NOTICE

AVIS

The quality of this microform is heavily dependent upon the quality of the original thesis submitted for microfilming. Every effort has been made to ensure the highest quality of reproduction possible.

La qualité de cette microforme dépend grandement de la qualité de la thèse soumise au microfilmage. Nous avons tout fait pour assurer une qualité supérieure de reproduction.

If pages are missing, contact the university which granted the degree.

S'il manque des pages, veuillez communiquer avec l'université qui a conféré le grade.

Some pages may have indistinct print especially if the original pages were typed with a poor typewriter ribbon or if the university sent us an inferior photocopy.

La qualité d'impression de certaines pages peut laisser à désirer, surtout si les pages originales ont été dactylographiées à l'aide d'un ruban usé ou si l'université nous a fait parvenir une photocopie de qualité inférieure.

Canada

UNIVERSITY OF ALBERTA

MEASUREMENT AND ANALYSIS OF MIXING AS IT RELATES TO

FLOCCULATION

by

STEPHEN J. STANLEY   Ⓒ

A THESIS

SUBMITTED TO THE FACULTY OF GRADUATE STUDIES A.   ᴕESEARCH

IN PARTIAL FULFILLMENT OF THE REQUIREMENTS FOR THE DEGREE

OF DOCTOR OF PHILOSOPHY

IN

ENVIRONMENTAL ENGINEERING

DEPARTMENT OF CIVIL ENGINEERING

EDMONTON, ALBERTA

FALL, 1995

THE AUTHOR HAS GRANTED AN IRREVOCABLE NON-EXCLUSIVE LICENCE ALLOWING THE NATIONAL LIBRARY OF CANADA TO REPRODUCE, LOAN, DISTRIBUTE OR SELL COPIES OF HIS/HER THESIS BY ANY MEANS AND IN ANY FORM OR FORMAT, MAKING THIS THESIS AVAILABLE TO INTERESTED PERSONS.

L'AUTEUR A ACCORDE UNE LICENCE IRREVOCABLE ET NON EXCLUSIVE PERMETTANT A LA BIBLIOTHEQUE NATIONALE DU CANADA DE REPRODUIRE, PRETER, DISTRIBUER OU VENDRE DES COPIES DE SA THESE DE QUELQUE MANIERE ET SOUS QUELQUE FORME QUE CE SOIT POUR METTRE DES EXEMPLAIRES DE CETTE THESE A LA DISPOSITION DES PERSONNE INTERESSEES.

THE AUTHOR RETAINS OWNERSHIP OF THE COPYRIGHT IN HIS/HER THESIS. NEITHER THE THESIS NOR SUBSTANTIAL EXTRACTS FROM IT MAY BE PRINTED OR OTHERWISE REPRODUCED WITHOUT HIS/HER PERMISSION.

L'AUTEUR CONSERVE LA PROPRIETE DU DROIT D'AUTEUR QUI PROTEGE SA THESE. NI LA THESE NI DES EXTRAITS SUBSTANTIELS DE CELLE-CI NE DOIVENT ETRE IMPRIMES OU AUTREMENT REPRODUITS SANS SON AUTORISATION.

Canada

UNIVERSITY OF ALBERTA

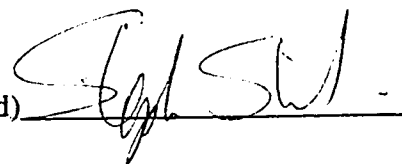## RELEASE FORM

NAME OF AUTHOR: STEPHEN J. STANLEY

TITLE OF THESIS: MEASUREMENT AND ANALYSIS OF MIXING
                          AS IT RELATES TO FLOCCULATION

DEGREE FOR WHICH THIS
THESIS HAS PRESENTED: DOCTOR OF PHILOSOPHY

YEAR THIS DEGREE
GRANTED: FALL 1995

(signed)_____

PERMANENT ADDRESS:

12220 42 Avenue

Edmonton, Alberta

T6J 0W9
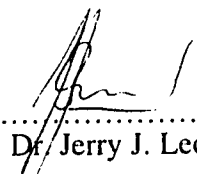
Dated: July 4, 1995
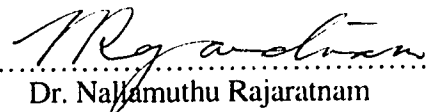
UNIVERSITY OF ALBERTA

FACULTY OF GRADUATE STUDIES AND RESEARCH
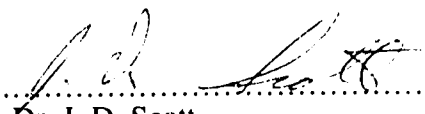
The undersigned certify that they have read, and recommended to the Faculty of

Graduate Studies and Research, for acceptance, a thesis entitled: MEASUREMENT AND

ANALYSIS OF MIXING AS IT RELATES TO FLOCCULATION submitted by: Stephen

J. Stanley in partial fulfillment of the requirement for the degree of DOCTOR OF

PHILOSOPHY IN ENVIRONMENTAL ENGINEERING.
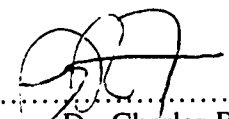
Dr. Daniel W. Smith - Supervisor

Dr. Gordon R. Finch

Dr. Jerry J. Leonard

Dr. Nallamuthu Rajaratnam

Dr. J. D. Scott

Dr. Charles R. O'Melia -
External Examiner

Date ....July 4, 1995............

DEDICATION

This work is dedicated to four people who have had a great influence on my life. My wife, Jennifer Stanley who has been encouraging, patient and understanding throughout this work. My parents, John Stanley and the memory of my mother, M.C. Denise Stanley who taught me all things were possible. And finally, to the memory of Dr. R. (Larry) Gerard who instilled in me the joy of research and knowledge.

Abstract

The coagulation and flocculation process is used in many water and wastewater treatment systems to change particulate characteristics to improve removal in the subsequent separation processes. The performance of the coagulation and flocculation process is dependent on complex interactions between many chemical and physical phenomena which include colloidal interactions, surface chemistry effects, and mixing and fluid processes. Due to the many complex interactions which affect process performance, the design, assessment and operation of flocculation systems must rely on bench and pilot-scale testing. However, to use results from small-scale tests, they must be scaled-up to the full-scale. It is generally assumed that the chemical processes are scale invariant and are accounted for by using the same water and chemical conditions in both systems. This is not the case for the physical process of mixing, as it has long been recognized that appropriate scaling of mixing is required to obtain similar results at different scales. Traditionally this has been accomplished through the use of the vessel-average root-mean-square velocity gradient, $\overline{G}$. It has been assumed if $\overline{G}$ is constant between scales the mixing environment will also remain constant. However, a number of studies have shown that $\overline{G}$ may not be appropriate for scaling of the flocculation process.

To investigate mixing in flocculation, detailed hydrodynamic measurements using a 2-D laser doppler anemometer were completed on two types of flocculators, with radial flow impellers: 1) a standard jar test apparatus; and, 2) the reactor zone of an upflow solids-contacting clarifier. Rather than rely on vessel-average parameters, localized velocities, energy dissipation rates, turbulent length scales and shear forces were determined for various zones of the flocculator. For these hydrodynamic factors it was also determined how they change with scale and impeller speed.

It was found that flow in impeller-agitated vessels is highly non-homogeneous, with areas of high energy dissipation and velocities occurring in the region of the impeller. It was also found that flow in the impeller discharge zone could be represented by a

swirling radial jet which provided the basis for the development of many scaling relations. Based on results gained from the analysis of turbulent flow in these flocculators, forces on the floc were determined for the various zones within the flocculator. It was found that local forces within the vessel can be much greater than those calculated based on vessel average values. Of importance, it was found that high forces on floc particles occur due to high turbulence or energy dissipation rates in the discharge stream of the impeller, mean shear stresses due to fluid flowing over the impeller blades and mean shear stresses caused by the impeller discharge jet impinging on vessel walls. The latter may be the most significant and explain many of the difficulties found in scaling up mixing for flocculation. Results also indicate that vessel average parameters such as average energy dissipation per unit mass, $\bar{\varepsilon}$ and $\bar{G}$ are not appropriate for the design, assessment and operation of flocculation facilities as local forces on the floc are not represented by them. A better approach for the scaling of the mixing process may be the matching of local floc forces for different scales. As results indicate that the dominant forces are those associated with the impinging jet, it appears that scaling of mixing based on matching these forces between flocculation systems is an improvement over the traditional use of $\bar{G}$.

ACKNOWLEDGMENTS

TABLE OF CONTENTS

LIST OF TABLES

LIST OF FIGURES

LIST OF SYMBOLS

A constant

A_{12} Hamaker constant

b width of impeller

C constant

D impeller diameter

d particle diameter

d_f maximum floc size

d_o diameter of jet at source

dU/dz laminar velocity gradient

F force on a floc

$\overline{G}$ vessel average root mean square velocity gradient

G local root mean square velocity gradient

K constant representing the floc density function

k kinetic energy

m impeller blade passage frequency

N impeller rotation speed

n_i, n_j number concentration of the class i and j particles and

N_{ij} collision rate for class i and j particles

N_p Power number

N_q Flow number

P power input

q radial and tangential resultant velocity

q_{max} radial and tangential resultant velocity along axis of radial jet

Q difference in dynamic pressure across a particle

R Reynolds number

$R_E(\tau)$ Eulerian autocorrelation function

t_k	Kolmogoroff time scale
T	diameter of vessel
u	mean radial velocity
u'	fluctuating radial velocity
V	liquid volume
v	mean tangential velocity
v'	fluctuating tangential velocity
V_{tip}	tip speed of impeller ($N\pi d$)
W	width of impeller
w	mean axial velocity
w'	fluctuating axial velocity
μ	absolute viscosity,
$\bar{\varepsilon}$	average rate of energy dissipation per unit mass
ξ	distance along the axis of the swirling radial jet
ν	kinematic viscosity
η	Kolmogoroff's microscale
ε	local unit mass energy dissipation rate
Φ_m	volume average power input,
k_1	wave number
Λ	width of jet
ρ	density
σ	interfacial tension
τ_o	shear stress

Subscripts

c	convective velocity
DI	inertial subrange

max	maximum
per	periodic fluctuating velocity
R	resistance
r	radial direction
rand	random fluctuating velocity
t	tangential direction
tot	total fluctuating velocity
VS	viscous subrange
z	axial direction

Chapter 1

Introduction

1.1 Overview

The most economical method of removing particulate matter from water during treatment is through the use of sedimentation. However, many particles are too small to settle out of suspension by gravity in an economical time. The agglomeration of these particles into larger, more settleable particles is essential to permit cost-effective removal in the subsequent sedimentation process. The process of agglomerating the particles in water treatment is known as coagulation and flocculation. In the literature, different interpretations of the terms "coagulation" and "flocculation" are found. In this study, coagulation will refer to the destabilization of the colloids and flocculation to the process that promotes particle-particle contact.

Particulate matter in water, of which those of most concern are classed as colloids, can be generally divided into those of inorganic origin or those of organic origin. Inorganic colloids include clay, silt and mineral oxides which generally originate from natural and cultural erosion processes. Organic colloids include humic and fulvic acids which are products of decay and leaching of organic debris and litter which have fallen in the water source. The impacts of the colloids on the water quality depend on their chemical, physical and biological properties. Some of the impacts include: reduction in clarity of the water; the large surface area of the colloids can serve as a potential adsorption sink for toxic substances, such as heavy metals, pesticides, viruses and other microbial contaminants; organic colloids can impart colour to the water, cause taste and odour problems, and produce harmful by-products upon oxidation; and colloids can limit the effectiveness of

microorganism disinfection. Therefore, the removal of particulate matter is required based on both aesthetic and health concerns.

Colloid particles in an aqueous dispersion carry an electric charge. The sign of this charge can be either positive or negative, although in most waters and wastewaters the colloids develop a negative charge (Stumm and Morgan, 1981). As all the colloids tend to carry the same charge (negative) they tend to repel one another. Therefore to effectively agglomerate the colloids into larger particles, the particles must be destabilized by neutralizing or reducing the charge. Following destabilization, less intense mixing of the particulates occurs to increase the rate of particulate collisions. In this slow mixing stage flocculation occurs only if particles: (1) collide with each other; and (2) can adhere when brought together by collision (i.e. the particles have low colloid stability). For the most part the first step is governed by transport processes. The primary mechanisms for the transport process are: (1) Brownian or perikinetic flocculation due to thermal fluid motion; (2) velocity gradient or orthokinetic flocculation due to bulk fluid and turbulent motions; and (3) differential settling due to larger particles overtaking and colliding with slower settling particles. In the second step, whether the particles adhere or attach is dependent on colloidal interactions. The two most familiar colloidal interactions are van der Waals attraction and electrical repulsion, known as DLVO forces (Derjaguin and Landau, 1941 and Verwey and Overbeek, 1948). In addition, non-DLVO forces such as hydration effects, hydrophobic effects, viscous or hydrodynamic interactions, steric interactions and bridging can also be important in assessing colloidal interactions (Gregory, 1989). The colloidal interactions tend to determine the collision efficiency and the strength of the aggregates. It should be noted that practically all colloidal interactions are of quite a short range, almost never extending over distances greater than the size of the particles (Gregory, 1989). This means that they have little influence over the transport of particles, although they are crucial in determining the collision efficiency. As a result the transport and attachment process can often be considered as separate steps.

In coagulation and flocculation the goal is to form the largest and strongest flocs as quickly as possible. Increasing the mixing intensity during flocculation will increase interparticle contacts; however it will also place greater forces on the floc. If forces are great enough this can cause break-up of the floc which negatively impacts the performance of the process. As a result, there is a relatively narrow range of optimum mixing conditions for flocculant mixing in which particle collision occur at a rate great enough to agglomerate particles in an economical time but the mixing is not too intense to cause significant break-up. Complicating this is that the floc's ability to resist forces placed on it by mixing is dependent on many site-specific conditions such as the colloidal interactions and hence optimum mixing conditions will vary from site to site and even at a given site with changing water quality conditions.

As the above discussion illustrates, the performance of coagulation and flocculation processes are dependent on complex interactions between many chemical and physical processes. Due to these complex interactions, much of the design, assessment, optimization and operation of flocculation facilities rely heavily on bench and pilot scale testing. A classic example is the use of the jar test in water treatment to determine coagulant dose and mixing conditions for the full-scale system. Another example is the common use of pilot-scale tests in design of new systems. However, to use results from the bench or pilot-scale, they must be scaled-up for application at full-scale.

It has generally been assumed that factors such as colloidal interaction and surface chemistry are not sensitive to scale. However, the importance of scaling hydrodynamic processes has long been recognized. Traditionally, vessel-average parameters such as the volume average root-mean-square velocity gradient, $\bar{G}$, have been used. It has been assumed that if $\bar{G}$ is held constant the mixing environment will remain constant (Camp and Stein, 1943). The use of constant $\bar{G}$ and $\bar{G}t$ has generally been used to obtain hydraulic similitude between various flocculation reactors. Recently considerable work has been

published that has questioned the use of $\overline{G}$ (Cleasby, 1984; Clark, 1985; Hanson and Cleasby, 1990; and Han and Lawler, 1992). Much of the recent work has highlighted that "local" hydrodynamics within the reactor, especially in the impeller zone, may be more important than vessel average parameters such as $\overline{G}$. Although this has been recognized for some time, most researchers have tried to account for this by simply assuming that $\overline{G}$ within the impeller zone is some multiple of the average value (AWWA, 1990), as little detailed turbulent flow information has been available for the flocculation reactors. The multiple used has been taken mostly from chemical engineering literature which has for some time reported studies of turbulent flow in stirred reactors.

However, most of this information from the chemical engineering literature is not directly related to coagulation and flocculation, as experimental conditions are generally outside those normally found in water treatment flocculation applications and most were completed using a the Rushton turbine. Most work in chemical engineering is concerned with blending and homogenization of fluid mixtures and, as a result, most studies are completed at high mixing intensity and the hydrodynamic parameters investigated are those most significant to blending. This work is more applicable to rapid mixing in coagulation with little literature available on hydrodynamic parameters under conditions found in most flocculation processes and little consideration of important parameters responsible for forces on flocs.

A recent study by Clark et al. (1994) entitled "Selection and Design of Mixing Processes for Coagulation" highlights the difficulty in scaling-up the coagulation and flocculation process using our current understanding of the mixing process. In their study four different types of flocculation impellers were investigated at three different scales. For each type of flocculator, mixing conditions were scaled by keeping a constant $\overline{G}$ for the three different sizes investigated. Although this is the standard practice, it was found that performance of the flocculators varied with scale. A similar trend found with all

flocculators was that performance deteriorated with increased size of the flocculator. This prompted the investigators to develop a number of recommendations for further study which included:

"there is a need for a detailed understanding of the fluid flow patterns induced by different flocculation impellers at different mixing intensities and of the impact of these fluid mechanics on floc size and floc structure"

"there is a need for a better understanding of how impeller fluid mechanics changes with scale and how these different fluid mechanics regimes affect flocculation-sedimentation performance"

The above study highlights the need for an improved understanding of the fundamentals of mixing in coagulation and flocculation. Given the general trend towards more stringent requirements for both water and wastewater treatment systems, the need to better understand the mixing process in flocculation and to be able to confidently scale-up results from the bench and pilot-scale to full-scale has become a significant requirement in process design and assessment.

In drinking water treatment there is renewed interest in optimizing the performance of the coagulation and flocculation processes. This can be related to the realization that coagulation and flocculation is not only important in the removal of general particulate matter but also important in the removal of microbial contaminants as part of the multi-barrier concept for microbial inactivation and that this process is also responsible for removal of significant organic contaminants which reduces the potential for the formation of disinfection by-products. Due to concerns with *Giardia* and *Cryptosporidium* the maintenance of a low turbidity in finished water is becoming a more important issue in drinking water treatment. The importance of turbidity as a parameter to indicate microbial

quality of drinking water is evident in the USEPA using turbidity to justify pathogen removal credits in their most recent standards (Letterman, 1994). In these standards maximum credits are earned with a finished water turbidity of ≤ 0.5 NTU 95% of the time. Miller (1994), for the protection of water against *Cryptosporidium* even recommends that filtered water should be less than 0.1 NTU. The coagulation and flocculation process is responsible for removal of a substantial portion of the turbidity in the treatment process and also affects the performance of filters that reduce turbidity further. The importance of coagulation and flocculation in removal of organic contaminants is also evident in the USEPA's (1994) decision to select enhanced coagulation as the "Best Available Technology" for the meeting of new disinfection by-product regulations. Enhanced coagulation involves the optimization of the process for the removal of organic material which acts as precursors to disinfection by-products (Cheng et al., 1995). Optimization normally involves bench and pilot-scale testing, which increases the need to be able to scale-up results successfully.

1.2 Theory of Coagulation and Flocculation

1.2.1 Introduction

Presented below is a summary of the theory of coagulation and flocculation. As this thesis is in a paper format, significant literature is presented with each chapter (paper) specific to the topic of that chapter. Chapters 2, 3, and 4 refer to literature on : analysis and measurement of turbulent low in impeller agitated mixing vessels; impacts of mixing on flocculation kinetics and floc characteristics; and scaling of hydrodynamic parameters and forces on the floc in mixing vessels, respectively. This information will not be repeated in this theory section. As a result, the purpose of this section is to give a general overview of the coagulation and flocculation field which will aid in determining how the work discussed

later in the thesis fits into the overall knowledge of coagulation and flocculation. This should highlight that, although the topic of this research (mixing in flocculation) is important to the coagulation and flocculation process, many other factors are also important which were not investigated as part of this study. The theory section will focus on colloidal interactions as this is a very important component of coagulation and flocculation theory, but was only touched on briefly in the work presented.

1.2.2 Colloidal Interactions

1.2.2.1 Colloids

Particulate matter in natural waters vary widely in origin, concentration and size. Particulate size may vary over several orders of magnitude, as shown in Table 1.1. Of primary interest in the coagulation and flocculation processes are the small particles (less than 10 μm) which settle very slowly, if at all, under gravity forces. These particles fall in the colloidal range. Because of their small size, interparticle forces can become very significant and play a large part in the stability of colloids. Colloidal particles are said to be stable if they are resistant to aggregation and unstable if aggregation occurs readily.

Some colloids are stable indefinitely and some are not. Colloids that are stable indefinitely are energetically or thermodynamically stable; they have been termed reversible colloids or hydrophilic colloids. These include water-soluble macromolecules such as starches, proteins, soap and detergent molecules called micelles, large polymers and some humic substances. Because they are thermodynamically stable in water, they can be induced to aggregate only by changing the solvency conditions, for instance by changing the temperature, pH or by adding large quantities of inorganic salts ("salting out").

Colloids that are not stable indefinitely are generally hydrophobic in nature and consist of materials with low solubility. They are often called irreversible colloids. In this case the particles are not stable in a thermodynamic sense, but may be kinetically stable by virtue or interparticle repulsion, so that particles are prevented from colliding and forming permanent aggregates (or flocs). Examples of irreversible colloids include clays, metal oxides and many microorganisms. Irreversible colloids given sufficient time will settle, however this time can be great. In water and wastewater treatment the primary concern with the agglomeration of thermodynamically unstable (irreversible) colloids, is to reduce the settling time.

Thermodynamically unstable colloids can be further categorized into those that agglomerate slowly (termed diuturnal) and those that agglomerate rapidly (termed caducous). The goal of the coagulation and flocculation process is to transform diuturnal colloidal systems into caducous systems.

1.2.2.2 Effect of Colloidal Interactions on Flocculation

When two particles approach each other several types of interaction can come into play which may have a major effect on the flocculation process. There are two different but related ways in which colloid interactions influence flocculation. First they have a direct effect on the collision efficiency. If, for example, there is a strong repulsion between the particles, then the chance of aggregate formation will be very low. As a result, one of the primary objectives in practical coagulation and flocculation is to ensure, by suitable chemical control, that any interparticle repulsion is reduced or eliminated so that the collision efficiency is as high as possible. The other aspect of colloid interactions is their effect on the strength of the aggregates, which is much less well understood but of great practical importance.

The two most familiar kinds of colloidal interactions are van der Walls attraction and electrical repulsion. These form the basis of the well-known DLVO theory of colloid stability which was developed independently by Derjaguin and Landau (1941) and Verwey and Overbeek (1948). Although the DLVO theory has allowed a large amount of experimental flocculation data to be explained, at least in a semi-quantitative manner; there are many cases where other types of interactions have to be considered. Some of these "extra" or "non-DLVO" forces include such things as hydration effects, hydrophobic effects and other effects arising from the presence of adsorbed polymer.

1.2.2.3 van der Waals Forces

The attractive van der Waals force is important in the interaction of colloidal particles. Without these forces, aggregation of particles would not occur even if the electrical repulsion forces were nullified, as hydrodynamic interactions would cause particles to flow around each other. van der Waals forces can be calculated using an approach developed by Hamaker (1937). It is based on the assumption of pairwise additivity of intermolecular forces. The interaction between two particles is calculated simply by summing the interactions of all molecules in one particle with all of the molecules in the other. Hamaker replaced the summation by a double integration procedure which leads to very simple expressions, especially when the separation distance is small. For two spheres, radii a_1 and a_2, separated by distance d, the interaction energy at close approach (d<<a) is given by:

$$V_A = -(A_{12}/6d)a_1a_2/(a_1+a_2) \qquad (1.1)$$

where V_A is the attraction energy between two spheres and A_{12} is the Hamaker constant for the media 1 and 2 of which the spheres are composed. The above equation applies only at close approach and to the interaction of media across a vacuum. As a result, modifications have been made to the Hamaker approach to make it more applicable to colloids in water

and to take into account other factors such as retardation effects. Approaches other than that by Hamaker have also been developed to determine van der Waals forces. For a more detailed explanation see for example Gregory (1989).

1.2.2.4 Electrical Interactions

The primary mechanism controlling the stability of both hydrophobic and hydrophilic particulates is electrical repulsion. The electrical charges existing at the particle surface originate in three principal ways (Stumm and Morgan, 1981):

1. Chemical reactions at the surface. Many particulate surfaces contain ionogenic groups, such as hydroxyls or carboxyl functional groups, which dissociate in water, producing a surface electrical charge that depends on the pH of the solution.

2. Imperfections in the crystal lattice. Under geologic conditions, silicon atoms in crystalline materials can be replaced by atoms with lower valence, such as an aluminum ion, giving an excess negative charge to the crystal material. This process, known as isomorphous substitution, produces negative charges on the surface of clay particles (van Olphen, 1983).

3. Adsorption of a surfactant ion. Preferential adsorption of one type of ion on the surface can arise from van der Waals interactions and from hydrogen or hydrophobic bonding.

It should be noted however, that most particulates have complex surface chemistry and surface electrical charges arise from several sources. When particles are dispersed in water, the charge on the particle surface is balanced by an equivalent number of oppositely charged counter-ions. This accumulation of ions is opposed by the tendency of ions to diffuse in the direction of decreasing concentration. The surface charge on a particle and

the associated counter-ion charge together constitute what in known as the electrical double layer (Kruyt, 1952). The widely accepted model for the double layer is that described by Stern, later modified by Graham (see Hunter, 1981), in which part of the counter-ion charge is located close to the particle surface (the "Stern layer") and the remainder is distributed in the diffuse layer. The Stern layer is approximately 0.5 nm deep, corresponding in size to the hydrated cation or nonhydrated anion. Figure 1.1 shows the structure of the electrical double layer.

The interaction between charged particles is governed predominately by the overlap of diffuse layers, so the potential most relevant to colloidal interactions is that at the plane between the Stern and diffuse layers (the Stern potential). There is no direct experimental method for determining the Stern potential, however it appears that the zeta potential is an adequate substitute (Lyklema, 1977), although there is still some controversy about this (Barouch and Matijevic, 1987). The zeta potential is the potential drop across the mobile part of the double layer that is responsible for electrokinetic phenomena. It is assumed that the liquid adhering to the solid (particle) surface and the mobile liquid are separated by a shear plane (slipping plane). The electrical potential (zeta potential) between the shear plane and the bulk solution can be determined by electrophoresis measurements (measurement of rate of movement of particles in an electric field).

The two major influences on electrical interaction between particles are the magnitude of the effective "surface potential" (generally assumed to be the zeta potential) and the extent of the diffuse layer, since it governs the range of the interaction. Surface potentials can be modified in two distinct ways. If the ionic strength is raised, then a greater proportion of the potential drop occurs across the Stern layer giving a smaller zeta potential. This is generally referred to as double-layer compression. Empirically, when the zeta potential is reduced below approximately ± 20 mV, rapid coagulation is likely to occur (Kruyt, 1952). However, this value may vary from system to system. In addition to

double-layer compression, the zeta potential can be lowered by the addition of specifically adsorbing counter-ions. These adsorb on the particles because of some specific, nonelectrostatic affinity and can be regarded as lying in the Stern layer. These can lead to charge neutralization and destabilization of the particles. In many cases, such ions can adsorb to such an extent that they reverse the sign of the zeta potential.

1.2.2.5 Combined Interactions - Colloid Stability

The classical theory on colloid stability was developed independently by Derjaguin and Landau (1941) and Verwey and Overbeek (1948) and is called the DLVO theory. It only considers van der Waals and electrical interactions and assumes that these contributions are additive and may be simply combined to give the total interaction. Although the DLVO theory does not take into account all colloid interactions, it provides an effective tool in the interpretation of many empirical facts in colloid chemistry (Stumm and Morgan, 1981). The total (net) interaction V_T is simply expressed as:

$$V_T = V_R + V_A \qquad\qquad (1.2)$$

where V_R is the electrical repulsion, and V_A is the van der Waals attraction. Numerous forms for this equation have been proposed based on different methods of calculating V_R and V_A. In Figure 1.2 the energies of interaction (V_R, V_A and V_T) are shown as a function of separation distance. Conventionally the repulsive potential is considered positive and the attractive energy negative. In the case chosen in Figure 1.2 the repulsion is greater than attraction giving a potential energy barrier and colloidal stability. Two colliding particles would need to possess sufficient energy to overcome this barrier for an aggregate to be formed. Once this barrier has been overcome the particles should be held in a deep primary minimum, from which escape would be unlikely. Another feature of Figure 1.2 is the secondary minimum in the V_T curve. In principle, aggregation could occur without the particles coming into close contact. However, the secondary minimum is seldom deep

enough to cause instability, but may help in explaining certain loose forms of adhesion or agglomeration (Stumm and Morgan, 1981).

In order to reduce the barrier energy and hence permit primary minimum flocculation to occur, the only practical method is to reduce the electrical repulsion (zeta potential). Methods for reducing the electrical repulsion were discussed earlier, which included "salting out" and charge neutralization.

When particles have been fully destabilized by the addition of sufficient salt or by charge neutralization, flocculation can occur at a rate which is dependent on the frequency of particle collisions. This is known as rapid flocculation, in which the term does not imply anything about the rate but implies that the rate cannot be increased by the addition of more salt. At lower salt concentration, slow flocculation occurs at a rate dependent on the magnitude of the potential energy barrier. The ratio of the slow flocculation rate, for a given condition to the most rapid rate observed is known as the collision efficiency factor, α, and represents the fraction of collisions which result in aggregate formation. The inverse of the collision efficiency is known as the stability ratio, W ($= 1/\alpha$).

The stability ratio must then depend on the form of the potential energy barrier; the higher the barrier, the smaller the proportion of successful collisions. Fuchs defined a stability ratio that is related to the area enclosed by the resultant curve of the energy of interaction (V_T) versus separation distance (see Verwey and Overbeek, 1948). The major contribution to this area comes from the region around the energy maximum, V_{max}, and as a result a first approximation of the stability ratio is given in terms of the V_{max}. This is conveniently expressed in units of kT, where k is the Boltzmann constant and T is the absolute temperature. V_{max} values of 5, 15 and 25 kT give stability ratios of about 40, 10^5 and 10^9, respectively. It should be noted that a simple relation between the energy barrier and stability ratio only applies in cases where diffusion is the only significant particle transport mechanism. If other transport mechanisms, such as fluid motion, are involved

the energy of colliding particles may be much greater than their thermal energy and aggregation may occur more readily (Gregory, 1989).

1.2.2.6 Other Colloidal Interactions

To fully explain the stability and the agglomeration properties of most colloids in natural waters, factors other than van der Waals attraction and electrical repulsion must also be considered. Other factors include hydration effects, hydrophobic interactions, steric interactions and polymer bridging.

As colloidal particles can be stabilized by a surface charge, it implies ionic groups at the surface, or adsorbed ions, together with some closely associated counter-ions (in the Stern layer). Since ions in aqueous solution tend to be hydrated, it is reasonable to suppose that surface ions are also associated with a certain amount of "bound water". The major consequence of hydration at a particle surface is an increased repulsion between approaching particles, because of the need for ions to lose their water of hydration if contact between particles is to be achieved. This involves work and hence an increase in free energy of the system. The range of these hydration forces is quite appreciable in relation to the range of double-layer repulsion and they may be expected to have an effect on colloid stability, especially at high ionic strength (Gregory, 1989). However, the exact role of hydration effects in practical application is still not fully understood.

Hydrophobic substances are readily soluble in many nonpolar solvents but only sparingly soluble in water; thus these substances tend to reduce the contact with water and seek relatively nonpolar environments. The possibility arises of another type of interaction which can give appreciable attraction, called hydrophobic interaction. The implication of hydrophobic interactions in aqueous dispersions has yet to be exp ored, but there are probably many examples where it is important in promoting coagulation and flocculation (Gregory, 1989).

In many cases small amounts of adsorbed polymer can promote agglomeration through bridging. However, if greater amounts of polymer are adsorbed, the polymers can result in enhanced stability by an effect known as steric stabilization. Many polymers have both hydrophilic and hydrophobic segments. The hydrophobic segments will tend to bond to the particle and the hydrophilic segments will tend to project into the aqueous solution. Stabilization occurs because as particles approach each other the hydrophilic segments will interact first and repel each other. This will not allow the particles to come in close contact. Many particles in the aquatic environment have adsorbed layers of natural organic material, such as humic substances (Tipping, 1988) which can have a dominant effect of colloidal stability. Also many microorganisms produce extracellular polymers which may adsorb. The stability of such colloids is usually higher than expected on the basis of the DLVO approach and it is likely that steric stabilization plays a part in many cases (Gregory, 1989). Humic substances are known to enhance the stability of inorganic colloids (Jekel, 1986) which can result in increased flocculant dosages.

When polymers are used at the appropriate doses they aid in formation of agglomerates through bridging. Long-chain polymers can be attached to more than one particle at one time. When more than one particle is attached to a single polymer molecule it is said to be bridged. For bridging to occur, the polymer needs to have a high molecular weight and adsorb such that a significant portion of the segments are not in contact with the particle but extended into the aqueous phase. However, if excess polymer is added the particle can be restabilized as there is insufficient free surface area on the particle for contacts to occur and the adsorbed layers may also cause steric repulsion.

1.2.2.7 Practical Particle Destabilization in Water Treatment

The above discussion has focused on two methods of particle destabilization: addition of salts which increase ionic concentrations (double-layer compression) and addition of specifically adsorbing counter ions which reduce surface charge (charge

neutralization). In water treatment, double layer compression is seldom the dominant

mechanism as the quantity of salt required tends to impact negatively on water quality. In

water treatment the dominant mechanism is generally either charge neutralization or

enmeshment, also termed sweep flocculation (O'Melia, 1972). Enmeshment results in

destabilization of particles through a mechanism which is not really described by classical

DLVO theory. It involves the addition of metal salts such as $Al_2(SO_4)_3$ or $FeCl_3$ at

concentrations generally much greater than would be required just for charge neutralization.

These concentrations are high enough to cause rapid precipitation of metal hydroxides in

which the colloidal particles can be enmeshed in these precipitates formed (O'Melia, 1972).

This has been termed sweep-floc by Packman (1965). Another important mechanism

which was briefly discussed previously is bridging. This is normally accomplished

through the use of organic polymers and recently with the use of polymeric inorganic

coagulants (Amirtharajah and O'Melia, 1990). Although the charge of the polymer is

opposite to that of the particles, such that it may be adsorbed to the particle surface, the

charge may not have to be great enough to neutralize the overall charge of the particle. As

the polymer bridges the distance between the particles, it is not required that particles come

in close contact where electrical repulsive force are significant. Polymers are also often

used as a coagulant aid where one of their primary purposes is to strengthen metal

hydroxide flocs which can be quite weak.

1.2.3 Transport Process

1.2.3.1 Flocculation Kinetics

Flocculation kinetics or the rate at which flocculation occurs are dependent both on

the rate at which particle-particle contacts occur, which is governed by transport processes

and the efficiency of these collisions, which, as discussed, is dependent on colloidal

interactions. Most of the work on flocculation kinetics can be related back to the original work by Smoluchowski (1917) who developed an expression for the rate of collisions between particles in laminar shear (orthokinetic flocculation). This work was extended to turbulent flow fields by Camp and Stein (1943) by defining the mean velocity gradient $\overline{G}$. Details of both these can be found in Chapter 2 and will not be presented here. As discussed, there has been a significant body of literature which has questioned the appropriateness of using a vessel average parameter such as $\overline{G}$, given the spatial variation in energy within the flocculator (see for example Clark (1985)).

Recent work in flocculation kinetics has focused on two new methods of analyzing the process. One of these methods involves the use of a multi-level floc model (Francois and Van Haute, 1985; and Clark and Flora, 1991). In these models the aggregation of particles can be described by dividing flocs into a number of different levels. In one model (Francois and Van Haute, 1985) the first level of flocs describe the primary particles which aggregate into compact aggregates whose diameter is dependent of the highest shear force experienced by the floc and are termed "flocculi", which are the second level. The flocculi can aggregate into higher level flocs (third level), which can finally form loose agglomerates (fourth level). Through break-up and regrowth of flocs, Clark and Flora (1991) showed that flocs can be described by the multi-level floc structure.

Another recent method of describing floc growth and kinetics is through the use of fractal dimensions of the floc, which can be related to floc characteristics such as floc density (Clark and Flora, 1991). As flocs grow, their fractal dimension tends to decrease. A wide range of fractal dimensions has been reported for various types of flocs, with reported values varying from 1.2 to 2.8 (Lagavankar and Gemmel, 1968; Wiesner and Mazounie, 1987; and Clark and Flora, 1991). A relatively recent model which uses fractal dimensions is the random cluster-cluster aggregation (CCA) model (Botet et al., 1986).

This model appears to estimate fractal dimensions which are close to those measured in practice.

At this point, these types of models are useful in a conceptual sense for understanding floc formation. However, currently, these models at the most use vessel-average parameters such as $\overline{G}$ to describe mixing characteristics.

1.2.3.2 Forces on a Floc and Floc Break-up

The break-up and maximum size of flocs are another important factors governing flocculation performance. With increased mixing, greater forces are place on the floc which can cause it to break up defeating the original purpose of making larger flocs. The ultimate size of the floc is determined by two opposing factors, namely the mechanical strength of floc and the applied breaking forces. Fluid induced stresses on the floc can be caused by shear stresses, drag stresses and differential pressure (i.e. normal stresses). For turbulent fluid induced stresses acting on particles it is necessary to consider the structure and scale of turbulence in relation to particle size and motion in the fluid flow. Generally turbulence production occurs at large scale with energy being transferred down through smaller scale eddies until it is dissipated at small scales. Of interest is the relation between the smallest length scales and particle size. The smallest sustainable eddy is given by the Kolmogorov's microscale, η. Eddies that are larger than the particle tend to entrain particles, thus causing little surface stress, with laminar shear being the dominate stress. If eddies are smaller than the size of the particles, these eddies can provide particle shear, surface drag and pressure forces. Forces on the floc will be different if the floc size is in the inertial convection subrange $(d \gg \eta)$ or the viscous subrange $(\eta \gg d)$. Chapter 5 discusses and formulates forces on the flocs for these two turbulent subranges.

Break-up of a floc occurs when the fluid forces on the floc exceed the strength of the floc. Unlike the related field of drop break-up where the drop strength can be related to

interfacial tension, drop viscosity and drop size, no universal relationship has been developed for floc strength. The mechanical strength of flocs is dependent on many factors. This includes colloidal interactions, which tend to impact the size and compactness of the floc matrix and the number and strength of bonds at the microparticle contacts (Gregory, 1989). The size and shape of the microparticles, type of coagulant or coagulant aid used and water quality parameters can also effect floc strength. Although the strength of flocs is of great practical importance, the effects of many of these factors on floc strength are still poorly understood (Gregory, 1989; Leentvaar and Rebhan, 1983). Tambo and Hozumi (1979) stated that the binding force of the floc is proportional to the net sectional area at the plane of rupture and a constant dependent on the mean binding strength of the floc. Their formula for floc strength which is presented in Chapter 5 incorporated a constant termed the floc density function and was proportional to the floc diameter squared. Parker et al. (1972) assumed that the strength of the floc was dependent on the floc yield strength, which is not directly related to floc diameter. Matsuo and Unno (1981) assumed that the strength of the floc could be related to a pseudosurface tension, analogous to what is done for drops. The maximum floc size is dependent on both the forces on the floc and floc strength, with many different formulas having been proposed for determining the maximum floc size. The difference in these formulas can mostly be related to the various methods proposed for estimating floc strength, as most studies tend to agree on the fluid forces placed on the floc. Greater detail on this will be presented in Chapter 5.

1.2.3.3 Scaling Studies in Coagulation and Flocculation

As discussed, since the volume average root mean square velocity gradient, $\overline{G}$, was first proposed by Camp and Stein (1943) it has been the standard for the scaling of mixing conditions in coagulation and flocculation. Given its wide spread use in the field, it is somewhat surprising that there is a lack of multi-scale flocculation studies to assess its appropriateness. Most work on the assessment of mixing for flocculation kinetics and floc

characteristics have been completed in a single size of mixing vessel. As a result, although these types of studies are useful, they only really assess the effect of changing mixing intensity by varying impeller speed. Of the few studies that have been completed with multi-scale flocculators most have shown the same trends. Oldshue and Mady (1978) tested water from the effluent of the rapid-mix stage of a surface water treatment plant. Water from the rapid-mix stage was flocculated in two small-scale batch flocculators, one measuring 460 mm in diameter and the other 760 mm. Both had impeller diameter, D, to tank diameter, T, ratios of 0.2 and used Rushton-type impeller. Flocculation time for each flocculator was 10 minutes and performance was determined by measuring turbidity after a 60 minutes settling period. The optimum $\overline{G}$ value was determined for each flocculator. It was found that the optimum $\overline{G}$ for the larger vessel was significantly less than for the smaller vessel. The optimum $\overline{G}$ for the smaller vessel was 116 s^{-1} while for the larger vessel it was 59 s^{-1}. From this result Oldshue and Mady suggested that the optimal batch flocculation $\overline{G}$ value decreases with increasing scale.

Clark and Fiessinger (1991) reported similar results in comparing two flocculators, one of 1 L and one of 20 L. The data indicated a higher turbidity and lower humic acid removal in the larger vessel than in the smaller one when operated at the same $\overline{G}$. The authors concluded that results were consistent with a decrease in optimum $\overline{G}$ value with scale, at least for batch operation.

The most recent multi-scale flocculation study was presented by Clark et al. (1994). In their study three flocculation vessel sizes were investigated (T = 434 mm, 857 mm and 1375 mm) with four different types of impellers. Impellers investigated included pitched blade, Rushton, foil and rake. Mixing was scaled based on keeping $\overline{G}$ = 25 s^{-1} in each vessel size. Flocculation performance was based on turbidity and total particle count after 20 minutes of sedimentation. Figure 1.3 shows results for one of their experimental set-ups. The figure indicates that as tank diameter increased so to did settled water turbidity

and particle counts. Turbidities were almost double between the small and large scale vessels. An explanation for this was not determined and instead recommendations for further study were given, which were summarized earlier.

Clark (1986) and Clark and Fiessinger (1991) have attempted to explain the sensitivity to scale. The basic argument is that flocculation can depend upon multiple characteristic mixing time scales. As the scale of the mixer increases, the mixing time scales generally change in different ways. They give the example that maintaining a constant average unit mass energy dissipation rate between scales will not result in maintaining a constant impeller tip speed, or turnover time. Much of the work in scale-up in flocculation has been completed by Clark and co-authors. In his most recent work (Clark et al., 1994) he states:

> " The most important point to be made is that the correct scale-up
> law of initial mixing and/or flocculation cannot be very precisely
> predicted from theory alone. In order to understand scale-related
> effects in initial mixing and flocculation, experiments in different-
> scale systems are required."

What seems to be clear from the few multi-scale studies that have been completed is that the maintenance of constant $\bar{G}$ between scales does not result in equal flocculation performance, which would question the use of $\bar{G}$ as a scaling parameter. These studies also seem to indicate a similar trend toward a decrease in mixing power requirements with increasing scale.

1.3 Problem Statement and Research Objectives

The literature summary highlights that although there is a significant need to scale-up mixing in the flocculation process, use of the standard approach of constant $\bar{G}$ appears to have produced less than satisfactory results. Although the few multi-scale flocculation

studies which have been completed have tended to show the same trends, little information is available to explain and quantify these results to improve the scale-up process. This can be partly related to a general lack of detailed hydrodynamic information for impeller agitated vessels under mixing conditions normally encountered in flocculation. The overall goal of this study was, thus, to examine the relationships between hydrodynamics within the flocculator and flocculation performance. This could be accomplished by the development of some fundamental relationships between local hydrodynamic parameters and flocculation performance and by defining scale-up and design relationships for hydrodynamic parameters. Specific objectives of this research were to:

1. Define turbulent flow in a standard jar test apparatus, as this is one of the fundamental methods used to assess coagulation and flocculation processes (Chapter 2)

2. Assess full-scale hydrodynamics in a upflow solids contact clarifier, a commonly used type of flocculator that has hydrodynamic conditions which are considerably different from a jar test apparatus (Chapter 3).

3. Develop scale-up methods and relationships from basic concepts which will allow, at least in part, hydraulic simultude between different types and scales of flocculators (Chapter 4).

1.4 References

American Water Works Association. (1990). *Water Quality and Treatment.*. Fourth Edition, F.W. Pontius Ed., McGraw-Hill, Inc., Toronto, 1194p.

Amirtharajah, A. and O'Melia, C.R. 1990. Coagulation Processes: Destabilization, Mixing and Flocculation. *Water Quality and Treatment*, F.W. Pontius Ed., AWWA, McGraw-Hill, Inc., Toronto, 269-366.

Argaman, Y. and Kaufman, W.J. 1970. Turbulence and Flocculation. *ASCE Journal Sanitary Engineering Division*, 98, 79-92.

Barouch, E. and Matijevic, E. 1987. Effects of Born repulsion on particle detachment. *Chem. Eng. Commun.*, 55, 29.

Botet, R., Jullien, R. and Kolb, M. 1986. in *Fractals in Physics*, L. Pietronero and E. Tosatti, Eds., Elsevier, Amsterdam.

Camp, T.R. and Stein, P.C. 1943. Velocity gradient and internal work in fluid motion. *Jour. Boston Soc. Civil Engineers*, 30, 10, 219-237.

Cheng, R.C., Krasner, S.W., Green, J.F. and Wattier, K.L. 1995. Enhanced coagulation: a preliminary evaluation. *Journal American Water Works Association*, 87, 2, 91-103.

Clark, M.M. (1985). Critique of Camp and Stein's RMS velocity gradient. *Journal of Environmental Engineering, ASCE*, 111, 6, 741-754.

Clark, M.M. 1986. Scale-up of laboratory flocculation results. In *Proceedings of the Annual Meeting of the AWWA*, Denver, CO.

Clark, M.M. and Fiessinger, F. 1991. Mixing and Scale-up. In *Mixing in Coagulation and Flocculation*. A. Amirtharajah, M.M. Clark, and R. Trussel. AWWA Research Foundation, Denver, CO. 282-308.

Clark, M.M. and Flora, J.R. 1991. Floc restructuring in varied turbulent mixing. *Journal of Colloid and Interface Science*, 147, 2, 407-421.

Clark, M.M., Srivastava, R.M., Lang, J.S., Trussel, R.R., McCollum, L.J. Baily, D., Christie, J.D., and Stolarik, G. (1994) Selection and Design of Mixing Processes for Coagulation. American Water Works Association Research Foundation and American Water Works Association, Denver, CO. 150p.

Cleasby, J.L. 1984. Is velocity gradient a valid turbulent flocculation parameter? *Journal of Environmental Engineering, ASCE, 110*, 5, 875-897.

Degremont. 1991. Water Treatment Handbook Sixth edition. Lavoisier Publishing, Paris France. 1459p.

Derjaguin, B.V. and Landau, L.D. 1941. Theory of the stability of strongly charged lyophobic sols and of adhesion of strongly charged particles in solution of electrolytes. *Acta Physicochim. URSS*, 14, 633.

Francois, R.J. and Van Haute, A.A. 1985. *Water Research*, 19, 10 1249- .

Gregory, J. 1989. Fundamentals of Flocculation. *Critical Reviews in Environmental Control Vol.* **19**, 3. pp. 185-230.

Hamaker, H.C. 1937. The London - van der Waals attraction between spherical particles. *Physica*, **4**, 1058.

Han, M and Lawler, D.F. (1992). The (relative) insignificance of G in flocculation. *Journal of the American Water Works Association, 84*, 10, 79-91.

Hanson, A.T. and Cleasby, J.L. (1990). The effects of temperature on turbulent flocculation: Fluid dynamics and chemistry. *Journal American Water Works Association,,* **82**, 11, 56-73.

Hunter, R.J. 1981. Zeta Potential in Colloid Science. Academic Press, London.

Jekel, M.R. 1986. The stabilization of dispersed mineral particles by adsorption of humic substances, *Water Research, 20*, 1543.

Kruyt, H.R. 1952. Colloid Science, Vol. 1, Elsevier, New York.

Lagavankar, A.L. and Gemmel, R.S. 1968. A size-density relationship for flocs *Journal American Water Works Association*, **60**, 1040-46.

Leentvaar, J. and Rebhun, M. 1983. Strength of ferric hydroxide flocs. *Water Research*, **17**, 8, 895-902.

Letterman, R.D. 1994. What Turbidity Measurements Can Tell Us. *Opflow*, **20** 8 .

Lyklema, J. 1977. Water at interfaces: a colloid chemical approach. *Journal of Colloid Interface Science, 58*, 242.

Matsuo, T. and Unno, H. 1981. Forces acting on floc and strength of floc. *Journal of Environmental Engineering, ASCE*, **107**, 3, 527-545.

Miller, K.J. 1994. Protecting Consumers from Cryptosporidiosis. *Journal American Water W rks Association*, **86**, 12, 8-12.

O'Melia, C.R. 1972. Coagulation and Flocculation. In *Physiciochemical Processes for Water Quality Control* Ed. by W.J. Weber Jr., John Wiley and Sons, Toronto, 61-107.

Oldshue, Y.J. and Mady, O.B. 1978. Flocculation performance of mixing impellers. *Chemical Engineering Progress*, **74**, 8, 103-108.

Packman, R.F. 1965. Some studies of the coagulation of dispersed clays with hydrolyzing salts. *Journal Colloid Interface Science*, **20**, 81.

Parker, D.S., Kaufman, W.J. and Jenkins, D. 1972. Floc break-up in turbulent flocculation processes. *Journal of the Sanitary Engineering Division. ASCE*, **88**, 1, 79-99.

Smoluchowski, M.W. 1917. Versuch einer Mathematischen Throrie der Koagulations Kinetik Kolloider Losungen. *Zeitschrift f. Physik. Chemie*, 92:126.

Stumm, W. and Morgan, J.J. 1981. *Aquatic Chemistry*. John Wiley and Sons, Toronto, 780p.

Tambo, N. and Hozumi, H. (1979). Physical Characteristics of Flocs - II. Strength of Floc. *Water Research*, **13**, 421-427.

Tipping, E. 1988. Colloids in the aquatic environment. *Chem. Ind. (London), 15*, 482.

USEPA, 1994. National Primary Drinking Water Regulations; Disinfectants and

    Disinfection Byproducts; Proposed Rule. *Fed. Reg.* 59:145:38668.

van Olphen, H. 1963. *An Introduction to Clay-Colloid Chemistry.* Wiley-Interscience,

    New York.

Verwey, E.J.W. and Overbeek, J. Th. G. 1948. *Theory of stability of Lyophobic*

    Colloids. Elsevier, Amsterdam.

Wiesner, M.R. and Mazounie, P. 1987. Raw water characteristics and the selection of

    water treatment configuations for particle removal. Pre-conference seminar, annual

    conference of the American Water Works Association, Kansas City, MO, June 14-

    18.

Table 1.1   Settling time for various sized particles (adapted from Degremont, 1991)

Particle Diameter (μm)	Type of particle	Settling time through 1 m of water	Specific area* (m^2/m^3)
10^2	Fine sand	2 minutes	6×10^4
10	Clay	2 hours	6×10^5
1	Bacteria	8 days	6×10^6
10^{-1}	Colloid	2 years	6×10^7
10^{-2}	Colloid	20 years	6×10^8
10^{-3}	Colloid	200 years	6×10^9

* Assuming spherical particles
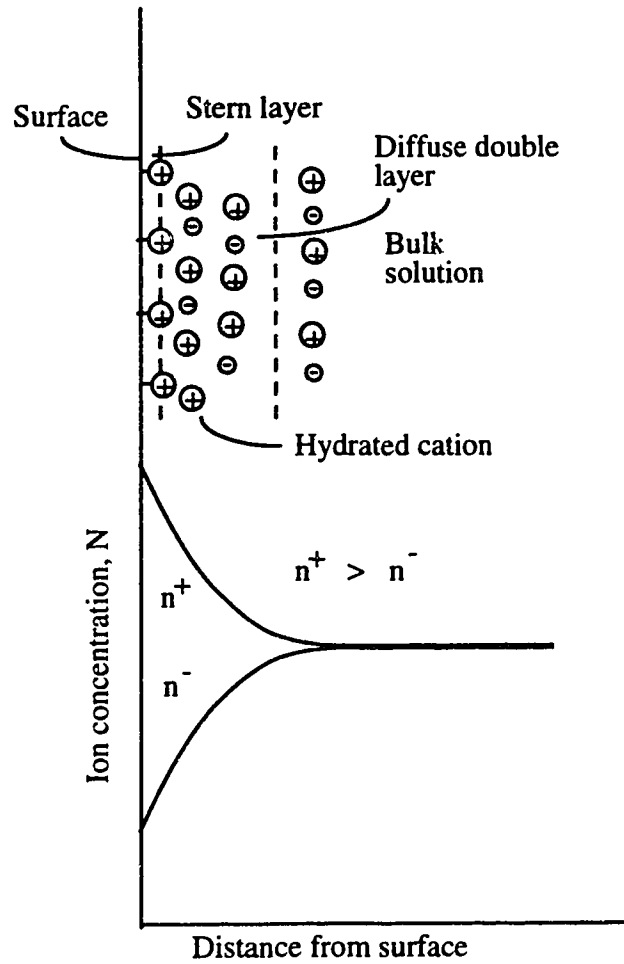
Figure 1.1   Electrical double layer for colloidal particles

Interaction Energy

V_E

Energy Barrier

V_T

Secondary Minimum

V_A

Primary Minimum

a) Colloids Stable

Interaction Energy

V_T

b) Colloids Destabilized
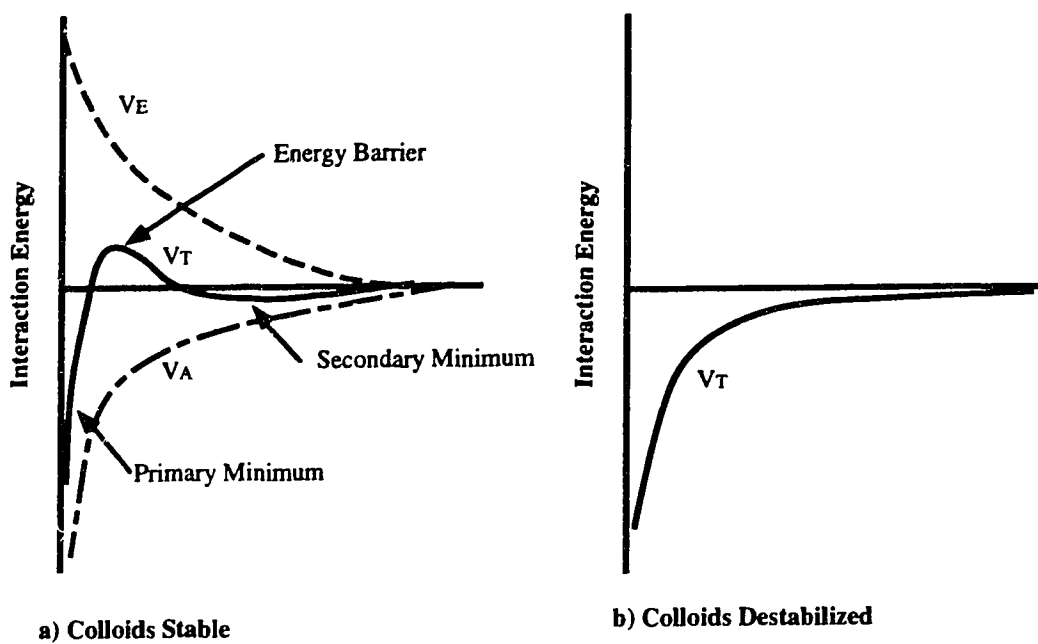
Figure 1.2   DLVO theory for colloidal particles.
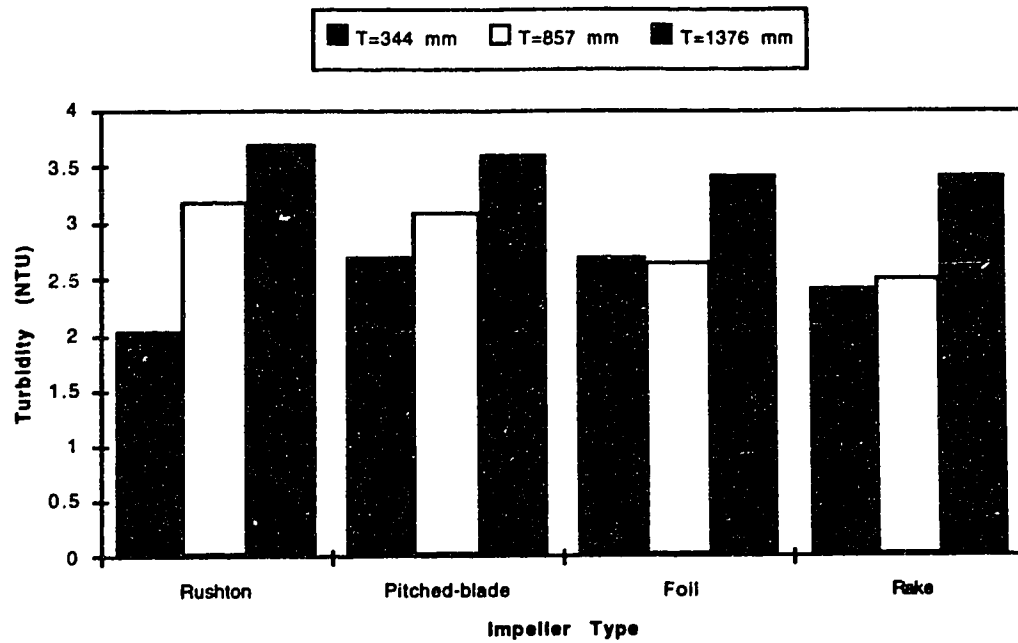
a)
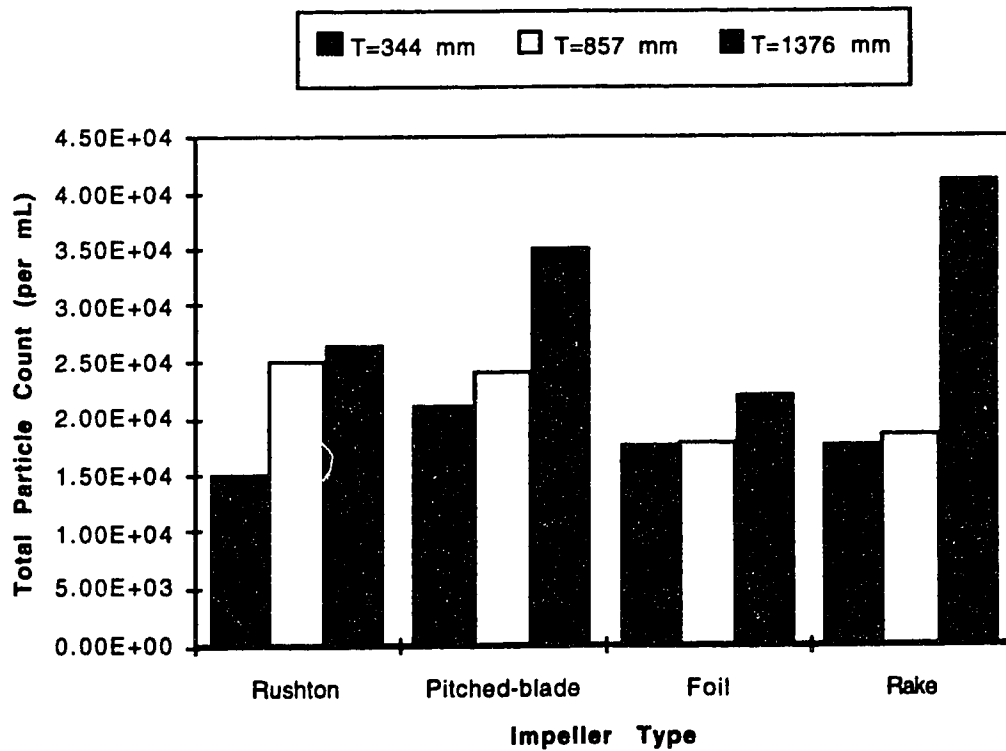
b)

Figure 1.3   Scaling results from Clark et al. (1994). a) Turbidity after 20 minutes
sedimentation; b) total particle count after 20 minutes sedimentation

Chapter 2

Measurement of Turbulent Flow in a Standard Jar Test Apparatus[1]

2.1 Introduction

The jar test has been used for over 70 years in the water treatment industry to evaluate coagulation and flocculation processes. It has been used both as a research tool in the study of the processes and as an operational tool for routine determination of plant coagulant dosing requirements. The objective of the jar test is to simulate existing plant operating conditions and under those conditions determine the optimum coagulant dose (Hudson, 1981). Simulation of plant operating conditions refers to both water quality and hydraulic conditions. It is the ability to simulate plant hydraulic conditions in the jar test that have long been criticized, questioned and studied. As a result, the interpretation of the ir ...ct of hydraulic conditions on flocculation performance which is determined at the jar test level has been difficult to relate to the full-scale.

Traditionally for the assessment, design and scale-up of mixing in water treatment coagulation and flocculation processes, the volume average root mean square velocity gradient, $\bar{G}$, has been used. It has been assumed that if $\bar{G}$ is held constant, the mixing environment will remain constant (Camp and Stein, 1943). The use of constant $\bar{G}$ and $\bar{G}t$ has generally been used for hydraulic simultude between the jar test and plant conditions. Recently considerable work has been published that has questioned the use of $\bar{G}$ (Cleasby, 1984; Clark, 1985; Hanson and Cleasby, 1990; and Han and Lawler, 1992). Much of the recent work has highlighted that "local" hydrodynamics within the reactor, especially in the impeller zone, may be more important than vessel average parameters such as $\bar{G}$. Although

---

this has been recognized for sometime, most of the researchers have tried to account for this by simply assuming that $\overline{G}$ within the impeller zone is some multiple of the average value (AWWA, 1990), as little detailed turbulent flow information has been available for the jar test apparatus. This multiple relating local impeller zone G to the vessel average $\overline{G}$ has generally been obtained from studies reported in the chemical engineering literature, for stirred tanks that are substantially different than those found in flocculation processes.

One of the first to document flow and turbulence in stirred tanks was Cutter (1966). With the development of better fluid velocity measuring techniques, primarily the laser doppler anemometer, more detailed information on hydrodynamics in stirred tanks has begun to appear in the literature. A series of papers has been published in the chemical engineering literature by Kresta and Wood (1991 and 1993), Weetman and Oldshue (1988), Wu and Patterson (1989) and Wu et al. (1989) which highlight the variations in hydrodynamics within the tank. However, most of this information is not directly related to coagulation and flocculation, as experimental conditions are generally outside those normally found in water treatment flocculation applications and most were completed on the Rushton turbine.

This paper presents a detailed analysis of turbulent flow in a standard jar test apparatus. To characterize the hydrodynamics, a 2-D laser doppler anemometer was used, which allows nonintrusive measurements of liquid velocity with high accuracy as well as the ability to measure rapidly changing flows. The experimental set-up was a standard 2 L square jar test apparatus with a 76 mm diameter flat blade impeller. This set-up is the typical standard since its introduction by Hudson and Wagner (1981) as a substitute for the cylindrical round glass beaker equipped with stators described by Camp (1969). The primary purpose of this paper is to present detailed turbulent flow information for researchers and water utility personnel to further understand the details of mixing in flocculation and variations in hydrodynamic characteristics within a stirred vessel.

The need for such studies has been highlighted in a recent American Water Works Association Research Foundation report on mixing processes for coagulation (Clark et al. 1994), which recommends "there is a need for a detailed study of the fluid flow patterns induced by different flocculation impellers at different mixing intensities". Clark et al. went on to state that the advancement in the area of flocculation will require the measurement of fluid flow patterns and energy dissipation induced by the different flocculation impellers at different scales. Once this is complete, characterization of the impact of impeller mixing on floc size and structure needs further study. A logical first step in beginning to fulfill these research requirements is to begin with one of the fundamental tools used in flocculation, the jar test apparatus.

2.2 Background

Coagulation, flocculation and sedimentation is generally the most economic method of removing large quantities of particulate matter from water. In natural waters many of these particles are colloidal in nature. For flocculation to occur particles must: 1) collide with each other; and 2) adhere when brought together by collision. For the most part the first step is governed by transport processes that are based on fluid and particle mechanics. If these particles are colloidal, the second step, whether the particles adhere or attach, is dependent on colloid interactions which are mostly based on colloid and surface chemistry. As a result, coagulation and flocculation is both a physical and chemical process. It should be noted that practically all colloidal interactions are of quite short range, almost never extending over distances greater than the size of the particles (Gregory, 1989). Consequently, they have little influence over the transport of particles, although they are crucial in determining the collision efficiency. As a result the transport and attachment processes can often be considered separate steps. This paper only considers the transport processes.

A brief overview of previous work on the role of transport processes on flocculation kinetics and floc break-up is presented. The purpose of this is not to critically review previous work but to determine which transport (hydraulic) parameters have been proposed to be important in the flocculation process. These parameters will be investigated in the jar test.

Most of the work on flocculation kinetics and break-up can be related back to the original work by Smoluchowski (1916) who developed an expression for the rate of collisions between particles of diameters d_i and d_j in laminar shear (orthokinetic flocculation) given as:

$$N_{ij} = \frac{1}{6} n_i n_j (d_i + d_j)^3 \left(\frac{dU}{dz} \right) \qquad (2.1)$$

where N_{ij} is the collision rate for class i and j particles, n_i and n_j are the number concentration of the class i and j particles and dU/dz is the laminar velocity gradient. Camp and Stein (1943) extended the Smoluchowski theory of orthokinetic flocculation to turbulent flow fields by defining the mean velocity gradient $\overline{G}$:

$$\overline{G} = \sqrt{\frac{\Phi_m}{\mu}} = \sqrt{\frac{P}{V\mu}} \qquad (2.2)$$

where Φ_m is the volume average power input, μ the absolute viscosity, P power input and V is the liquid volume. Camp and Stein replaced the laminar shear term by $\overline{G}$ to obtain:

$$N_{ij} = \frac{1}{6} n_i n_j (d_i + d_j)^3 \left(\frac{\Phi_m}{\mu} \right)^{\frac{1}{2}} \qquad (2.3)$$

Saffman and Turner (1956) developed a similar expression which was based more fundamentally on fluid mechanic principles in their work on flocculation of rain droplets in clouds. Assuming isotropic turbulence they found:

$$N_{ij} = 0.16 n_i n_j (d_i + d_j)^3 \left(\frac{\varepsilon}{v}\right)^{\frac{1}{2}}$$

(2.4)

where ε is the local unit mass energy dissipation rate and v is kinematic viscosity. It appears the only difference in [2.3] and [2.4] is a slight difference in the numerical constant as $\overline{G}$ is often expressed as:

$$\overline{G} = \sqrt{\frac{\varepsilon}{v}}$$

(2.5)

However, as Clark (1985) outlined there can be an important difference between Φ_m , the total spatial-average, steady unit volume energy dissipation rate and ε which is the local dissipation rate due to turbulent motions. Small-scale dissipation may only account for 0.7 of the total dissipation (Clark 1985) and as [2.4] is non-linear in ε , spatial variation in energy dissipation in the flocculator can not be accounted for by average values.

Although much more complex models have been developed to describe the kinetics of flocculation in terms of floc size distributions and mechanisms of floc formation, almost all incorporate ε , $\overline{G}$, and/or mean velocity gradients as the hydraulic parameter governing the process.

The break-up and maximum size of flocs is another important factor governing flocculation performance. With increased mixing, greater forces are placed on the flocs which can cause them to break-up. The ultimate size of the floc is determined by two opposing factors, namely the mechanical strength of floc and the applied breaking forces. Fluid induced stresses on the floc can be caused by shear stresses, drag stresses and pressure (i.e. normal stresses). To determine turbulent-flow-induced stresses acting on particles it is necessary to consider the structure and scale of turbulence in relation to particle size and motion in the fluid flow. Figure 2.1 gives an idealized view of scales found in turbulent flow. Generally turbulence production occurs at large scale with energy

being transferred down through smaller scale eddies until it is dissipated at small scales. Of interest is the relation between the smallest length scales and particle size. The smallest sustainable eddy is given by the Kolmogorov microscale, η, which based on dimensional arguments is given by:

$$\eta = \left(\frac{v^3}{\varepsilon}\right)^{1/4}$$
(2.6)

When eddies are larger than the particle, the eddies tend to entrain particles, thus causing little surface stress, with laminar shear being the dominant stress. If eddies are smaller than the size of the particles, these eddies can provide particle shear, surface drag and pressure forces. As a result the relation between η and particle size is important. Generally the maximum floc size, d_f, which is governed by break-up forces is given in the form of:

$$d_f = K\varepsilon^{-n}$$
(2.7)

where K is a constant representing the floc density function and n is a function of whether $\eta >> d_f$ or $\eta << d_f$. For $\eta >> d_f$ (viscous subrange) Tambo and Hozumi (1979) reported values of 0.28 to 0.33 for a while for $\eta << d_f$ (inertial subrange) values were between 0.3 to 0.4. However, these values were based on vessel average values of ε. Numerous other studies have developed other values for a with different values depending on the subrange of the turbulence in which the particle size falls. For floc break-up it appears that the dissipation rate ε is important along with the microscale η.

2.3 Experimental

The experimental set-up was a standard 2 L (115 mm x 115 mm x 150 mm) square jar test apparatus with a 76 mm diameter flat blade impeller, as described by Hudson and

Wagner (1981). Radial, axial and tangential velocities were measured with a Dantec 2-D laser doppler anemometer (LDA) in the forward scatter mode using a 300 mW Argon-ion laser (see Appendix A). The receiving optics were set at a deflection angle of 60° from a true forward scatter mode to allow more complete measurement in the impeller zone. Although the LDA was only capable of measuring velocities in two dimensions at one time, three dimensional velocity measurements could be obtained by combining data from two points lying on the same horizontal plane, at the same radius, separated by an angle of 90°. If the two points are separated by 90° one measuring point would give axial and radial velocities and the other measuring point, axial and tangential velocities. As a result, two vertical planes, perpendicular to the vessel walls, separated by 90° form the basis for most of the measured data presented in this study. To allow measurement of reversing flows the frequency of one beam for each velocity component was shifted by 40 MHz using a Bragg cell. Bandpass input filters were set at a bandwidth of 0.4 MHz. Signal processing was accomplished with a Particle Dynamics Analyzer, covariance signal processor. It has the ability to handle higher data rates and lower signal-to-noise ratios than traditional counter and tracker signal processors. The laser system contains a built-in laser diode which generates calibration signals that are fed via a fibre optic cable to the receiving optics to ensure that the equipment is automatically calibrated. All velocity measurements were validated based on signal-to noise levels and fringe counts. To eliminate velocity bias, moments were calculated by residence time weighting. For the set-up used in this study the measuring volume at the beam crossing was 0.12 mm x 0.12 mm x 2.4 mm. Measurements were used to determine the general flow field within the jar, velocity gradients, dissipation rates and turbulent length scales. Some difficulty in measuring velocities close to the center of impeller was experienced due to blockage of the laser and receiving optics by blade passage. The impact of this was minimized by location of the receiving optics, using two planes for measurements and some limited testing for the radial velocity plane in which the blade direction was reversed. This only impacts a few

measurements used in describing the general flow patterns and not detailed results presented at the edge of the impeller where this is not an issue.

Testing was conducted from 20 to 100 RPM which corresponds to values of $\overline{G}$ from 10 to 125 s⁻¹ which is a typical range used in water treatment for flocculation. $\overline{G}$ values were determined by measuring torque with a model TRPA5 Rotary Parallel Shaft torque transducer manufactured by Industrial Measurements Ltd. Figure 2.2 shows the relation between impeller rotation speed and $\overline{G}$ at 20° C. Values obtained are very similar to those reported previously by Cornwell and Bishop, 1983.

Ideally measurement of the complete turbulent frequency spectrum would be desired. However, with any measurement technique there are always some limitations. The highest frequency of interest is that given by the Kolmogorov time scale, t_k, which can be determined by:

$$t_k = \left(\frac{v}{\varepsilon}\right)^{\frac{1}{2}} \tag{2.8}$$

which, for the impeller zone, is in the range of 0.006 s or 175 Hz. The Nyquist criterion requires a sampling rate of at least 350 Hz for proper characterization of that frequency. However, the size of the measuring volume sets the phase ambiguity noise limit. The frequency at which phase ambiguity noise becomes a significant factor can be determined by considering the dimension of the measuring volume perpendicular to the fringes (0.12 mm) and the wave number k_1 as defined by Hinze (1987):

$$k_1 = \frac{2\pi f}{\overline{U}} = \frac{1}{\lambda} \tag{2.9}$$

Substituting into this equation the typical velocity in the impeller zone and the dimension of the measuring volume for λ (all wavelengths smaller than this will be completely contained in the measuring volume) gives a maximum measurable frequency,

f, of about 100 Hz. This phenomena is shown in Figure 2.3 which shows the frequency spectrum for a typical measurement point. For turbulent flow in local equilibrium the frequency spectrum should show a -5/3 slope when plotted on a log-log scale. As the figure indicates, this occurs up to a frequency of about 100 Hz; at higher frequencies the spectrum appears to be composed of phase ambiguity noise. Using the dead-time mode of velocity sampling the measurement frequency could be set in the range of the maximum measurable frequency as well as provide independent velocity measurements for autocorrelation analysis of the data which was completed later. For each sampling point 5,000 velocity measurements were taken. Water used in the experiments was seeded with <5 μm TiO_2 particles due to their good light scattering properties.

2.4 Results

Figure 2.4 shows the general flow pattern in the reactor at 60 RPM. High radial velocities are found in the impeller region with large circulation patterns both above and below the impeller. Figure 2.5 shows the instantaneous velocity at the edge of the impeller ($2r/D = 1.02$ or 1.5 mm from the edge of the impeller). The average radial velocity is 0.35 of the tip speed ($N\pi D$). It is also important to note the periodic nature of the velocity near the impeller. Generally instantaneous turbulent velocities, u_i, are divided into a mean component, $\overline{U_i}$ and a fluctuating component, u_i' which is defined as:

$$u_i' = u_i - \overline{U_i} \qquad (2.10)$$

However, not all velocity fluctuations near the impeller are random in nature but are periodic. These periodic fluctuations, called pseudo-turbulence by Van't Riet et al. (1976), need to be removed before the actual turbulence can be properly characterized. This is done by separating the random fluctuation, $u'_{rand}(t)$ from the periodic part, $u'_{per}(t)$.

$$u'_{tot}(t) = u'_{rand}(t) + u'_{per}(t)$$ (2.11)

The periodic component can be represented by a Fourier series as a function of time or frequency. Analysis of the energy spectra in the region of the impeller indicated that two major peaks were evident from the periodic component, one at the frequency of the blade passage and one at twice the frequency of the blade passage which probably result from passage of trailing vortices (Wu and Patterson, 1989). As a result, only two terms of the Fourier series are required. Assuming no correlation between the periodic and random turbulent components, the Eulerian autocorrelation function, $R_E(\tau)$, can be written as:

$$R_E(\tau) = \frac{\overline{u'(t)u'(t-\tau)}_{tot}}{\overline{u'^2}} = \frac{\overline{u'(t)u'(t-\tau)}_{rand} + \overline{u'(t)u'(t-\tau)}_{per}}{\overline{u'^2}}$$ (2.12)

where τ is the time delay in the autocorrelation function. Substituting in the two terms of the Fourier series the periodic component is given as:

$$\frac{\overline{u'(t)u'(t-\tau)}_{per}}{\overline{u'^2}} = A_1 \cos(2m\pi t) + A_2 \cos(4m\pi t)$$ (2.13)

where m is the impeller blade passage frequency and A_1 and A_2 are constants, the amplitude of the two periodic components. Values for A_1 and A_2 were calculated using the autocorrelation coefficient function at large values of τ where the correlation is only the result of the impeller blade passage frequency. Figure 2.6 shows a typical autocorrelation coefficient function for both a measurement point near the impeller and one away from the impeller in the bulk of the tank. The figure indicates that near the impeller at large values of τ, velocities are correlated with the frequency of the blade passage. Away from the impeller the correlation disappears. More details on the use of the Eulerian autocorrelation coefficient function to determine the periodic fluctuating velocities can be found in Wu and Patterson (1989).

Figure 2.7 shows mean radial velocities in the region of the impeller for rotation

speeds of 20 to 100 RPM. As has been found in most studies of impellers, the figure

shows that they scale on the tip speed of the impeller or (NπD). It was also found that the

tangential velocity, the velocity gradient and the total, random and periodic fluctuating

velocities also scale with NπD. Figure 2.8 shows this for the total fluctuating radial

velocities at different impeller speeds. It was found that the maximum total RMS velocity

was 0.3 $u'_{r(tot)}/(N\pi D)$. Figure 2.9 shows the total, random and periodic fluctuating

velocities for 60 RPM. The periodic component is the largest at the middle of the impeller

(2z/W = 0). This results in the maximum random fluctuating velocities being the highest

slightly above and below the middle of the impeller. Similar findings have been found with

the Rushton turbine (Wu and Patterson, 1989)

A number of different methods can be used to calculate the turbulent local

dissipation rate, ε. Four methods have generally been used to calculate dissipation rates

which can be briefly described as: 1) the gradient hypothesis method which uses the

constitutive equation for the $k - \varepsilon$ model where k is kinetic energy; 2) Taylor's hypothesis

which is used to convert time derivatives to spatial derivatives; 3) dimensional arguments

which lead to the estimation of ε from k using a constant length scale; and, 4) the

autocorrelation coefficient function which is used to calculate the Eulerian integral time

scale, which is then combined with k to estimate ε. Kresta and Wood (1993) reviewed

the various methods and found that either the dimensional or autocorrelation methods

worked reasonably well in stirred tanks. A combination of both methods was used to

calculate dissipation rates in this study, with the dimensional arguments being used in the

impeller zone and the autocorrelation methods being used in the bulk of the tank.

The dimensional argument is based on the fact that all the kinetic energy, k, being

transferred from the large scale eddies where production is occurring must be dissipated by

the small scale eddies. The rate of energy transfer per unit mass which must be dissipated is given by:

$$\varepsilon = \frac{\text{kinetic energy}}{\text{decay time}} \qquad (2.14)$$

where kinetic energy is given by:

$$k = \frac{\overline{u'_z}^2 + \overline{u'_r}^2 + \overline{u'_t}^2}{2} \qquad (2.15)$$

where the fluctuating velocities are only the random component and z, r, and t denote the axial, radial and tangential velocities respectively. The decay time is given as L / u' where L is the characteristic length scale and u' the characteristic velocity which is given by $k^{1/2}$. In the impeller zone L has been shown to be one-half the impeller width (Kresta and Wood, 1991). L may also be determined by equating it to the Eulerian integral length scale, determined by the autocorrelation coefficient function, which was done in the bulk of the tank. The Eulerian integral time scale is given by:

$$\tau_E = \int_0^\infty R_E dt \qquad (2.16)$$

The time scale can be converted to a length scale with use of a suitable convection velocity, U_{c_i}:

$$L_i = U_{c_i} \tau_E \qquad (2.17)$$

The convection velocity can be approximated with the local mean velocities if Taylor's frozen field hypothesis can be applied. However, for high-intensity turbulent shear flows, such as those found in stirred tanks, this hypothesis may not be applicable. Based on work done by Heskestad (1965), Van Doorn (1981) developed the following equation for the convection velocity in three-dimensional flows:

$$U_{c_i}^2 = U_i^2\left(1 + 2\frac{U_j^2}{U_i^2} + 2\frac{U_k^2}{U_i^2} + \frac{\overline{u'_i^2}}{U_i^2} + 2\frac{\overline{u'_j^2}}{U_i^2} + 2\frac{\overline{u'_k^2}}{U_i^2}\right)$$
(2.18)

Near the impeller, the integral length scale was assumed to be close to half the impeller width, hence its use in this zone. Justification for its use can also be related to the successful use of a swirling rad:al jet model to describe flow in the impeller zone (Kresta and Wood, 1991; Kolar et al., 1982). It has long been recognized that, in a jet, the integral length scale can be related to half the jet width. Examination of Figure 2.6 shows that the width of the discharge jet from the impeller can be related to the width of the impeller. To check this, the Eulerian integral length scale was also determined based on the autocorrelation procedure in the impeller zone and found to correspond to half the impeller width. The half-width of the impeller was used in the impeller zone as it allows calculation of dissipation rates based on an easily measured quantity (the width of the impeller) and provides the basis of scale-up. As mentioned, in the bulk of the tank the autocorrelation procedure was used to determine the length scale, as in this region the Eulerian integral length scale can not be related to a simple geometric measurement.

Although all three velocity components were used in the determination of k, if one assumes isotropic turbulence, which was found to be generally true, the dissipation rate can be expressed as:

$$\varepsilon = A\frac{u'^3}{L}$$
(2.19)

where A is a constant of proportionality (close to unity). Equation (2.19) provides the basis for the development of a scaling relation for ε as it was found that the fluctuating velocities scale on (NπD). Hence, ε should scale on:

$$\frac{\varepsilon}{(N\pi D)^3 / D} = \text{dissipation scale constant}$$
(2.20)

For the impeller speeds investigated the dissipation scale constant varied from 0.1

to 0.12 in the impeller zone, as shown in Figure 2.10. Again the maximum dissipation rate

occurs slightly above and below the middle of the impeller. Figure 2.11 shows the

variation in local dissipation rates in the reactor at 60 RPM. As indicated by the figure

much of the dissipation occurs in the impeller zone.

2.5 Discussion

The hydraulic parameters investigated can be determined at different impeller speeds

based on the results of this study and the use of the appropriate scaling relationship. The

general form of the equation can be expressed as follows

$$\text{value of hydraulic parameter} = C \text{ (parameter scaling relationship)} \quad (2.21)$$

where C is the hydraulic parameter scaling constant. Table 2.1 gives the constants as well

as the scaling relationship for the hydraulic parameters investigated at the middle tip of the

impeller ($2r/D = 1.02$ and $2z/W = 0$). Also included in Table 2.1 are the constants that

have been reported for the Rushton turbine. The reason that results from the Rushton

turbine are included in the table is that most of the information used to date to try to account

for variations in hydrodynamics in the jar test have been taken from studies on the Rushton

turbine as it is by far the most studied type of impeller.

As indicated in Table 2.1 all of the velocity components scale with the tip speed of

the impeller ($N\pi D$). However, the values found for mean velocities in the jar test apparatus

are significantly less than those previously reported for the Rushton turbine. The primary

reason for the lower values are that the Rushton turbine has 6 blades where the flat blade

has just two.

The turbulent fluctuating velocities are only slightly less for the jar test. The ratio between periodic and random components of the fluctuating velocity were about the same as those found for the Rushton turbine. The biggest difference between the jar test and the Rushton turbine is the scaling constant for dissipation rates. Constants have been reported that are higher than those found in the jar test. It should be noted that, as shown in Figure 2.10, the maximum dissipation rate does not occur at the center of the impeller but slightly above and below the center due to the influence of the periodic component of the fluctuating turbulent velocity. The primary reason for the difference between the scaling constants between the jar test and the Rushton turbine can be related to the use of the scaling factor for dissipation rates, $(N\pi D)^3 / D$. The denominator represents a scaling factor for the Eulerian integral length scale. As mentioned, in the impeller zone this can be related to the width of the impeller. The use of impeller diameter can be related to the standard geometry of the Rushton turbine where the width of the impeller is equal to D/5. Since the integral length scale has been related to half of the width it can be given as D/10. For simplicity the constant 10 is dropped, allowing only one dimension of the impeller to be required for all the scaling factors. In the case of the jar test, the impeller width is equal to D/3 and the integral length scale would be in the order of D/6. This difference accounts for much of the difference in the scaling constants.

Even though the dissipation rates determined are less than those for the Rushton turbine, the local unit mass energy dissipation rate, ε, in the impeller zone is higher than the volume average power input, Φ_m. Figure 2.12 shows the variation in the local unit mass energy dissipation rate, ε, and the volume average dissipation rate, Φ_m for various impeller speeds. As indicated by the figure the local dissipation rate is 4 to 6 times higher than the vessel average dissipation rate.

An important factor determining the forces which are acting on a floc particle is the relationship between the floc size and the smallest scale of the turbulence, the

Kolmogorov's microscale, η. Since measurement of the total turbulent frequency spectrum is not possible, the Kolmogoroff microscale can be calculated using equation (2.6) if the dissipation rate is know. Figure 2.13 shows the calculated microscale, η, based on the local unit mass energy dissipation rate, ε in the impeller zone and based on the vessel average dissipation rate. For both, the kinematic viscosity used assumed the water was at 20°C. As expected, because of the higher dissipation rate in the impeller zone, the local microscale is smaller than one based on the vessel average dissipation rate. The significance of this finding may be greater than just the difference in the value of the microscale. Typically in water treatment flocculation processes the maximum size of the floc is in the range of 100 µm. As indicated in the figure, for most of the typical $\overline{G}$ values used in water treatment, the size of the microscale may be smaller than the maximum floc size. For those trying to determine the forces on the floc this finding can be significant.

Information given in Figures 2.7 through 2.12 and Table 2.1 can be used to calculate hydrodynamic quantities in the impeller zone and highlights the variations in these quantities within the vessel. As the circulation time in a small vessel, such as a jar test apparatus, is in the order of seconds and normal flocculation time is in the order of 5 to 30 minutes, many of the floc characteristics (especially floc size) are probably governed by hydrodynamic conditions found in the impeller zone. With the circulation time being much smaller than the flocculation time, the flocs will pass through the impeller zone numerous times during the time the flocculation test is run. As floc size is dependent on the forces applied to it, this area of increased turbulence will tend to govern the equilibrium floc size. It may therefore be more approperiate to match impeller zone hydrodynamic conditions between the jar test and full-scale for hydraulic simultude. However, little detailed information is available on hydrodynamic characteristics in larger scale flocculators. As stated earlier, this study constitutes one of the first steps required to further understand the role of mixing in flocculation, in that it presents detailed information on hydrodynamic conditions in the jar test apparatus. Further study is required to determine similar hydraulic

information for full-scale and pilot-scale flocculators. In addition there is a need for better understanding of the effects of local hydrodynamics (especially in the impeller zone) on floc characteristics and process performance, as most previous studies have relied on vessel average parameters to assess mixing in flocculation.

2.6 Conclusions

Detailed laser doppler anemometer measurements were taken to characterize turbulent flow in a standard jar test apparatus. General flow patterns, turbulent flow parameters, local dissipation rates and turbulent length scales were determined. Results indicated that significant variation in these parameters occurred within the jar test apparatus. Local dissipation rates in the impeller zone were on the order of 4 to 6 times higher than the volume average dissipation rate. The size of the microscale in the impeller zone was found to be less than ones determined based on vessel-average dissipation rates. In some instances the impeller zone microscale may be smaller than the size of floc, which is important for those trying to determine forces that may be acting on the floc. Scaling constants found in this study were compared to those reported for the Rushton turbine. Constants for mean velocities and local dissipation rates were found to be less than those reported for the Rushton turbine. Differences in the scaling constant for dissipation rates can be partly related to the traditional scaling factor used in impeller studies.

The primary purpose of this work was to present detailed turbulent flow information for researchers and water utility personnel to further understand the details of mixing in flocculation and highlight the variations in hydrodynamic characteristics within a mixing vessel.

2.7 References

Armstrong, S.G. and Ruszkowski, S. (1988). The flow field in the discharge stream of disk turbines. *Proc. 6th Eur. Conf. on Mixing*, Pavia, Italy, BHRA Fluid Eng. Cntr., Springer, 1-6.

American Water Works Association. (1990). *Water Quality and Treatment..* Fourth Edition, McGraw-Hill, Inc., Toronto, 1194p.

Bertrand, J. Couderc, J.P. and Angelino, H. (1980a). Power Consumption, Pumping Capacity and Turbulence Intensity in Baffled Stirred Tanks: Comparison Between Several Turbines. *Chem. Eng. Sci.* **35**, 2157-2163.

Bertrand, J. Couderc, J.P. and Angelino, H. (1980b). Ecoulement dans le Courant de Refoulement d'une Turbine a Disque et Six Plates Dans une Cuve Munie de Chicanes. *Chem Eng. J.* **19**, 113-123.

Camp, T.R. (1969). Hydraulics of Mixing Tank. *Jour. Boston Soc. Civil Engineers,* **56**,1,1-11.

Camp, T.R. and Stein, P.C. (1943). Velocity gradient and internal work in fluid motion. *Jour. Boston Soc. Civil Engineers* **30**, 10, 219-237.

Clark, M.M. (1985). Critique of Camp and Stein's RMS velocity gradient. *Journal of Environmental Engineering, ASCE, 111*, 6, 741-754.

Clark, M.M., Srivastava, R.M., Lang, J.S., Trussel, R.R., McCollum, L.J. Baily, D., Christie, J.D., and Stolarik, G. (1994) Selection and Design of Mixing Processes for Coagulation. American Water Works Association Research Foundation and American Water Works Association, Denver, CO. 150p.

Cleasby, J.L. (1984). Is velocity gradient a valid turbulent flocculation parameter? *Journal of Environmental Engineering, ASCE, 110*, 5, 875-897.

Cooper, R.G. and Wolf, D. (1968). Velocity Profiles and Pumping Capacities for Turbine-Type Impellers. *Can. J. Chem. Eng.*, **46**, 94-100.

Cornwell, D.A. and Bishop, M.M. (1983). Determining Velocity Gradients in Laboratory and Full-scale Systems. *Journal of the American Water Works Association,* 75, 470-475.

Costes, J. and Couderc, J.P. (1982). Pumping Capacity and Turbulence Intensity in Baffled Stirred Tanks; Influence of the Size of the Pilot Unit. *Proc. 4th Eur. Conf. on Mixing,* Leewenhorst, 25-24.

Cutter, L.A. (1966). Flow and turbulence in a stirred tank. *A.I.Ch.E. J.* 12, 35-45.

Fort, I. and Mala, J. (1982) Hydrualic Characteristics of Turbine Impeller. *Coll. Czech. Chem. Comm.* 47, 421-432.

Gregory, J. (1989). Fundamentals of Flocculation. *Critical Reviews in Environmental Control. Vol.* 19, 3. pp. 185-230.

Gunkel, A.A. and Weber, M.E. (1975). Flow Phenomena in Stirred Tanks I: The Impeller Stream. *A.I.Ch.E. J.* 21, 931-949.

Han, M and Lawler, D.F. (1992). The (relative) insignificance of G in flocculation. *Journal of the American Water Works Association,* 84, 10, 79-91.

Hanson, A.T. and Cleasby, J.L. (1990). The effects of temperature on turbulent flocculation: Fluid dynamics and chemistry. *Journal of the AWWA,,* 82, 11, 56-73.

Hekestad, G. (1965) A generalized Taylor hypothesis with application for high Reynolds number turbulent shear flows. *J. Appl. Mech.* 32, 735-739.

Hinze, J.O. (1987). *Turbulence, an Introduction to Its Mechanisms and Theory,* 2nd Edn., McGraw-Hill Classic Textbook Reissue, McGraw-Hill, Toronto.

Hudson, H.E. Jr.(1981). *Water Clarification Processes: Practical Design and Evaluation.* Van Nostrand Reinhold Company, New York, NY, 353p.

Hudson, H.E. Jr. and Wagner, E.G. (1981). Conduct and use of jar tests. *Journal of the American Water Works Association,* 73, 4, 218-224

Keller, D.B.A. (1985). To Determine the Pumping Capacity of a Disk Turbine Impeller at

Different Reynolds Numbers. *Proc. 5th Eur. Conf. on Mixing*, Wurtzburg,

Germany, 25-34.

Kolar, V. Filip, P. and Curev, A.G. (1982) The swirling radial jet. *Appl Sci. Res.* **39**,

329-335.

Komasawa, I.R., Kuboi, R. and Otake, T. (1974). Fluid and Particle Motion in Turbulent

Dispersion: I: Measurement of Turbulence of Liquid by Continual Pursuit of Tracer

Particle Motion. *Chem Eng. Sci.* **29**. 641-650.

Kresta, S.M. and Wood, P.E. (1991). Prediction of the three dimensional turbulent flow in

stirred tanks. *A.I.Ch.E.J.*, **37**, 448-460.

Kresta, S.M. and Wood, P.E. (1993). The flow field produced by a pitched blade turbine:

Characterization of the turbulence and estimation of the dissipation rate. *Chem.*

Eng. Sci., **48**, 10, 1761-1774.

Mahouast, M. Cognet, G. and David, R. (1987). Analysis of Turbulent Mixing in a

CFSTR from LDV Measurements. *ASME 3rd Int. Symp. on Laser Anemometry*,

ASME, FED, 55, 157-166.

Mahouast, M., David, R. and Cognet, G. (1988). Periodic Phenomena Generated in the

Discharge Flow by a Rushton Turbine in a CSTR and Investigation of the Reynolds

Stresses. *Proc. 6th Eur. Conf. on Mixing*, Pavia, Italy, BHRA Fluid Eng. Cntr.,

Springer, 23-28.

Nouri, J.M., Whitelaw, J.H. and Yianneskis. (1987). The Scaling of the Flow Field with

Impeller Size and Rotational Speed in a Stirred Reactor. *2nd Int. Conf. on Laser*

Anemometry-Advances and Applications, Strathclyde, UK, 489-500.

Saffman, P.G. and Turner, J.S. (1956) On the collision of drops in turbulent clouds. *Jour.*

Fluid Mechanics **1**, 16-28.

Smoluchowski, M.W. (1917). Versuch einer Mathematischen Theorie der Koagulations

Kinetik Kolloider Losungen. *Zeitschrift f. Physik. Chemie*, 92:126.

Tambo, N. and Hozumi, H. (1979). Physical Characteristics of Flocs - II. Strength of

   Floc. *Water Research*, **13**, 421-427.

van Doom, M. (1981) On Taylor's hypothesis in turbulent shear flows. Internal note

   811123, University of Missouri-Rolla.

Van der Molen, K. and Van Maanen, H.R.E. (1978). Laser Doppler Measurements of the

   Turbulent Flow in Stirred Vessels to Establish Scaling Rules. *Chem. Eng. Sci.* **33**,

   1161-1168.

Van't Riet, K., Bruijn, W. and Smith, J.M. (1976). Real and pseudo-turbulence in the

   discharge stream from a Rushton turbine. *Chem. Eng. Sci.*, **31**, 407-412.

Weetman, R.J. and Oldshue, J.Y. (1988). Power, flow, and shear characteristics of

   mixing impellers. *Proc. 6th Eur. Conf. on Mixing*, Pavia, Italy, BHRA Fluid Eng.

   Cntr., Springer, 43-50.

Wong, C.W. and Huang, C.T. (1988). Flow Characteristics and Mechanical Efficiency in

   Baffled Stirred Tanks with Turbine Impellers.*Proc. 6th Eur. Conf. on Mixing*,

   Pavia, Italy, BHRA Fluid Eng. Cntr., Springer,

Wu, H. and Patterson, G.K. 1989. Laser doppler measurements of turbulent flow

   parameters in a stirred mixer. *Chem. Eng. Sci.*, **44**, 2207-2221.

Wu, H., Patterson, G.K. and van Doom, M. 1989. Distribution of turbulence energy

   dissipation rates in a Rushton turbine stirred mixer. *Expts Fluids*, **8**, 153-160.

Table 2.1. Summary of hydrodynamic characteristics of impeller agitated vessels

Hydraulic Parameter	Scaling Relation	Jar Test Scaling Constant	Rushton Turbine Scaling Constant*
Mean radial velocity, U_r, m/s	$N\pi D$	0.35	0.5 - 1.20 average = 0.82
Mean tangential velocity, U_t, m/s	$N\pi D$	0.34	0.66 - 1.054 average = 0.85
Total radial fluctuating velocity, $u'_{r(tot)}$, m/s	$N\pi D$	0.28 - 0.31	0.3 - 0.35
Periodic radial fluctuating velocity, $u'_{r(per)}$, m/s	$N\pi D$	0.1 - 0.12	0.12 - 0.2
Random radial fluctuating velocity, $u'_{r(ran)}$, m/s	$N\pi D$	0.17 - 0.22	0.15 - 0.20
Maximum dissipation rate, ε, m^2/s^3	$(N\pi D)^3/D$	0.1 - 0.14	0.2 - 0.7

* obtained from (Cooper and Wolf, 1968; Komasawa et al. 1974; Gunkel and Weber, 1975; V.D. Molden and V. Maanen, 1978; Bertrand et al. 1980a; Bertrand et al. 1980b; Fort and Mala, 1982; Costes and Couderc, 1982; Keller, 1985; Nouri et al., 1987 and Mahouast et al., 1987; Mahoust et al., 1988; Armstrong and Ruszkowski, 1988; Wong and Huang, 1988; Wu and Patterson, 1989; Wu et al., 1989; Kresta and Wood, 1991)
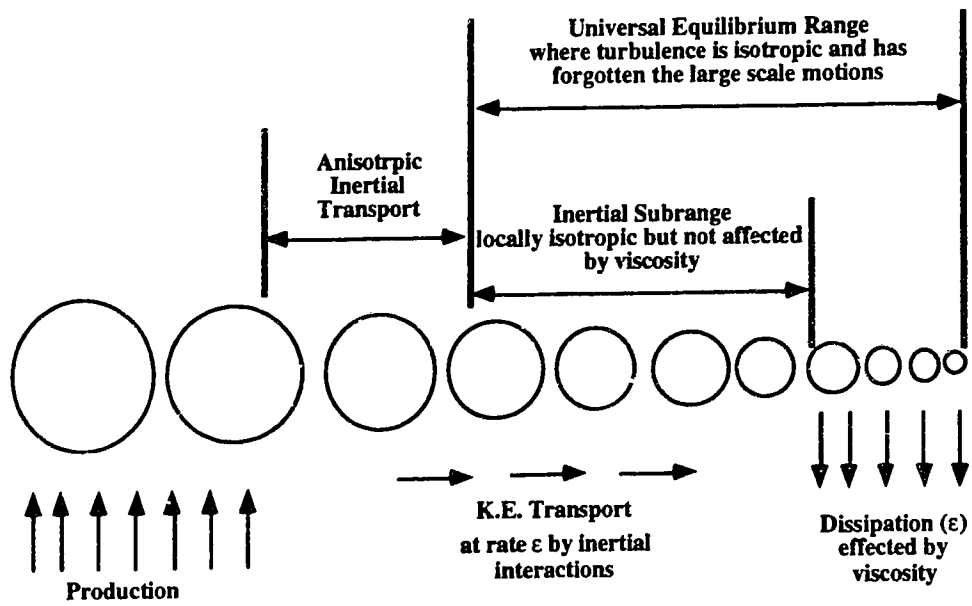
Figure 2.1. Idealized visualization of turbulent length scales.
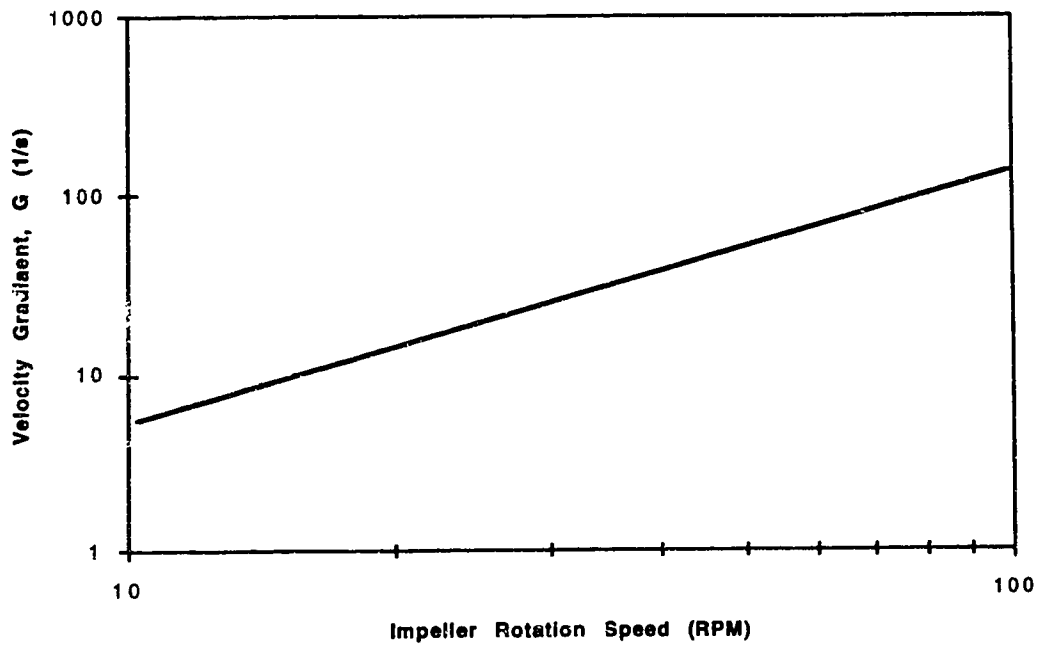
Figure 2.2. Relation between impeller speed and mean velocity gradient, G, at 20°C
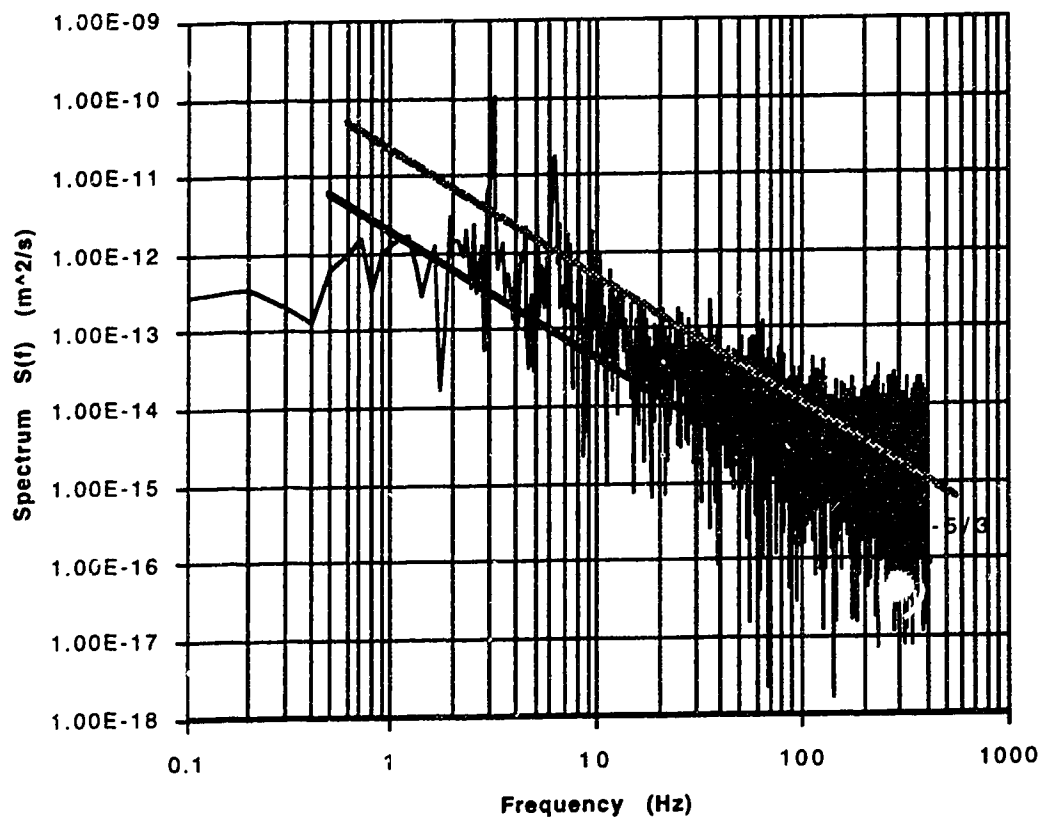
Figure 2.3. Frequency spectrum showing phase ambiguity noise.
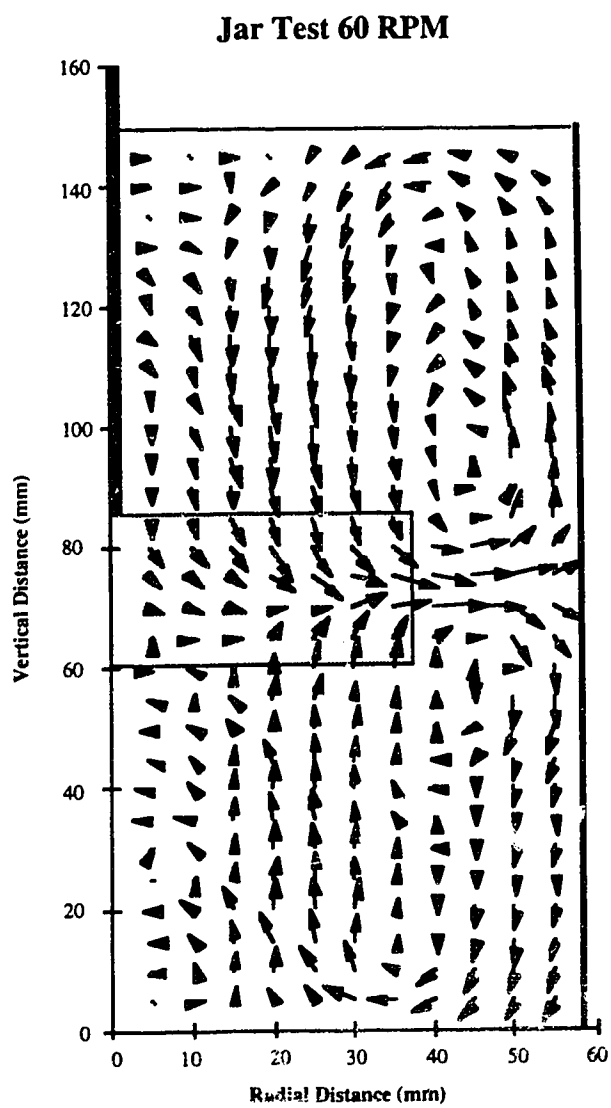
Jar Test 60 RPM

Figure 2.4. General flow patterns with in jar test at 60 RPM.
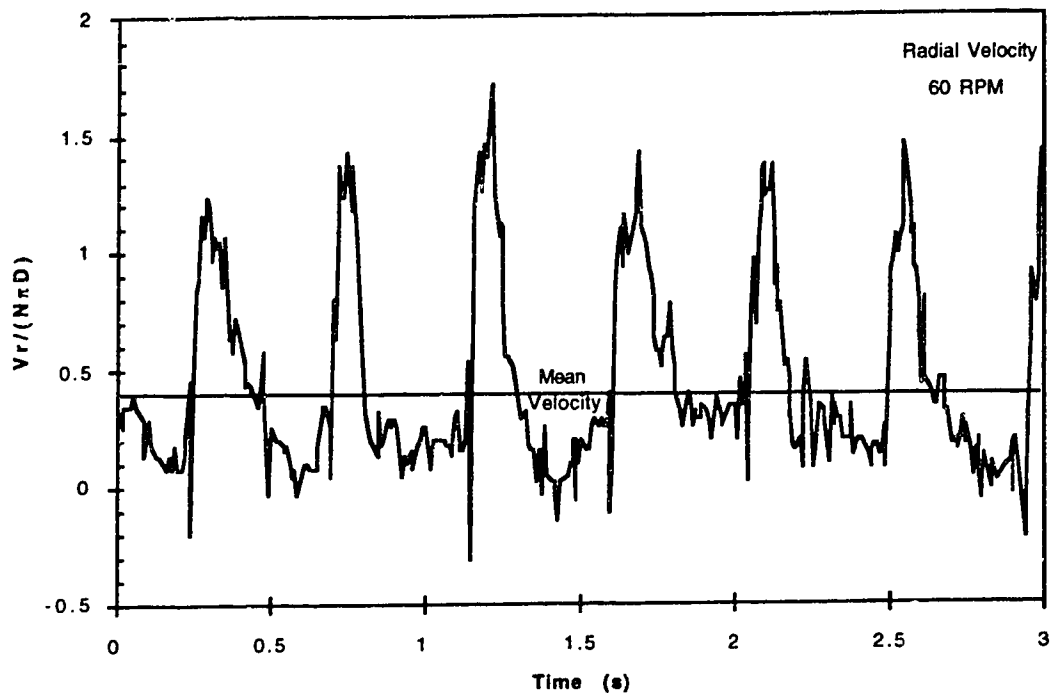
Figure 2.5. Instaneous radial velocities at the tip of the impeller.
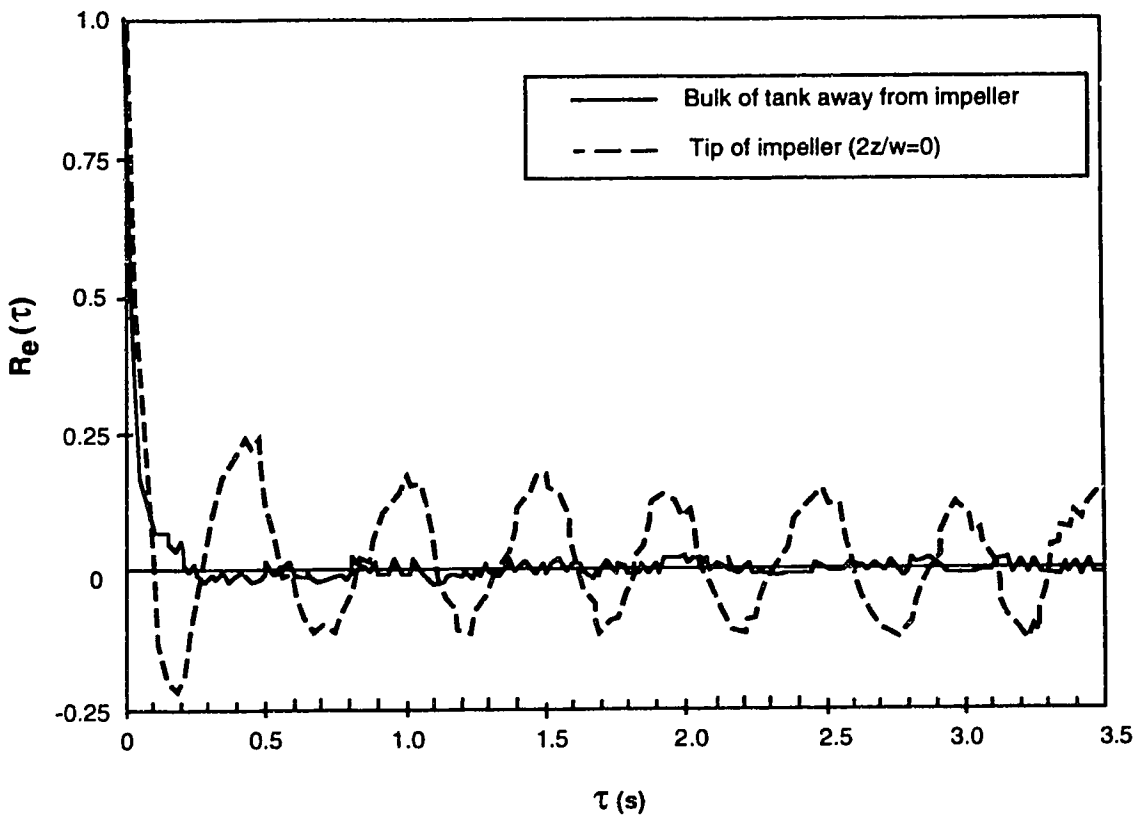
Figure 2.6.   Comparison of the Eulerian autocorrelation function in the impeller zone and in the bulk of the tank.
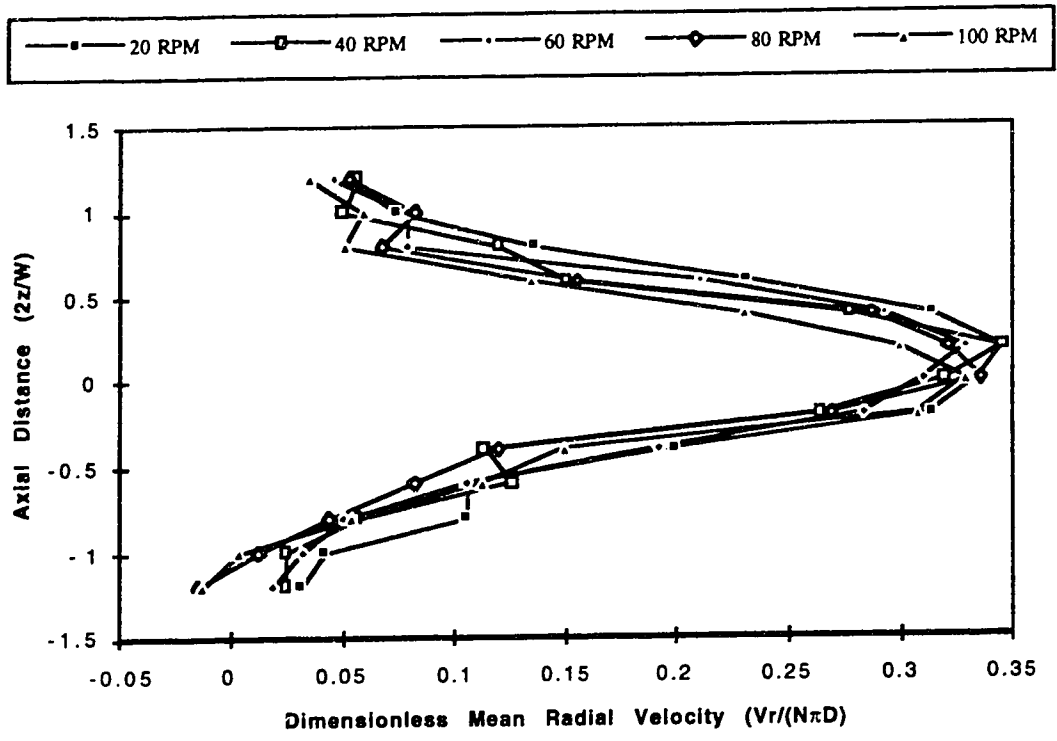
Figure 2.7.   Mean radial velocities in the impeller region (2r/d=1.02), made
dimensionless by tip speed.
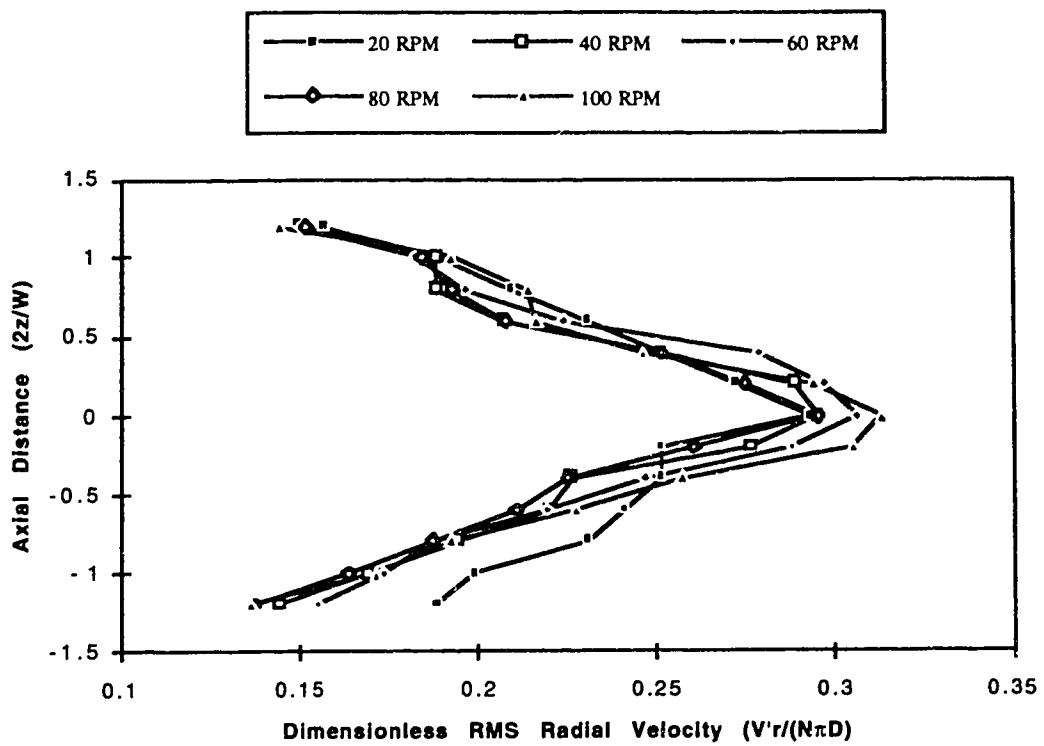
Figure 2.8.   Radial RMS fluctuating velocities in the impeller region (2r/d=1.02), made dimensionless by tip speed..
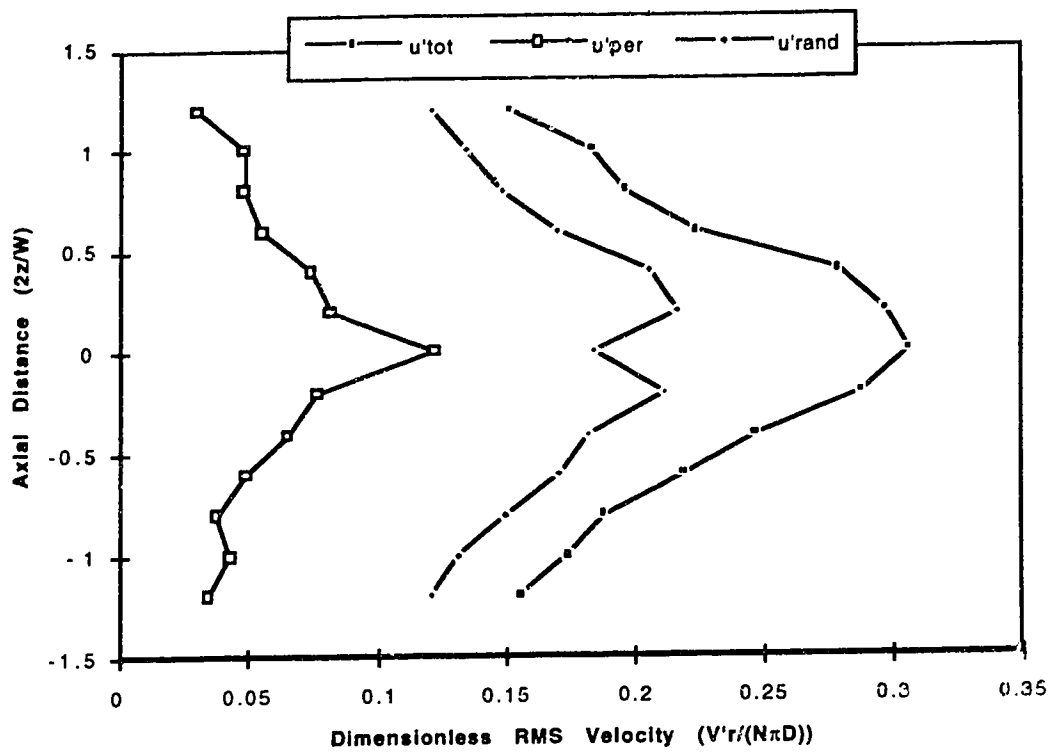
Figure 2.9.   Radial total, periodic and random fluctuating velocities in the impeller
zone (2r/d=1.02) at 60 RPM.
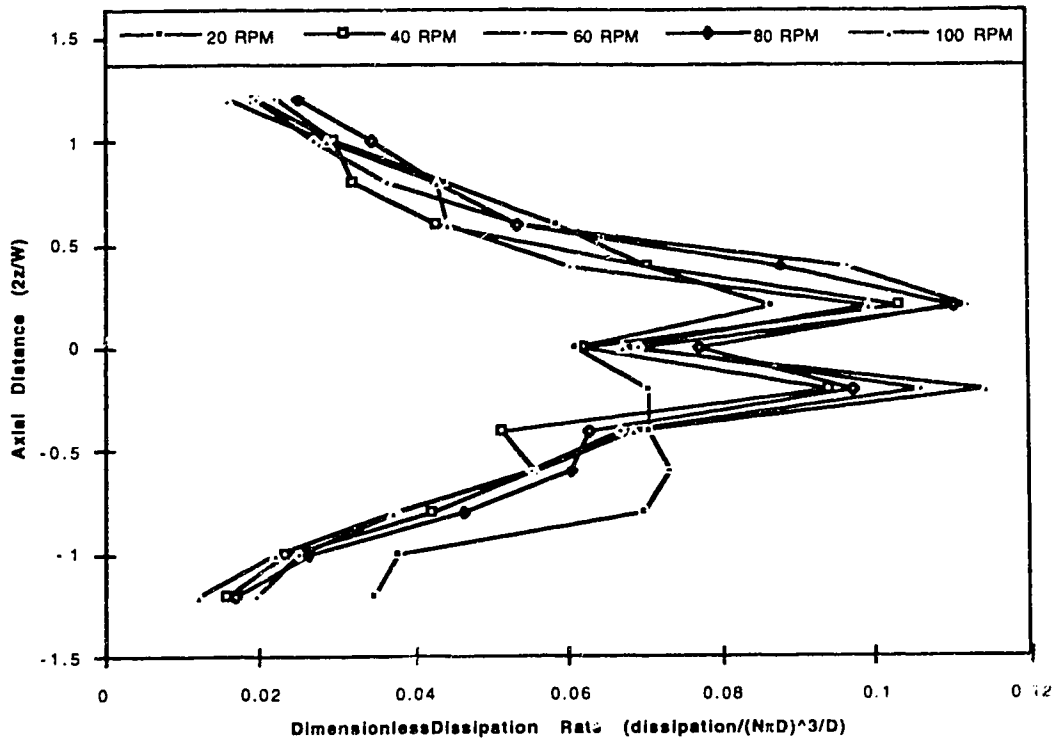
Figure 2.10.   Dissipation rates in the impeller zone (2r/d=1.02), made dimensionless by $(V_{tip})^3 / D$.
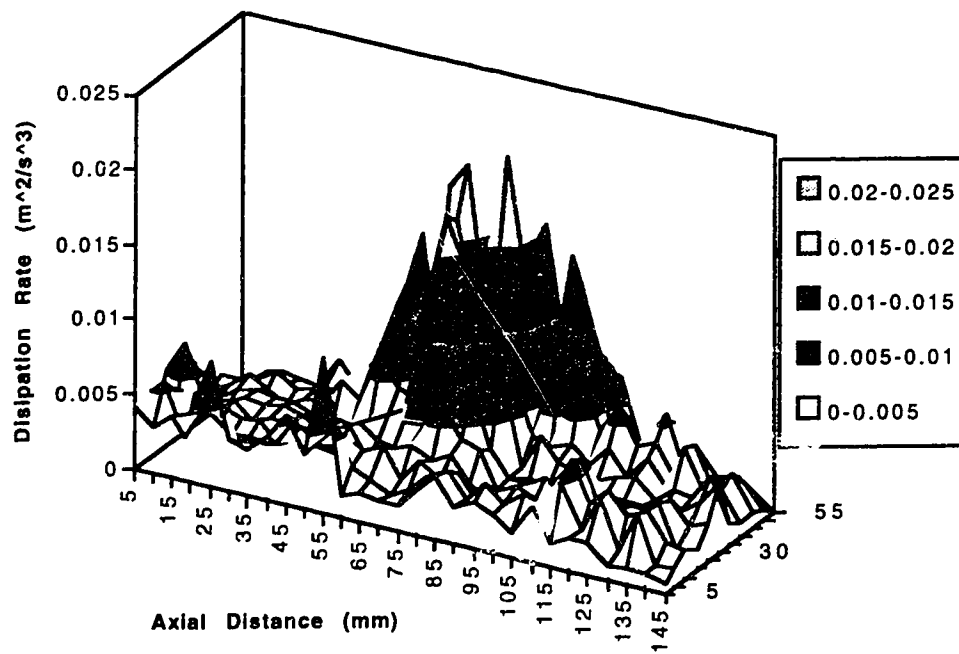
Figure 2.11. Variation in local dissipation rates in the jar test at 60 RPM.
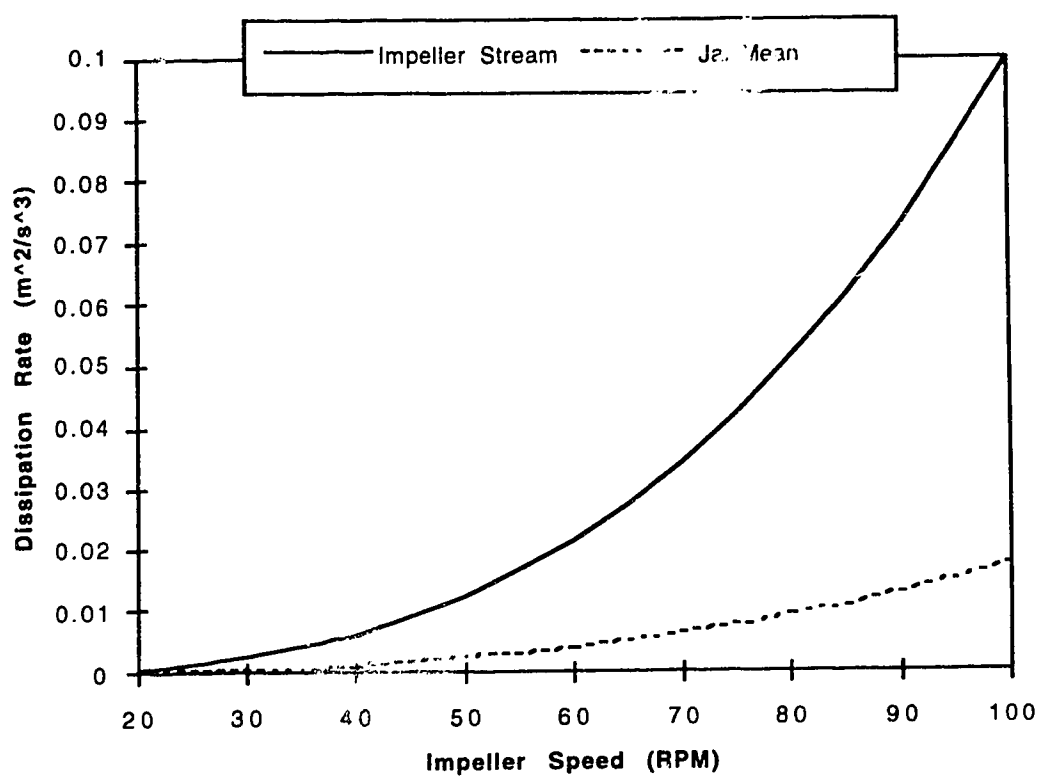
Figure 2.12. Comparison of vessel average dissipation rates to local dissipation rates in the impeller zone.
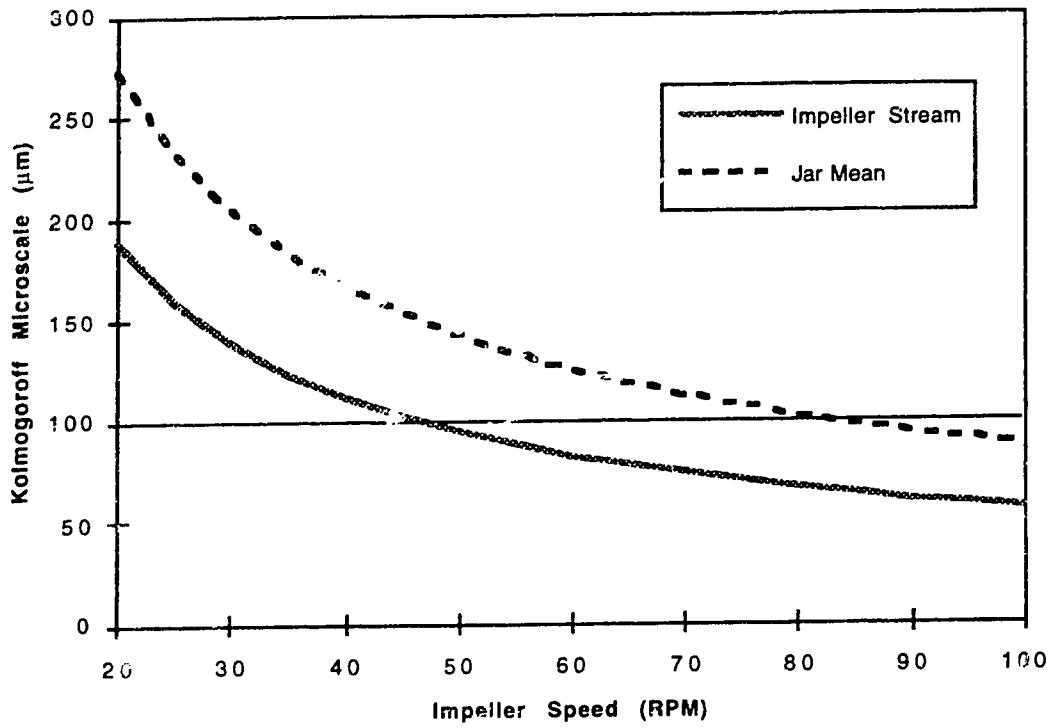
Figure 2.13.   Comparison of the Kolmogoroff microscale based on vessel average
dissipation rates and local dissipation rates in the impeller zone.

Chapter 3

Characterization of Impeller-Agitated Flow in an Upflow Solids-Contacting Clarifier[1]

3.1 Introduction

Following from the original work by Smoluchowski (1917) and the extension of this work to turbulent flow by Camp and Stein (1943), a large body of research has been conducted to investigate the impact of mixing on flocculation performance. However, most of the experimental work has been conducted at bench-scale or pilot-scale, with mixing conditions being documented by vessel-average parameters such as the root mean square velocity gradient, $\overline{G}$. There has also been recently been a greater recognition for the need to more fully document mixing condition within flocculators, that consider spatial variations in flow and energy within the stirred vessel, especially in the impeller zone (Clark et al. 1994). These variations are not considered when vessel-average parameters are used, as they assumed homogeneous mixing conditions exist throughout the flocculator. With this recognition and the development of advanced velocity measurement techniques, more detailed information has begun to be reported in the literature on turbulent flow impeller-agitated mixers. However, much of this information is found in the chemical engineering literature (Kresta and Wood, 1991 and 1993; Weetman and Oldshue, 1988; Wu and Patterson, 1989; and Wu et al., 1989) for experimental conditions outside the range of those normal found in flocculation practices. Some information directly related to flocculation, for example Stanley and Smith (1995), has been reported; however it is mostly for bench or pilot-scale systems, with simple impeller systems. Little detailed hydrodynamic data have been presented for real flocculators such as full-scale which often have much more complex flow patterns than batch tanks with impellers placed in them.

Presented is a study to characterize detailed hydrodynamic mixing conditions in the impeller zone of an upflow solids-contacting clarifier, located at a large water treatment plant used to flocculate and clarify alum coagulated surface water. Hydrodynamics were characterized through the use of three different scale models of the clarifier and limited testing on the full-scale system. Mixing characteristics were measured by: a 2-D laser doppler anemometer which allowed a detailed description of turbulent flow for the two smallest scale models; a propeller meter to document mean velocities in the largest of the scale models; and a tracer test on the full-scale clarifier to estimate bulk flow characteristics.

The objectives of this chapter are three fold:

1. Document detailed mixing hydrodynamics in the impeller zone for a complex flocculator/clarifier which is used in many water treatment facilities.

2. Show the application of physical modeling for the assessment of treatment process hydraulics.

3. Develop and confirm scaling factors which are required to relate model results to the full-scale. It should be noted, that the theory and concepts used in the development are also useful for those wanting to characterize other radial flow impeller systems and to scale-up bench or pilot-scale mixing processes to the full-scale.

3.2 Background

The E.L. Smith Water Treatment Plant in Edmonton, Alberta, Canada is a relatively new plant (constructed in 1976) with a nominal capacity of 200 ML/d. The plant employs the following processes: alum coagulation, clarification, chlorine dioxide disinfection, fluoridation, partial softening with lime and recarbonation, rapid sand filtration and chloramine disinfection to provide a residual. The clarifiers consist of three identical upflow solids-contacting clarifiers. Under normal operating conditions two of the clarifiers are used for alum clarification and one for lime softening. Each clarifier is a 42.7 m x 42.7 m x 7.7 m deep concrete basin, with a draught tube and impeller mixer in the center and high rate shallow depth plastic tube settlers installed approximately 1 m below the launder system along the outer edges of the clarifier, as shown in Figure 3.1. In the alum clarifiers, the chemical coagulant is introduced and rapid mixing occurs by means of an in-line mixer in the raw water supply line at a point just upstream of the two clarifiers. The influent raw water is introduced directly into the circular draught tube via a tangential entry. The raw water influent is mixed with recirculated sludge and forced upward and out of the draught tube due to the presence of an impeller-generated recirculated flow. After exiting the draught tube, the flow may either be recycled back into the draught tube through the bottom or may exit the clarifier through the tube settlers and launders. There are two primary purposes for the draught tube and impellers: 1) to provide mixing energy for the flocculation of particles: and, 2) to recycle sludge to increase particle concentration and improve the efficiency of flocculation. As shown in Figure 3.1 the clarifier can be divided into three main components: 1) the draught tube; 2) the flocculation zone, which is considered to be the volume outside the draught tube and inside the tube settler area; and 3) the sedimentation zone, the region above and below the area covered by tube settlers. The existing impellers and clarifiers are a proprietary design of Ecodyne Ltd. They are typically operated at impeller speeds of 4 to 10 RPM depending upon the conditions necessary to

produce an acceptable degree of flocculation. Details of the impeller and draught tube are given in Figures 3.2 and 3.3.

Because little information in available on mixing conditions in this type of clarifier, the City of Edmonton commissioned this study to better understand hydrodynamic conditi ns in their clarifiers. Results from it are to be used to aid in the selection of mixing cond ions for ench and pilot-scale studies. In addition, the increased understanding of the mixing process gained through this study should also help in the operation and optimization of the process. Complicating the lack of information on these types of clarifiers is the difficulty of assessing even simple traditional mixing parameters such as $\overline{G}$ for these combined flocculators/clarifiers, as there is no definable volume for the flocculator. The volume could be taken to be anywhere from the volume of the draught tube to the volume of the flocculation zone to the total volume of the clarifier. This was an additional reason that more detailed study was required.

3.3 Theory

Due to the complexities of impeller-generated turbulent flow the traditional approach in analysis and assessment has been based on vessel-average or bulk parameters. Through dimensional analysis (Rushton, 1951) it has been shown that bulk mixing in impeller-agitated flow can be describe by the following dimensionless quantities:

$$R = \frac{D^2 N}{v} \qquad (3.1)$$

$$F = \frac{DN^2}{g} \qquad (3.2)$$

$$N_p = \frac{P}{\rho D^5 N^3} \qquad (3.3)$$

where D is the diameter of the impeller, N is the rotation speed, v is the kinematic

viscosity, g acceleration due to gravity, ρ the density of the fluid, P the power input into

the tank, R is the Reynolds number (ratio of inertial to viscous forces), F the Froude

number (ratio of inertial to gravitational forces) and N_p the power number (analogous to a

drag coefficient). It has generally been founded that if impeller-agitated mixers are well

baffled, the effect of the Froude number, F, is effectively suppressed.

Additional parameters used to describe bulk flow include:

$$N_q = \frac{Q}{ND^3} \qquad (3.4)$$

$$\overline{G} = \sqrt{\frac{P}{\mu V}} = \sqrt{\frac{\overline{\varepsilon}}{v}} \qquad (3.5)$$

where Q is the impeller generated flow rate, μ is the absolute viscosity, $\overline{\varepsilon}$ the average rate

of energy dissipation per unit mass, V is the volume of the tank, N_q is the flow number or

the pumping number and $\overline{G}$ is the root mean square velocity gradient which has long been

used in the field of coagulation and flocculation.

The importance of the concepts of energy and dissipation in flocculation mixing

processes is well recognized, as is indicated by the traditional use of parameters such as $\overline{G}$

in describing mixing processes for flocculation. This parameter has been shown to be

important in the description of flocculation kinetics as well as floc characteristics, such as

floc size. The use of these bulk parameters has allowed a relatively complicated process to

be described adequately well by a few easily obtained values. However, bulk parameters

do not describe local variations within the impeller-agitated mixer, especially in the impeller

vicinity. As such, the analysis of turbulence, which requires examination of the flow field

within the tank, allows a more refined specification of flow, energy and dissipation which

have long been known to be important to the flocculation process.

With the development of improved velocity measurement techniques, such as the laser doppler anemometer, detailed studies of turbulent flow in impeller-agitated tanks have begun to appear in the literature. These studies have highlighted the spatial variations of flow and energy dissipation within the tank. They have found that energy dissipation near the impeller region is much higher than in the bulk of the tank (see for example: Kresta and Wood, 1991 and 1993; Weetman and Oldshue, 1988; Wu and Patterson, 1989; Wu et al., 1989; and Stanley and Smith, 1995). These studies have also shown some unique characteristics of impeller-agitated flow, because in some systems not all velocity fluctuations near the impeller are random in nature but are periodic. These periodic fluctuations, called pseudo-turbulence by Van't Riet et al. (1976), need to be removed, if they are present, before the actual turbulence can be properly characterized. This is done by separating the random fluctuation, $u'_{rand}(t)$ from the periodic part, $u'_{per}(t)$.

$$u'_{tot}(t) = u'_{rand}(t) + u'_{per}(t) \qquad (3.6)$$

Methods for their removal are discussed in Wu and Patterson (1989) and Stanley and Smith (1995).

The documentation of the kinetics of flow and the mechanics of energy dissipation in the tank appear to be the most significant to the flocculation process. This involves the use of measurements to calculate the variations in ε, the local unit mass energy dissipation rate, within the tank. A number of different methods can be used to calculate the turbulent local dissipation rate, ε, see for example Kresta and Wood (1993) or Stanley and Smith (1995). In stirred tanks the most appropriate methods are based on the fact that all the kinetic energy, k, being transferred from the large scale eddies where production is occurring must be dissipated by the small scale eddies. An estimate of kinetic energy, k, is given by:

$$k = \frac{\overline{u'_z}^2 + \overline{u'_r}^2 + \overline{u'_t}^2}{2} \qquad (3.7)$$

Knowing the rate at which kinetic energy is transferred down through the eddies, an estimate of ε can be obtained from:

$$\varepsilon = A\frac{k^{\frac{3}{2}}}{L} \qquad (3.8)$$

where A is a constant of proportionality (close to unity) and L is a characteristic length scale. Although all three velocity components were used in this study for the determination of k, if one assumes isotropic turbulence, which was found to be generally true, the dissipation rate can be expressed as:

$$\varepsilon = A\frac{u'^{3}}{L} \qquad (3.9)$$

where u' is the characteristic velocity which is given by $k^{1/2}$. This form of the equation can be used to provide the basis for scaling factors for ε. L is usually determined by equating it to the Eulerian integral length scale, which can be determined by the autocorrelation coefficient function (Wu and Patterson, 1989) or by relating it to a physical dimension of the flow. The latter approach can be justified by the success of describing impeller-agitated flow with the swirling radial jet model (Kolar, Filip and Curev, 1984; Kolar, Filip and Curev, 1985; Filip, Kolar and Curev, 1985a; Filip, Kolar and Curev, 1985b; Filip, Kolar and Curev, 1986; and Kresta and Wood, 1991). Studies of jets have shown that the Eulerian integral length scale can be related to 1/2 of the total jet width (Antonia, Satyaprakash and Hussian, 1980). The initial width of the jet produced by a radial impeller has been shown by many to be equal to the width of the impeller blade and hence the Eulerian integral length scale can be related to 1/2 the blade width, near the impeller. Calculation of the length scale by the autocorrelation coefficient function in the discharge stream from the impeller has also found that it can be approximated by the half-width of the impeller blade (Wu and Patterson, 1989; and Stanley and Smith, 1995).

To characterize the swirling radial jet it must be recognized that the jet produced by the impeller has both a radial and tangential velocity component. The axis of the jet does not therefore follow the traditional radial and tangential coordinate systems used in mixing tank analysis. A new geometric variable, ξ, originally described by Kolar, Filip and Curev (1982) is used to represent the distance along the axis of the swirling radial jet.

$$\xi = \sqrt{r^2 + e^2} \tag{3.10}$$

where r is the radial distance from the center of the tank and e is described as:

$$e = \frac{\int\limits_{-\infty}^{+\infty} \rho 2\pi r u^2 dz}{\int\limits_{-\infty}^{+\infty} \rho 2\pi r^2 uv dz} \tag{3.11}$$

where u is the mean radial velocity, v the mean tangential velocity and z is the coordinate in the axis direction. Equation 3.11 may be seen to represent the ratio of the radial momentum to the angular momentum within the swirling radial jet. In practice, e may be fully defined for a given set of conditions from a single measurement of the radial and tangential velocities at the impeller's periphery:

$$\beta_o = \tan^{-1}\left(\frac{v_o}{u_o}\right) \tag{3.12}$$

so that e may be determined directly from

$$e = r_o \sin \beta_o \tag{3.13}$$

which then allows coordinate ξ to be determined for any radius, r. Finally, knowing u and v, a vector sum of these may be made in order to define a new velocity, q, which is the local velocity along the axis of the swirling radial jet. With the use of transforms of q and ξ, characteristics of the impeller induced jet, such as the width of the jet and maximum jet

velocity can be determined using traditional formula's for radial jets as described by Rajaratnam (1976).

$$\Lambda \propto (\xi \,/\, b) \tag{3.14}$$

$$\frac{q_{max}}{q_o} \propto \frac{1}{(\xi \,/\, b)} \tag{3.15}$$

where Λ is the width of the jet at any ξ, q_{max} the velocity along ξ, q_o the velocity at source of the jet (tip of impeller), and b the diameter of the jet source (the width of the impeller).

The representation of the impeller as a swirling radial jet provides the basis of the development of many of the scaling relations, as similarity analysis in turbulent jets is a well developed field of study.

3.4 Experimental Arrangement

Documentation of flow conditions in the upflow solids-contacting clarifier was accomplished through the measurement of turbulent flow in three scaled models and limited testing on the full-scale clarifier. The three model-scales, maintaining geometric similarity, used in the study were 1:55, 1:41 and 1:10, which correspond to impeller diameters of 76.6 mm, 103.7 mm and 427 mm, respectively. Two small scale models (scales 1:55 and 1:41) were constructed to represent the impeller and draught tube only, with no externally applied inflow. They were constructed of transparent acrylic or polycarbonate as the velocity measurements were accomplished with the use of a laser doppler anemometer. The impellers were constructed from stainless steel. For these two models the draft tube and impeller were placed in a large tank, which approximated the flocculation zone. Another model, at a scale 1:10 was constructed by Northwest Hydraulic Consultants Ltd., a company specializing in hydraulic model studies. This scale model represents a true

geometric reproduction of the entire clarifier, complete with a tangential infow pipe, flocculation zone, settling zone, tube settlers and perforated launders.

The experimental program can be divided into four main components:

1. Measurement of turbulent flow using the LDA for the free impeller (no draught tube) at the 1:55 and 1:41 scale to investigate the applicability of the swirling radial jet analogy to describe impeller-generated flow. This was required as the impeller is quite different to others that have been reported in the literature given its 10 blades and cap on the top.

2. Detailed measurements of turbulent flow quantities for the 1:55 and 1:41 scale impellers with the draught tube in place using the LDA. Bulk parameters such as N_q, R and N_p were also determined.

3. Measurement of velocities in the 1:10 scale model both with and without tangential inflow using a propeller meter. Results from this component were used to confirm scaling relations developed with detailed LDA velocity data at the two smaller scale models and determine the impact of the tangential inflow whi $\because$ $\because$ not considered at the 1:55 and 1:41 scale models.

4. Some limited tracer test data analysis to estimate flow properties at full scale.

In the 1:55 and 1:41 scale models radial, axial and tangential velocities were measured with a Dantec 2-D laser doppler anemometer (LDA), in the forward scatter mode using a 300 mW Argon-ion laser (see Appendix A). The receiving optics were set at a deflection angle of 60° from a true forward scatter mode to allow more complete measurement in the impeller zone. Although the LDA was only capable of measuring velocities in two dimensions at one time, three dimensional velocity measurements could be obtained by combining data from two points lying on the same horizontal plane, at the same

radius, separated by an angle of 90°. If the two points are separated by 90°, one measuring point would give axial and radial velocities and the other measuring point, axial and tangential velocities. As a result, two vertical planes, perpendicular to the vessel walls, separated by 90° form the basis for most of the measured data presented in this study. To allow measurement of reversing flows the frequency of one beam for each velocity component was shifted 40 MHz via a Bragg cell. Bandpass input filters were set at a bandwidth of 0.4 MHz. Signal processing was accomplished with a Particle Dynamics Analyzer, covariance signal processor. It has the ability to handle higher data rates and lower signal-to-noise ratios than traditional counter and tracker signal processors. The laser system contains a built-in laser diode which generates calibration signals that are fed via a fibre optic cable to the receiving optics to ensure that the equipment is automatically calibrated. All velocity measurements were validated based on signal-to noise levels and fringe counts. To eliminate velocity bias, moments were calculated by residence time weighting. For the set-up used in this study the measuring volume at the beam crossing was 0.12 mm x 0.12 mm x 2.4 mm. Care was taken to ensure that the frequency of data collection was below the phase ambiguity noise limit. More details on the LDA system and concerns with the phase ambiguity noise limit can be found in Stanley and Smith (1995).

To measure velocities in the 1:10 model, a Nixon propeller meter attached to a Novonic Streamflow processor was used. Given the spatial limitations presented in the model only radial and tangential velocities could be measured. This meter was calibrated by means of a velocity measurement across a rectangular flume under conditions of steady flow. Consistent vertical location of the current meter was ensured by mounting the meter to a moveable point gauge and radial location was maintained by referencing the radial position to a fixed reference point.

To measure the impellers' power consumption at the 1:55 and 1:41 scales, torque was measured with a model TRPA5 Rotary Parallel Shaft torque transducer manufactured

by Industrial Measurements Ltd. This device was connected to a special conditioning unit which gives readout in Nm directly.

3.5 Results

3.5.1 Free Impeller

'   '55 and 1:41 impellers were tested with no draft tube over a range from 25 to 20C   e 3.4 shows the general flow patterns for the 1:55 scale at 50 RPM. As sho, ι the gure flow enters from the bottom and is discharge radially from the impeller. Figure 3.5 shows radial mean velocities, u, at $2r/D = 1.175$. Note that velocity profiles tend to collapse on one another when velocity is scaled by the tip speed of impeller $(N\pi D)$. Similar results were found for other velocity components. Figure 3.6 shows similar results for the fluctuating radial velocity, u', again scaled with the tip speed of the impeller. Once again all components of the fluctuating velocities collapsed when made dimensionless with the tip speed. Of interest, unlike the previous study of the flat blade paddle impeller used in the jar test apparatus (Stanley and Smith, 1995), it was found by analysis of the autocorrelation coefficient function that there did not seem to be a strong periodic component to the fluctuating velocities. This may be a result of the large number of blades. Similar results were found by Kresta and Wood (1992) for a pitched blade impeller.

In total, five cross-sections through the impeller discharge were taken starting at the edge of the impeller ($2r/D=1.044$) to $2r/D=2.2$. As discussed, measurements were taken for two planes separated by 90° to allow all 3 velocity components to be measured. Using these data the maximum velocity along the axis of the jet could be determined as well as the width of the jet. If the impeller can be represented by a swirling radial jet, values should correspond to those reported for these jets. Limited data are available for a swirling radial

owever, the use of ξ and q should now allow comparison with a radial jet, as the

transform of the coordinate systems accounts for the swirl. Rajaratnam (1976) based on experimental work by Heskestad (1966) found that the maximum velocity of a radial jet can be given by

$$\frac{u_m}{U_o} = \frac{3.5}{(r/b_o)}\frac{r_o}{b_o} \tag{3.16}$$

where U_0 is the velocity at the jet source, r the radial distance, r_0 the radius of the jet and b_0 the width of the jet at its source. For the impeller studied, r_0 is equal to the radius of the impeller and rearranging yields:

$$\frac{u_m}{U_o} = \frac{3.5}{r/r_o} \tag{3.17}$$

Figure 3.7 shows the variation in maximum velocity, q_{max}, the resultant of the tangential and radial velocity with ξ, the distance along the axis of the jet. The data are presented in a format compatible with Eq. (3.17) above. The value r has been replaced with ($\xi + r_0$). Note that the decrease q_{max} appears to be linear with ($r_0/(\xi + r_0)$) as would be predicted by Eq. 3.17. The general slope of the measured values ranges from 2.5 to 3, which compares to the 3.5 constant reported by Rajaratnam in Eq. 3.17. The value obtained for the impeller is slightly smaller however the difference could be the result of the use of v_{tip} ($N\pi D$) to represent U_0, as examination of the figure indicates that the value of q_{max} never quite reaches v_{tip} at the edge of the blade . The best fit line for the data can be summarized as:

$$\frac{q_{max}}{V_{tip}} = \frac{2.65}{(\xi + r_o)/r_o} \tag{3.18}$$

Another important quality of a jet is the growth of the jet-width with distance from the source. For a radial jet Rajaratnam (1976), again based on experimental work by Heskestad (1966), wrote the width of the jet could be determined by:

$$\frac{\Lambda}{b_0} = 0.11\frac{r}{b_o} \qquad\qquad (3.19)$$

where b_0 is the width of the jet at its source.

For comparison, the width of the jet produced by the free impeller was determined with distance from the impeller. It was found that if the radial coordinate 2r/D was used, the growth was decidedly not linear and not in agreement with Eq. 3.19. However, if ξ was used the growth of the jet was much more linear, It was also found that the initial width of the jet was somewhat dependent on N (the impeller rotation speed). A simple multiparameter linear regression analysis with ξ and N was conducted to determine their effect on Λ. Results are presented below:

$$\text{Scale 1:55} \qquad \frac{\Lambda}{b} = 1.259 - 0.0019N + 0.1335\xi + 0.0026\xi N. \qquad (3.20)$$

$$\text{Scale 1:41} \qquad \frac{\Lambda}{b} = 1.0015 - 0.0027N + 0.0968\xi + 0.0001\xi N \qquad (3.21)$$

Obviously the approach is limited by the relatively small sample size available (five radii, at five N's for the 1:55 scale and three dimensionless radii, at two N's for the 1:41 scale). However, the analysis is useful in indicating several fundamental properties of the jet. First the analysis indicates a slight negative dependence of the jet-width upon N, a behavior clearly noted in the experiments. Secondly, although a dependence of Λ upon N exists, it is seen to be only a fraction of the calculated dependence of Λ upon ξ. Thirdly, it is seen the average dependence of Λ upon ξ is 0.115, a value very close to that reported by Rajaratnam (1976) for a radial jet without swirl (Eq. 3.19). Finally by setting $\xi = 0$ it is seen that the dimensionless jet-width is of the order of unity near the impeller, or equal to the width of the impeller. This gives further justification of the use of the half-width of the impeller to represent the Eulerian integral length scale in the impeller region as it has been long recognized in the study of jets that it can be represented by the half-width of the jet.

Using Eqs. 3.20 and 3.21 it can also be shown that the jet width and hence Eulerian integral length scale would only increase by 10% between 2r/D = 1.004 and 2r/D = 1.175, the locations where most of the measurements were taken.

The local dissipation rates, ε, in the vicinity of the impeller were therefore determined using Eq. 3.7 and 3.8, and setting L equal to the half-width of the impeller for locations near the impeller. Figure 3.8 shows the calculated values of ε. Note that even though the dimensional values vary over four orders of magnitude, the curves tend to collapse on one another, when made dimensionless by dividing by $((N\pi D)^3 / D)$ or $((N\pi D)^3 / b)$. The use of these scaling factors can be related to Eq. 3.9, noting the fact that the fluctuating velocities scale as the tip speed of the impeller. $((N\pi D)^3 / D)$ is the factor most commonly used in impeller studies; however, it is only a licable for comparison with other types of impellers when the D/b ratio (diame   width of impeller) is constant, as D is being used to represent the length scale which is really dependent on b. For Rushton turbines, the most frequently studied turbine, the D/b ratio is 5. For this impeller the ratio is 3.95. For this reason it is better to use $((N\pi D)^3 / b)$ as it does not require a constant D/b ratio for comparison purposes. Note the maximum dimensionless dissipation value is about $\varepsilon / ((N\pi D)^3 / b) = 0.032$. Very similar results were found for the 1:41 scale model.

In addition, bulk parameters such as N_q, R and N_p were also determined for the free impeller and will be discussed later.

3.5.2 Draught Tube - No Tangential Inlet

After developing the basis for further analysis based on results from the free impeller, testing was conducted on all three scale models with the draught tube in place. As mentioned, velocity measurements were obtained with a LDA for the 1:55 and 1:41 scale models and a propeller meter for the 1:10 scale model. As a result, detailed turbulent

measurement could only be obtained for the two smallest models as the proppeller meter can only measure mean velocities. In addition, bulk parameters were also determined for the scale models.

Figure 3.9 shows the general flow patterns with the impeller and the draught tube. Note that the flow is pumped from below and exits through the top. As mentioned, the purpose of the impeller is two-fold: 1) provide mixing energy for flocculation; and, 2) recycle sludge from the bottom of the clarifier. Therefore, the pumping number, N_q, is an important parameter. N_q is determined by defining a control volume around the impeller to determine Q, and then substituting this value into Eq. 3.4. Other studies have indicated that the control volume should be as close to the impeller as possible to avoid contributions from the entrainment of surrounding fluid into the discharge jet being included in the calculation of Q. Table 3.1 shows some of the calculated values obtained. A few trends should be noted in the results. First of all there appears to be a trend of decreasing N_q with increasing R, which was evident in all three of the scales. As expected, the draught tube also tends to slightly reduce N_q, which indicates that it slightly restricts the flow to the impeller. If one compares the results between the different scales, especially if one considers similar R, the values of N_q are comparable. In general, Godfrey and Amirtharajah (1991) suggested that the pumping numbers of impellers are generally given as:

$$N_q = 0.75 \pm 0.15 \qquad (3.22)$$

Most of the values for N_q in this study are slightly lower than this reported range. This may be because only one side of this impeller is available for drawing in the surrounding fluid as the top is covered.

The power number, N_p, was determined for the 1:55 and 1:41 scale models with the use of the torque transducer to calculate P and the use of Eq. 3.3. In accordance with

the published literature, the values of N_p were found to vary with R up to a R = 1x 10^4, after which the values remained constant. The constant values for R > 1x 10^4 are given in Table 3.2. Values were found to be much more consistent than for N_q and there was excellent agreement between the two scales. An increase in N_p with the addition of the draught tube was observed which indicates that more power is required to maintain the same rotation speed with the draught tube in place. This would be expected due the additional shear that the walls of the draught tube would impart to the fluid.

To assess the scaling of velocities measured over a wide range of impeller scales and speeds, results obtained from all three model scales were compared. Figure 3.10 shows mean radial velocities from all model scales at a number of different rotation speeds, scaled on the tip speed of the impeller. As indicated in the figure, the curves collapse quite closely, especially considering the tip speed of the impellers range from 0.2 m/s to 1.56 m/s (1:55 @ 50 rpm to 1:10 @ 70 rpm) and impeller diameters, from 76.6 mm to 427 mm and two different methods were used to measure velocities. Figure 3.11 shows similar results for the fluctuating radial velocity (only the 1:55 and 1:41 scales). It should be noted that comparison of Figure 3.10 and 3.11 with Figures 3.5 and 3.6 shows that there is not a big difference in the flow at the edge of the impeller for the free and confined (draught tube) cases. Figure 3.10 shows that the mean flow patterns still have a jet velocity profile. Table 3.3 gives the values for all three velocity components, made dimensionless by the v_{tip}, for the confined and unconfined case. The table also shows that in terms of velocities there does not seem to be a big difference between the confined and unconfined case.

As the width of the jet at the edge of the impeller still seems to scale on the width of the impeller, the local dissipation rates, ε, were calculated based on L being approximated by the half-width of the blade. Figure 3.12 shows values of ε for the 1:55 and 1:41 scale models. Again there appears to be little difference between the free impeller case and the draught tube case, with both having a maximum value of ε of $\varepsilon / (V_{tip}^3 / b) = 0.032$.

3.5.3 Draught Tube - Tangential Inlet

As mentioned, the 1:55 and 1:41 scale models did not have the ability to assess the impact of the tangential inflow on impeller hydraulics. Studies were therefore conducted to assess effect of the tangential inflow on the 1:10 scale model. Tests were completed on the 1:10 model with no tangential inflow, a tangential inflow equivalent with a full-scale flow of 100 ML/d and one equivalent to a full-scale inflow of 200 ML/d, which is the capacity of the clarifier. In this part of the study the inflow was scaled by the Froude criterion which is typical practice for scaling bulk flows and velocities in free surface models. Some initial dye tests were conducted which showed visually that flow entering through the tangential inlet did not flow into the impeller zone, but simply left through the top of the draft tube. Velocity measurements were also taken in the impeller stream. Although it was found that the tangential inlet does effect general flow patterns in the whole clarifier, the effect in the impeller zone was small. At the 1:10 scale model, only mean velocities could be taken. An easy method to compare what effect the tangential inlet has on flow through the impeller is to compare flow numbers, N_q. Figure 3.13 shows the calculated values of N_q, for the two small scale models (1:55 and 1:41) with no tangential inflow and results from the 1:10 model with no tangential inflow (0Q), an inflow equivalent to 100 ML/d (100Q) and an inflow equivalent to 200 ML/d (200Q). Although there is some scatter in the data there does not appear to be a trend that separates the test with inflow and those without. Based on these results the author is confident that detailed turbulent measurements in the impeller vicinity taken at the 1:55 and 1:41 scale models with no inflow, should be applicable to the full-scale with tangential inflow.

To provide some information at full-scale, some limited tracer testing was completed. The results discussed are only a small portion of tracer testing completed to determine general flow patterns through the entire clarifier. The test involved a step dose addition of NaCl tracer to the water entering the clarifier. The tracer was added

immediately upstream of the rapid mixer in the raw water line to ensure good mixing. To try to determine the flow produced by the impeller, samples were taken and analyzed for sodium, at the bottom of the draught tube, at the point where the raw water entered through the tangential inlet and at four locations at the top of the draught tube. Samples were taken at 1 minute intervals for a 30 minute time period. It was found that there was a background concentration of 6.98 mg/L of Na and a step dose of 9.62 mg/L of Na was added. Samples were analyzed using a flame emission photometric method , Standard Method 3500-Na (APHA-AWWA-WEF, 1992). Knowing the flow through the tangential inlet and the tracer concentration in water entering through the bottom and exiting through the top an estimate of the flow through the bottom, which results from the impeller can be estimated. Although this calculated flow can only be considered an estimate, a large variation from that predicted from scaling factors developed in the models would indicate the unsuitability of scaling results from the model scale to full scale. As the tracer test only supplies bulk flow information, an appropriate comparison parameter is the flow number, N_q. Under the conditions studied (impeller speed $\approx$ 6 rpm and inflow rate = 180 ML/d) the value of N_q was found to be approximately 0.6, which is similar to results from the scale models.

3.6 Discussion

Results from the study of the scale models indicate that the free impeller can be considered analogous to a swirling radial jet. Even when the impeller is placed in a draught tube, which significantly complicates the flow patterns near the impeller, this analogy appears to remain valid. Although, the analogy between impeller-agitated flow and a swirling radial jet has been proposed for some time: little detailed turbulent flow information has been taken to confirm this; studies that have been done have examined simple impeller systems (Rushton turbines), in large tanks (free impellers); and testing has not covered a wide range of scales. Results from this study indicate that the analogy is

valid for a different type of impeller in a much more complex flow condition (draught tube) over a range of impeller sizes varying from a diameter of 76.6 mm to 4267 mm. The significance of this finding is that the swirling radial jet provides a theoretical basis to describe many characteristics of the impeller generated flow as well as the basis of scaling factors.

Using the jet analogy, many characteristics of the discharge from the impeller can be determined. Jet characteristics have traditionally been defined based on: U_0, mean velocity at jet source; d_0, diameter of the jet source; and u', the turbulent fluctuating velocity. Measurements taken as part of this study have found that U_0 can be approximated by q, the resultant of the radial and tangential mean velocities. It has also been found that q and other mean velocity values scale on the tip speed of the impeller and as indicated in Table 3.3 the value of q can be estimated as:

$$\frac{q}{(N\pi d)} \approx 1 \tag{3.23}$$

It was also found that turbulent fluctuating velocities also scale on the v_{tip}, which indicates that the u'/U should remain constant. Although each component of the turbulent fluctuating velocity varied slightly, a characteristic fluctuating velocity can be given by $k^{1/2}$. As shown in Table 3 the dimensionless value for the free impeller and confined impeller, given as $k^{\frac{1}{2}} / (N\pi D)$, were 0.31 and 0.26, respectively. As $k^{1/2}$ is representing u' and U_0 is equal to the v_{tip}, the value reported for $k^{\frac{1}{2}} / (N\pi D)$ would be equivalent to u'/U_0. The concept of a constant u'/U has long been recognized in turbulent jets. Antonia et al. (1980) reported a value of u'/U_0 of 0.32 for a circular jet which was similar to the value from Wygnanski and Fielder (1969) of 0.31 for the same kind of jet. For a radial jet, u'/U was reported by Heskestad (1966) to be 0.33. Note that values are similar to those found for an impeller, even though the devices generating the jet are significantly different. Given that the fluctuating turbulent velocities are similar and the Eulerian integral length scale can be

determined by the half-width of the jet, the values for dissipation rates should also be similar.

As indicated by the above discussion, results from this study can be described by a swirling radial jet and characteristics of this impeller-agitated flow are similar to those produced by other types of true jets. This gives confidence in the characterization and scale-up of the results from the model study. Fluctuating turbulent velocities and therefore dissipation rates could only be determined at the 1:55 and 1:41 scale. For the 1:10 scale model only mean velocities could be determined and at full-scale only a bulk flow determination could be made. However, it was found that mean velocities could be scaled with v_{tip}, all the way up to the full-scale. Given the above discussion on maintenance of a constant u'/U, even with different types of jets (impeller generated and true jets), scaling based on a constant $\varepsilon / ((N\pi D)^3 / b)$ should be valid. Using $\varepsilon / ((N\pi D)^3 / b) = 0.032$ the value of the local dissipation rate, ε, near the impeller for the full scale system should vary from 0.021 to 0.33 m^2/s^3 for rotation speeds of 4 rpm and 10 rpm, respectively. Using Eq. 3.5 the localized G values would be 144 s^{-1} and 574 s^{-1} near the impeller for 4 and 10 rpm, respectively. As the results indicate, the local values of G near the impeller are much greater than volume average values that are normally associated with flocculation in water treatment, with vessel average $\bar{G}$ normally being in the range of 10 to 70 s^{-1}. Although it has been recognized that energy and values of G are higher in the impeller zone, this is one of the first studies to quantify these values in a real flocculator. Given the importance of mixing energy and hence $\bar{G}$ on floc characteristics and process performance, this highlights the need for further study of detailed hydrodynamics in the impeller zone, and relating it to forces on the flocs and process performance. The assumption of homogeneous mixing conditions in a flocculator is clearly a gross simplification of the impeller-agitated mixing process. It should be noted that the clarifier studied produces a good clarified water and often operates at or near the maximum rotation speed.

A recent American Water Works Association Research Foundation Report on mixing processes for coagulation (Clark et al. 1994), recommended:

there is a need for a better understanding of how impeller fluid mechanics changes with scale and how these different fluid mechanics regime affect flocculation-sedimentation performance.

This will demand:

the measurement of fluid flow patterns and energy dissipation induced by different flocculation impellers at different scale

This study provides some of this information for only one type of flocculation impeller used in the water treatment industry. However, the concepts and theory used in the analyses of the results and the development of scaling factors should be valid for other radial flow impeller-agitated flocculators. Although few studies are available which have presented detailed turbulent flow for multi-scale systems, information is available for single scale systems. Wu et al. (1989) measured turbulent flow in a tank containing a Rushton turbine with a 93 mm diameter. By transforming data from their study into a dimensionless format similar to this study, their results showed that $k^{\frac{1}{2}} / (N\pi D)$ in the impeller zone varied from 0.19 to 0.29, a value comparable to this study and similar to that reported for radial jets. They did not use the radial jet analogy in the calculation of the local dissipation rate, ε, but determined the Eulerian integral length scale based on the analysis of the autocorrelation coefficient function. Converting their results to the form $\varepsilon / ((N\pi D)^3 / b)$ shows that the value varied from 0.018 to 0.07. Again, the results are within the range found in this study. Stanley and Smith (1995) investigated turbulent flow in for a 76 mm flat paddle used in a standard jar test apparatus. They found $k^{\frac{1}{2}} / (N\pi D)$ to be in the range of 0.26 and $\varepsilon / ((N\pi D)^3 / b)$ to range from 0.033 to 0.047, again very similar to this study.

It appears that the analogy of the swirling radial jet to radial flow impellers is applicable over a wide range of scales, as shown in this study, and substantially different types of impellers. Results seem to indicate that mean velocities and turbulent fluctuating velocities scale on the tip speed of the impeller and appear to remain constant for different scales, types of impellers and even in comparison to true radial jets. An estimate of local dissipation rate near the impeller should therefore be possible just based on tip speed and impeller geometry. For different types of impellers, not mentioned in this study it is still necessary to confirm the scaling constants. However, based on the theory of radial jets, the form of the scaling relationships should remain the same. The applicability of the scaling parameters were highlighted by their ability to describe the flow in a complex mixing situation which involved an impeller, a draught tube, a tangential inlet, with a range of impeller diameters from 76.6 mm to 4267 mm, and varying impeller speeds.

3.7 Conclusions

Detailed analysis of the hydrodynamics of the impeller region in an up-flow solids-contacting clarifier was conducted. The system studied has much more complex flow patterns than most previous impeller-agitated mixing studies due to the presence of a draught-tube and a tangential inlet. Results were obtained through a series of studies on three scale-models and limited testing on the full-scale clarifier. Results were analyzed and scaling parameters were determined based on analogy of the impeller-generated flow to a swirling radial jet. The use of this analogy was confirmed by studies on the free impeller.

Despite the presence of the draught tube it was found that mean and fluctuating velocities scaled on the tip speed of the impeller. Use of the swirling radial jet analogy allowed the scaling of local dissipation rates based on the following relation $\varepsilon / ((N\pi d)^3 / b)$ which was found to be constant and equal to 0.032. Results compared

favorably to other impeller studies and true radial jets, indicating the applicability of concepts used to assess other flocculation impellers.

In the full-scale system it was found that local dissipation rates near the impeller varied from 0.021 to 0.33 m^2/s^3 under normal operating conditions. Calculated localized G values were found to range from 144 s^{-1} and 574 s^{-1} near the impeller. These high values highlight the need for further study of the impact of local mixing conditions on flocculation performance as these values are considerably greater than those normally associated with flocculation processes in water treatment.

3.8 References

Antonia, R., Satyaprakash, B. & Hussain, A. (1980). Measurements of Dissipation Rate and Some other Characteristics of Turbulent Plane and Circular Jets, *Phys. Fluids*, **23**, *4*, April, 695-700.

APHA-AWWA-WEF. (1992). Standard Methods for the Examination of Water and Wastewater. 18th Edition

Camp, T.R. and Stein, P.C. (1943). Velocity gradient and internal work in fluid motion. *Jour. Boston Soc. Civil Engineers* **30**, 10, 219-237.

Clark, M.M., Srivastava, R.M., Lang, J.S., Trussel, R.R., McCollum, L.J. Baily, D., Christie, J.D., and Stolarik, G. (1994). Selection and Design of Mixing Processes for Coagulation. American Water Works Association Research Foundation and American Water Works Association, Denver, CO. 150p.

Filip, P., Kolar, V. & Curev, A.G. (1985a). Space Flow Geometry of the Radial Free, Wall and Liquid Jets with Swirl. *Applied Scientific Research*, **42**, 185-196.

Filip, P., Kolar, V. & Curev, A.G. (1985b). Complex Swirling Radial Jets, *Z. Angew. Math. u. Mech*, **65**, *9*, 441-446.

Filip, P., Kolar, V. & Curev. A G. (1986). A Note on the Radial Wall Jet with Swirl, *Acta Mechanica*, **60**, 41-47.

Godfrey, J.C. and Amirtharajah, A. (1991). Mixing in Liquids. from Mixing in Coagulation and Flocculation, American Water Works Association Research Foundation, 35-79.

Heskestad, G. (1966). Hot-wire measurements in a radial turbulent jet. Trans. ASME, J Appl. Mech. 417-424.

Kolar, V., Filip, P. & Curev, A.G. (1982). The Swirling Radial Jet, *Applied Scientific Research*, **39**, 329-335.

Kolar, V., Filip, P. & Curev, A.G. (1984). Hydrodynamics of a Radially Discharging

Impeller Stream in Agitated Vessels, *Chemical Engineering Communications*, **27**,

313-326.

Kolar, V., Filip, P. & Curev, A.G. (1985). The Swirling Radial Jet Model and its

Application to a Radial Impeller Stream, from *5th European Conference on Mixing*,

Wurzburg, West Germany, 10-12 June, 1985, 483-490.

Kresta, S.M. and Wood, P.E. (1991). Prediction of the three dimensional turbulent flow in

stirred tanks. *A.I.Ch.E.J.*, **37**, 448-460.

Kresta, S.M. and Wood, P.E. (1993). The flow field produced by a pitched blade turbine:

Characterization of the turbulence and estimation of the dissipation rate. *Chem.

Eng. Sci.*, **48**, 10, 1761-1774.

Rajaratnam, N. (1975). Turbulent Jets, Elsevier Science Publishers Ltd., Amsterdam.

Rushton, J.H. (1951). The use of pilot plant mixing data. *Chemical Engineering Progress*,

47, 9, 485-488.

Smoluchowski, M.W. (1917). Versuch einer Mathematischen Theorie der Koagulations

Kinetik Kolloider Losungen. *Zeitschrift f. Physik. Chemie*, 92:126.

Stanley, S.J. and Smith, D.W. (1995). Measurement of turbulent flow in a standard jar test

apparatus. *Journal of Environmental Engineering, ASCE*, (Accepted for

publication).

Van't Riet, K., Bruijn, W. and Smith, J.M. (1976). Real and pseudo-turbulence in the

discharge stream from a Rushton turbine. *Chem. Eng. Sci.*, **31**, 407-412.

Weetman, R.J. and Oldshue, J.Y. (1988). Power, flow, and shear characteristics of

mixing impellers. *Proc. 6th Eur. Conf. on Mixing*, Pavia, Italy, BHRA Fluid Eng.

Cntr., Springer, 43-50.

Wu, H. and Patterson, G.K. (1989). Laser doppler measurements of turbulent flow

parameters in a stirred mixer. *Chem. Eng. Sci.*, **44**, 2207-2221.

Wu, H., Patterson, G.K. and van Doorn, M. (1989). Distribution of turbulence energy

dissipation rates in a Rushton turbine stirred mixer. *Expts Fluids*, **8**, 153-160.

Wygnanski, I. and Fielder, H. (1969). Some measurements in the self-preserving jet. *J.*

Flui Mech., **38**:577-612.

Table 3.1. Pumping number, N_q

Scale	Description	N (rpm)	Reynolds No., R_i	Pumping No. N_q
1:55	free impeller	50	5.0×10^3	0.72
1:55	free impeller	100	9.9×10^3	0.62
1:55	free impeller	200	1.99×10^4	0.57
1:41	free impeller	55	1.0×10^4	0.57
1:41	free impeller	100	1.82×10^4	0.42
1:55	draught tube	50	5.0×10^3	0.55
1:55	draught tube	100	9.9×10^3	0.54
1:55	draught tube	200	1.99×10^4	0.49
1:41	draught tube	55	1.0×10^4	0.55
1:41	draught tube	100	1.82×10^4	0.47
1:10	draught tube	10	3.10×10^4	0.63
1:10	draught tube	50	1.54×10^5	0.50
1:10	draught tube	70	2.15×10^5	0.44

Table 3.2. Power Numbers, N_p

Scale	Description	Power No. N_p
1:55	free impeller	2.3
1:41	free impeller	2.3
1:55	draught tube	3.0
1:41	draught tube	3.0

Table 3.3. Dimensionless characteristics of the impeller, $z/b = -0.5$

Description	Scale	2r/d	u/v_{tip}	v/v_{tip}	w/v_{tip}	q/v_{tip}
Free Impeller	1:55	1.044	0.44	0.73	0.18	0.85
	1:41	1.044				
Confined Impeller (Draught tube)	1:55 1:41 1:10	1.044 1.044 1.044	0.48	0.88	0.07	1.00

Description	Scale	2r/d	u'/v_{tip}	v'/v_{tip}	w'/v_{tip}	$k^{1/2}/v_{tip}$
Free Impeller	1:55	1.044	0.26	0.25	0.25	0.31
	1:41	1.044				
Confined Impeller (Draught tube)	1:55 1:41 1:10	1.044 1.044 1.044	0.25	0.20	0.18	0.26
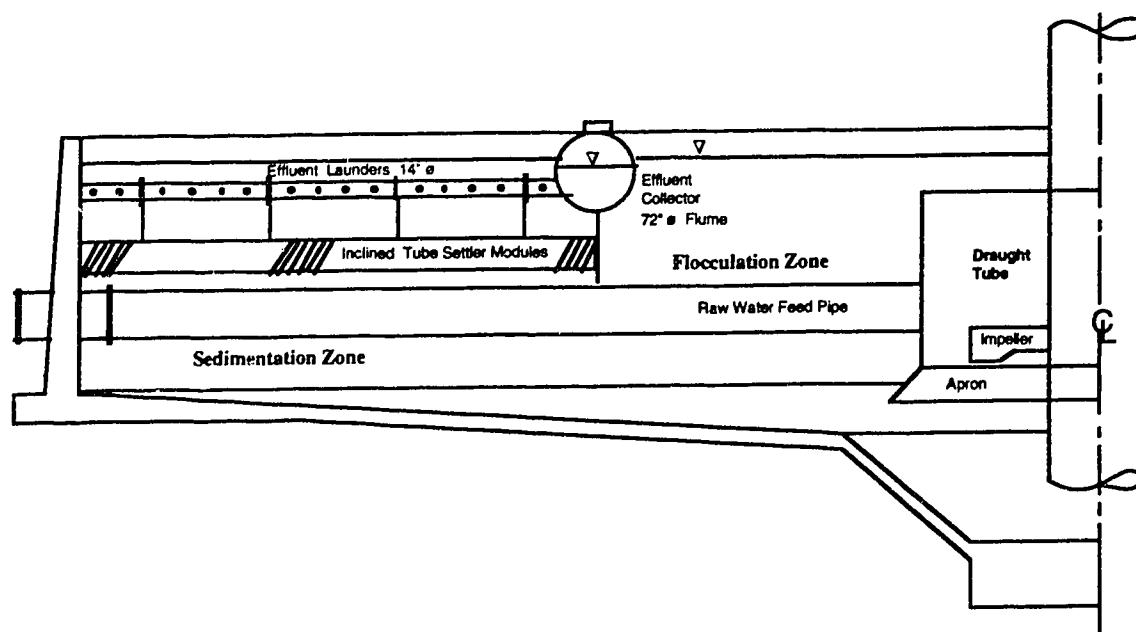
Figure 3.1.   Configuration of upflow solids-contacting clarifier at E.L. Smith Water
Treatment Plant (half section
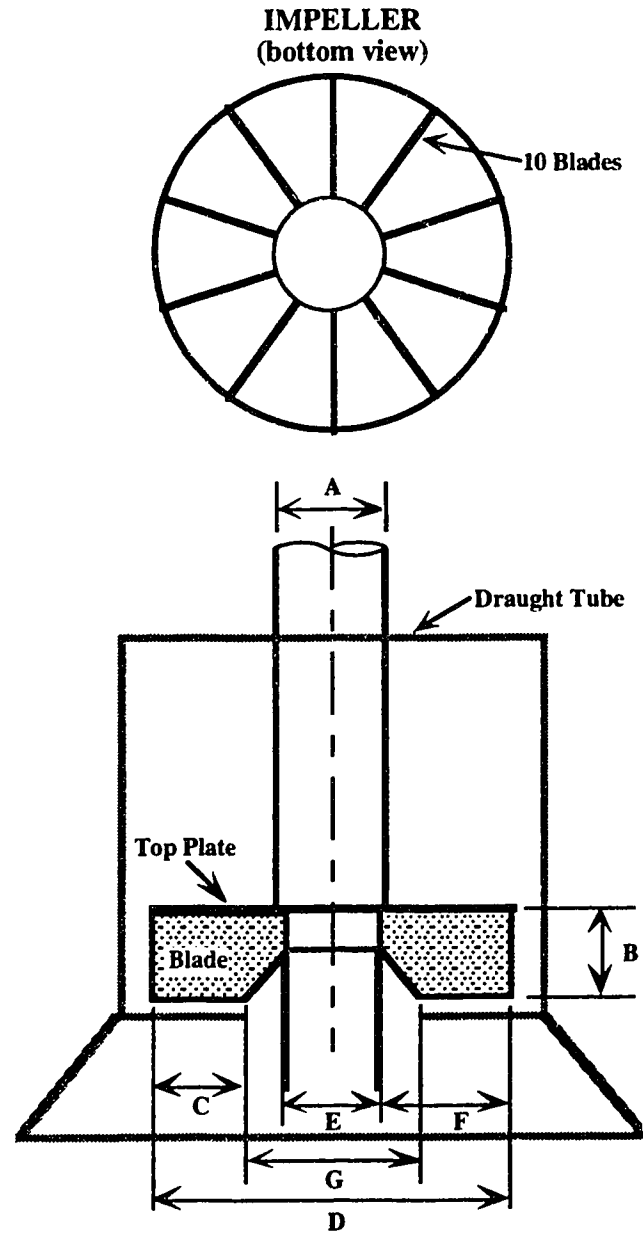
IMPELLER
(bottom view)

10 Blades

A

Draught Tube

Top Plate

Blade

B

C   E   F

G

D

All dimensions in mm

Dimension	1:55	1:41	1:10	Full-scale
A	24.6	33.3	140	1369
B	19.4	26.3	108	1083
C	18.5	25.0	103	1029
D	76.6	103.7	427	4267
E	19.5	26.4	107	1067
F	28.6	38.7	160	1600
G	39.7	53.7	221	2210

Figure 3.2. Impeller details
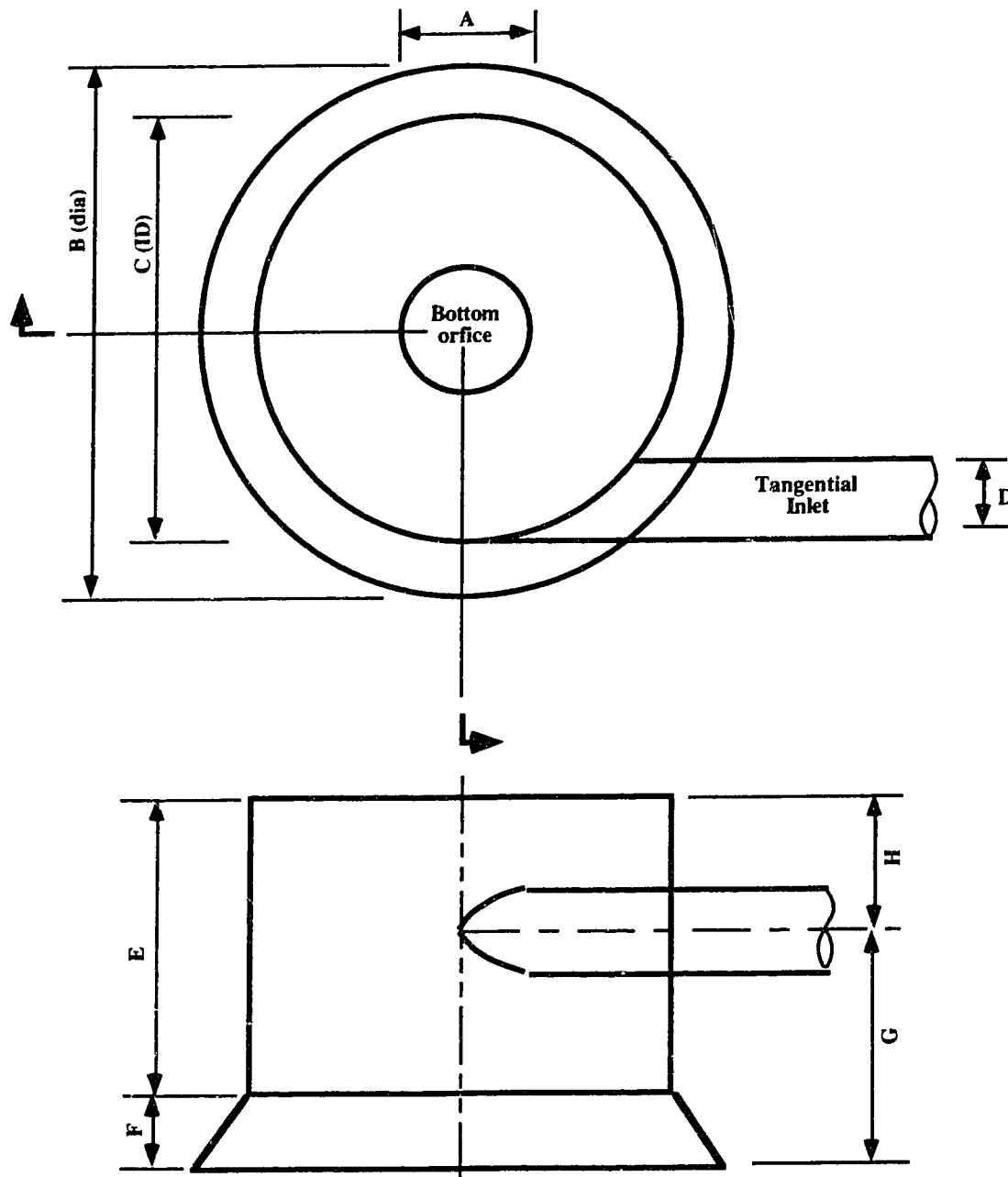
All dimensions in mm

Dimension	1:55	1:41	1:10	Full-scale
A	40.0	53.7	221	2210
B	137.0	18.5	760	7600
C	108.0	146.0	601	6007
D	-	-	152	1520
E	73.0	98.8	406	4064
F	19.1	26.2	107	1065
G	-	-	208	2083
H	-	-	198	1981

Figure 3.3 Draught Tube details
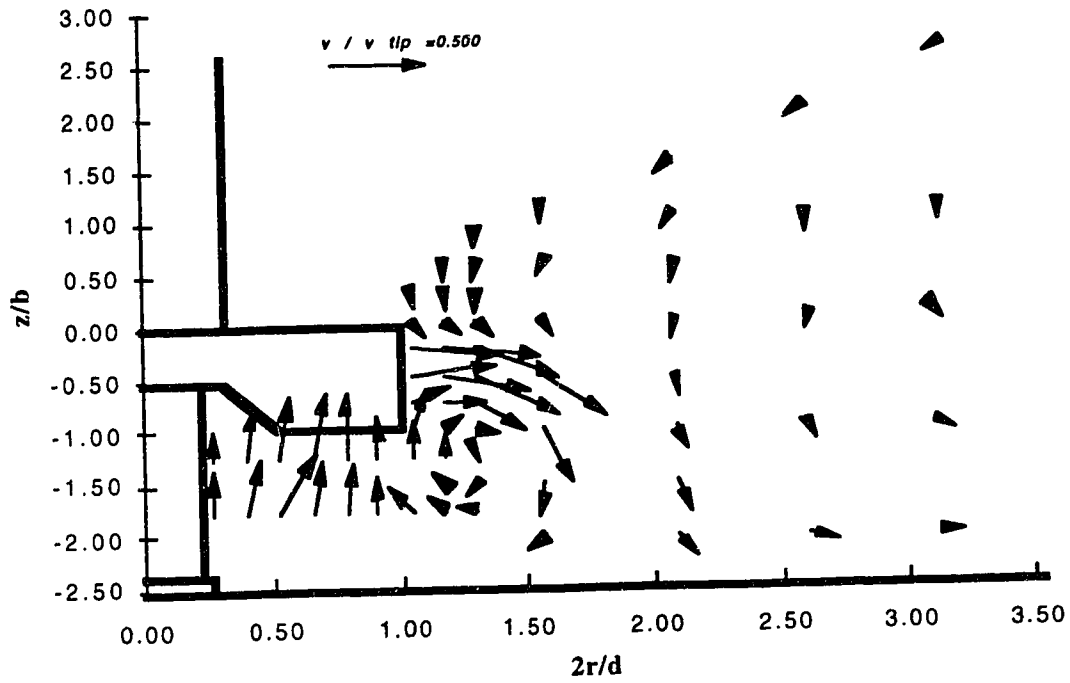
Figure 3.4. General flow patterns for free impeller. 1:55 scale; normalized by tip speed; d=76.6mm; b=19.4mm; 50 rpm
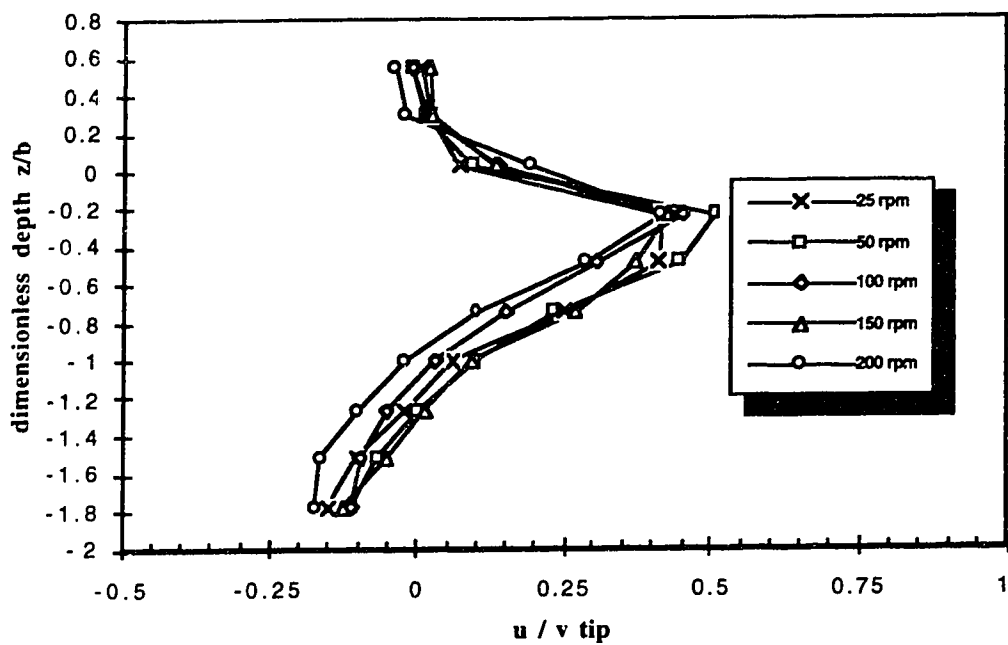
Figure 3.5.   Mean radial velocities for free impeller. 1:55 scale; normalized by tip speed;
d=76.6mm; b=19.4mm; 2r/d=1.175
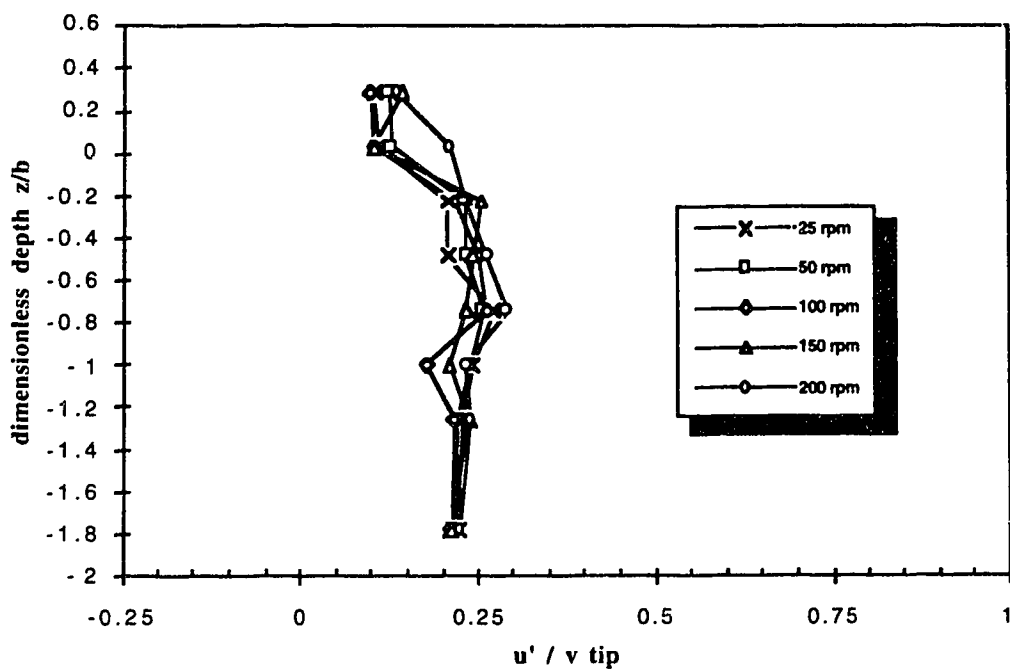
Figure 3.6.   Fluctuating turbulent radial velocities for the free impeller. 1:55 scale; normalized by tip speed; d=76.6mm; b=19.4mm; 2r/d=1.044
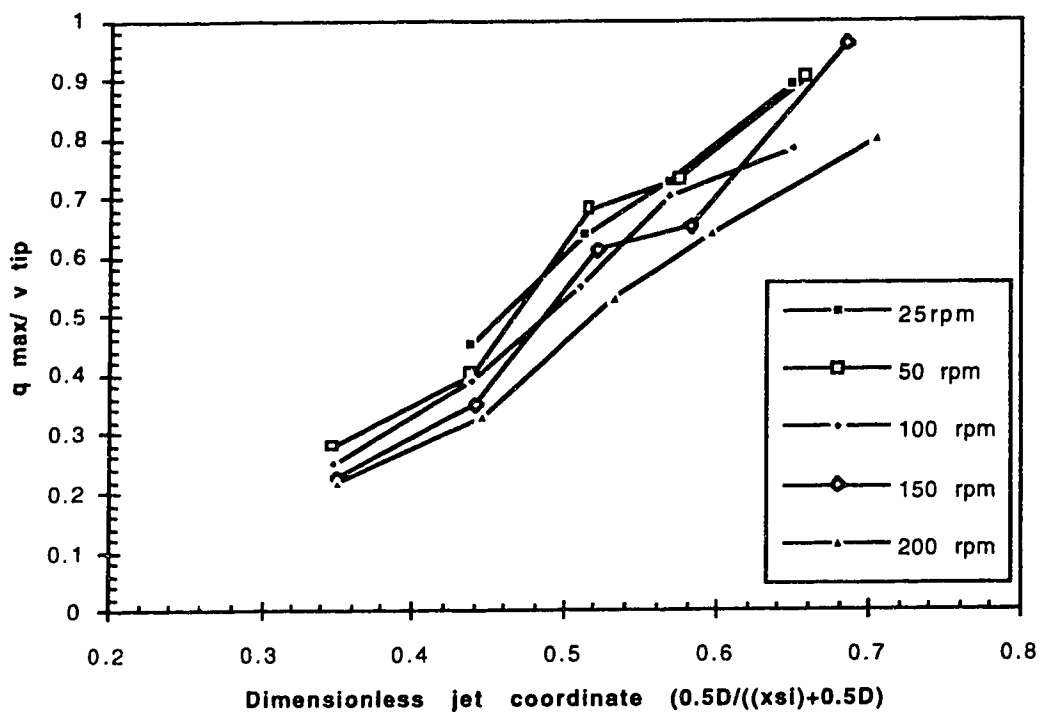
Figure 3.7.   Maximum resultant velocity along axis of the swirling radial jet. Free
impeller; 1:55 scale; normalized by tip speed; d=76.6mm; b=19.4mm.
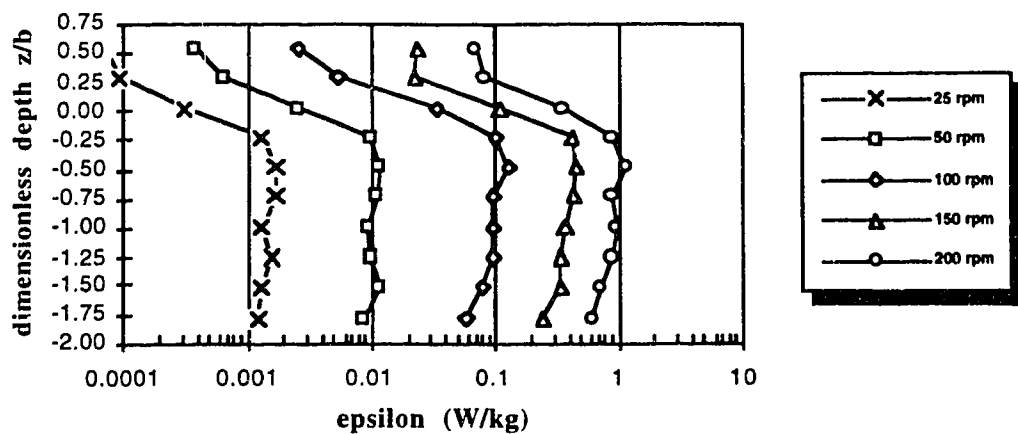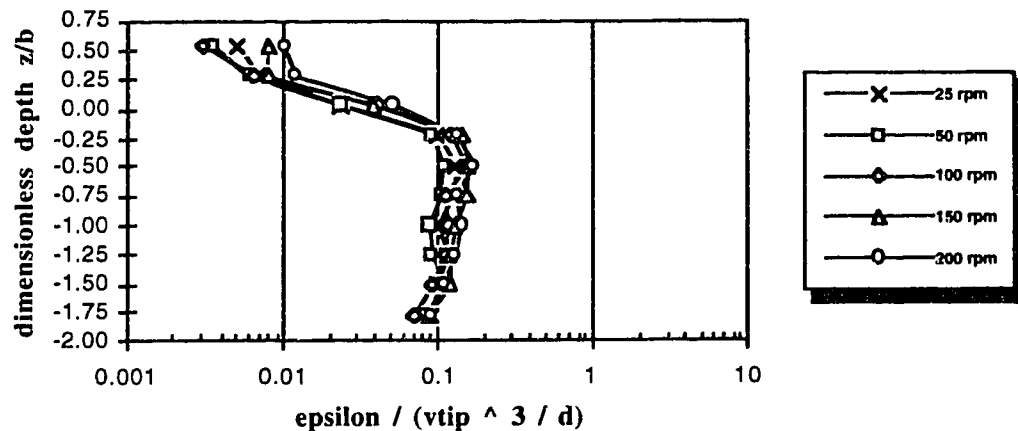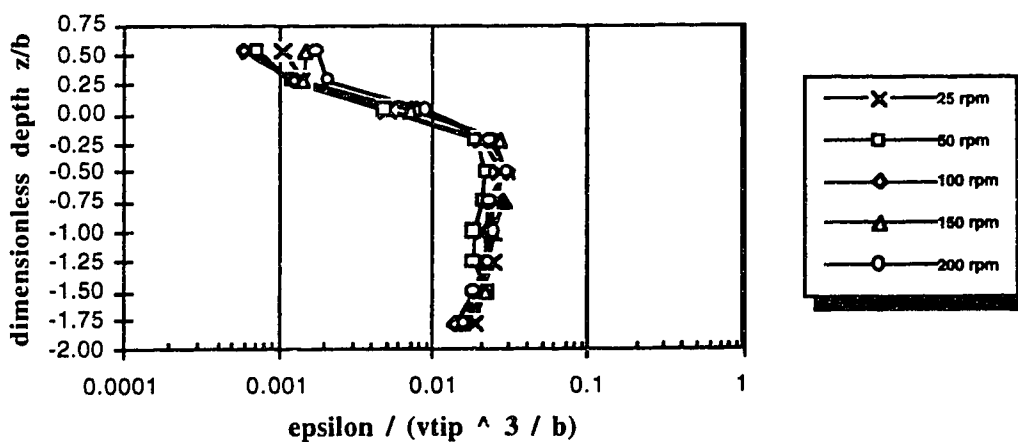
Figure 3.8. Local dissipation rates near the impeller. Free impeller; 1:55 scale; d=76.6mm; b=19.4 mm; 2r/d=1.175. a) dimensional; b) dimensionless-normalized by $\varepsilon / ((N\pi d)^3 / d)$; c) dimensionless- normalized by $\varepsilon / ((N\pi d)^3 / b)$
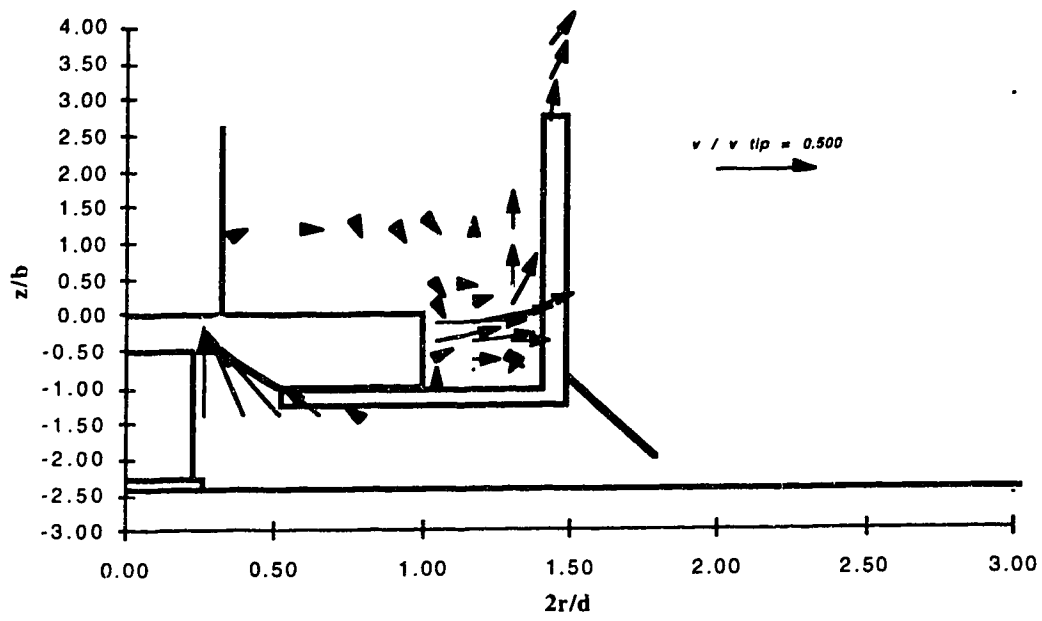
Figure 3.9.   General flow patterns for impeller with draught tube. 1:55 scale;
d=76.6mm; b=19.4 mm; 100 rpm
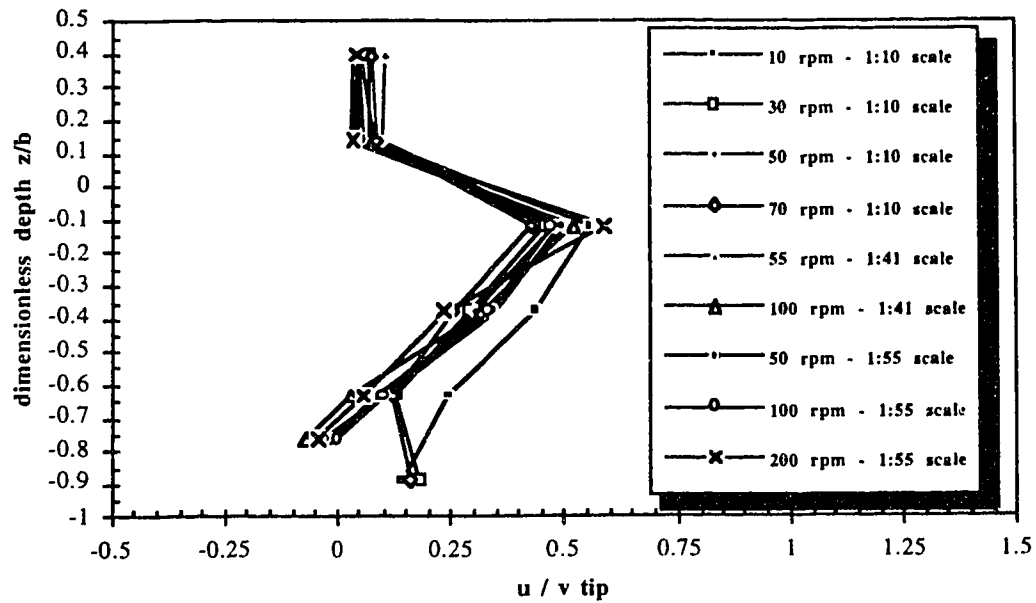
Figure 3.10. Radial velocity for impeller with draught tube. Normalized with tip speed;
Sclae 1:55, 1:41, and 1:10; d=76.6mm, 103.7mm and 426.2mm;
b=19.4mm, 26.3mm and 108.3mm; 2r/d=1.044.
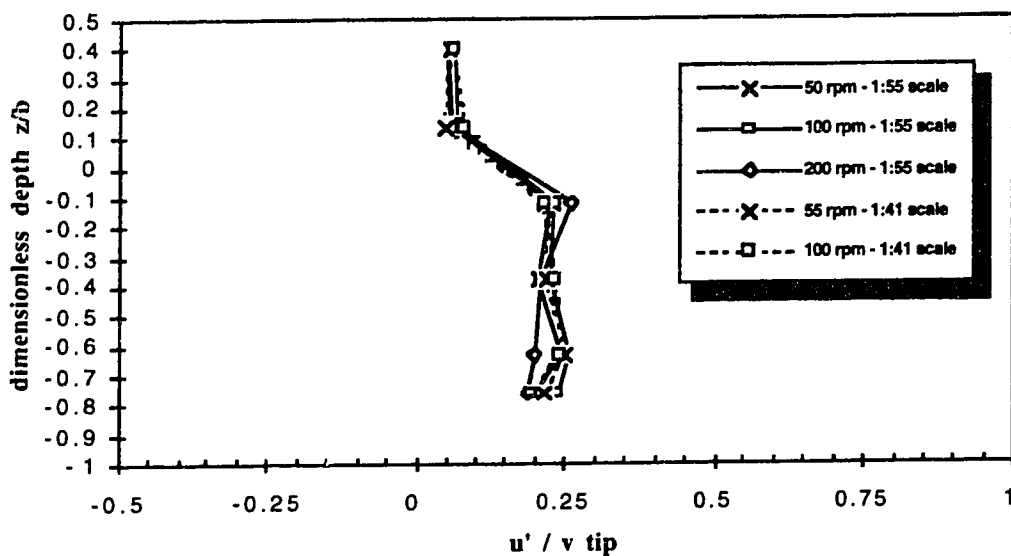
Figure 3.11.   Fluctuating turbulent radial velocities for impeller and draught tube. 1:55 and 1:41 scale; normalized by tip speed; d=76.6mm and 103.7mm; b=19.4mm and 26.3; 2r/d=1.044.
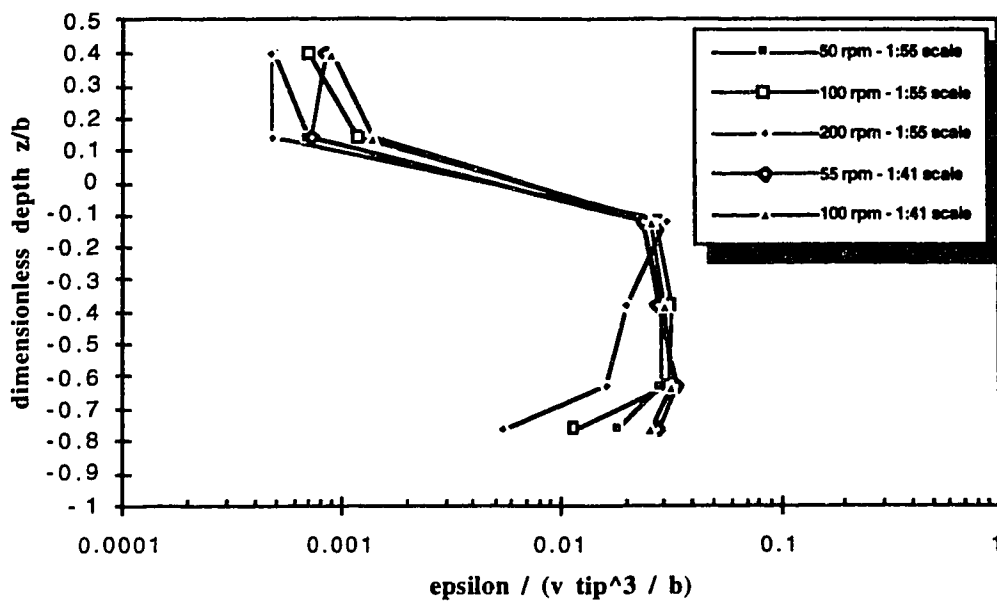
Figure 3.12. Local dissipation rates near the impeller. Impeller and draught tube; 1:55 and 1:41 scale; d=76.6mm and 103.7mm; b=19.4mm and 26.3mm; 2r/d=1.044; Dimensionless- normalized by $\varepsilon / ((N\pi d)^3 / b)$
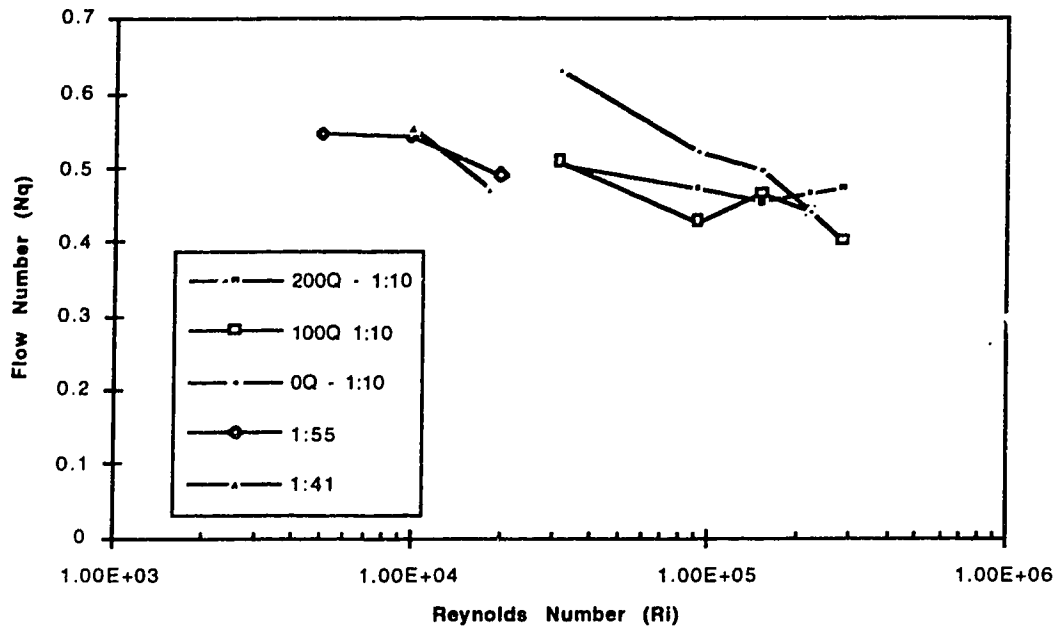
Figure 3.13. Variation in Flow Number, N_q, with tangential inflow. 1:55 and 1:41 scale
no tangential inflow; 1:10 - 0Q=no inflow, 100Q=100 ML/d inflow, 200Q=
200 ML/d inflow.

Chapter 4

Scaling of Forces on a Floc Particle[1]

4.1 Introduction

The process of flocculation is used in many water and wastewater treatment systems. The goal of flocculation is to form larger floc particles which can be more efficiently removed in the subsequent solids separation processes. Performance of the flocculation process and the subsequent separation processes is largely dependent on characteristics of the floc which is formed. For example, if the separation process used is sedimentation and the larger and more dense the floc is, the better the performance of the sedimentation process. Important floc characteristics such as size, strength and density are dependent on many factors. Some of these factors include: particulate matter being flocculated, coagulant or coagulant aid used, colloidal interaction, surface chemistry and hydrodynamic forces placed on the floc. As a result, floc characteristics are dependent on complex interactions between many chemical and physical processes. Due to these complex interactions, much of the design, assessment, optimization and operation of flocculation facilities relies heavily on bench and pilot scale testing. A classic example is the use of the jar test in water treatment to determine coagulant dose and mixing conditions for the full-scale system. However, to use results from the bench or pilot-scale they must be scaled-up for application at full-scale.

Rightly or wrongly, it has generally been assumed that factors such as colloidal interaction and surface chemistry are not sensitive to scale. However, the importance of scaling hydrodynamic forces on the floc, which are imposed by mixing have long been recognized. Traditionally, vessel-average parameters such as the volume average root-

---

mean-square velocity gradient, $\overline{G}$, has been used. It has been assumed that if $\overline{G}$ is held constant, the mixing environment should also remain constant (Camp and Stein, 1943). Standard practice for the scale-up of mixing has therefore involved maintaining a constant $\overline{G}$ between small-scale tests and the full-scale.

Although this has long been the practice, the success of using $\overline{G}$ as the scaling parameter for flocculant mixing is questionable and, as a result, successful scale-up of the flocculation process has also had to rely a great deal on experience. An example of some of the difficulties in scaling the flocculation process is highlighted in a recent study by Clark et al. (1994). In their study four different types of flocculation impellers were investigated at three different scales. For each type of flocculator, mixing conditions were scaled based on keeping a constant $\overline{G}$ for the three different sizes investigated. Although this is the standard practice it was found that performance of the flocculator varied with scale. A similar trend was found with all flocculators: performance deteriorated with increased size of the flocculator. This prompted the investigators to develop a number of recommendations for further study which included:

"there is a need for a detailed understanding of the fluid flow patterns induced by different flocculation impellers at different mixing intensities and of the impact of these fluid mechanics on floc size and floc structure"

"there is a need for a better understanding of how impeller fluid mechanics changes with scale and how these different fluid mechanics regimes affect flocculation-sedimentation performance"

In another multi-scale study Oldshue and Mady (1978) found that the optimum value of $\overline{G}$ for geometrically scaled vessels decreased with increased scale of the flocculator. This phenomenon has also been reported in the study of drop size in impeller

agitated mixing (Konno et al. 1983). Traditionally it has been assumed that the scale-up criterion for drop size was based on an equal power input per unit mass, which is equivalent to a constant $\overline{G}$. However, Konno et al. (1983) found that when the scale of the mixing vessel was increased keeping 100% geometric similarity, significantly different drop size distributions were found, even though equal power input per unit mass between the two scales was kept. The investigators concluded that the equal power input per unit mass is inappropriate as a scale-up criterion for the break-up process.

The above three studies cited illustrate some of the difficulties in scaling mixing and forces on flocs using vessel average parameters such as $\overline{G}$. Given the general trend towards more stringent requirements for both water and wastewater treatment systems, the need to better understand the mixing process in flocculation and to be able to confidently scale-up results from the bench and pilot-scale to full-scale has become a significant requirement in process design and assessment. This will require a more refined and fundamental approach to mixing and the forces it places on the floc.

There is a significant body of literature on the fundamentals of fluid-solid interactions and the forces that are placed on the floc (Matsou and Unno, 1981; Tambo and Hozumi, 1979; and Parker et al. 1972). Although many of these researchers developed rigorous and complex models describing hydrodynamic forces on a floc, due to the lack of data describing the complex flows found in impeller-agitated mixing vessels, most researchers simplified models such that the hydrodynamics could be described by easily measured vessel-average parameters such as $\overline{G}$. With the development of improved velocity measurement techniques, such as the laser doppler anemometer, detailed studies of turbulent flow in impeller-agitated vessels have begun to appear in the literature (see for example: Kresta and Wood, 1991 and 1993; Weetman and Oldshv 1988; Wu and Patterson, 1989; Wu et.al., 1989; Stanley and Smith, 1995; Stanley et al. 1995). These studies have highlighted the spatial variations of flow and energy dissipation within the

vessel and have shown that these are not represented by vessel-average parameters such as $\overline{G}$. This available information allows quantification of many of the terms developed previously to describe forces on flocs and eliminates the need to simplify equations to incorporate only easily measured vessel-average parameters. As a result, much of the original fundamental work on forces on flocs needs to be revisited.

Presented this chapter is an analysis of the scale-up of forces on flocs. Assuming that chemical processes are scale invariant, these forces tend to dictate many of characteristics of the floc and performance of the subsequent separation processes. Based on detailed characterization of turbulent flow in two types of flocculators with a 2-D laser doppler anemometer, forces on a floc were determined and scaling of these forces was discussed.

In scaling two different types of situations are normally encountered. In pilot-scale work the small scale is often geometrically scaled from the full-scale. This tends to simplify the scaling relationships, although the work by Clark et al. (1994), Oldshue and Mady (1978) and Konno et al. (1983) indicate that even in this simplified situation traditional scaling relations do not appear to be appropriate. A more complex situation that is often encountered is the scaling of two different physical arrangements that are not geometrically similar. An example of this is the jar test apparatus. In this case a two blade flat impeller in a square tank is used to represent all types of flocculators found in full-scale applications. For both situations, the scaling of forces on a floc will be discussed.

4.2 Forces on a Floc

Many floc characteristics, especially floc size, are dependent on two opposing factors, namely the mechanical strength of floc and the applied breaking forces. The mechanical strength of flocs is dependent on many factors. These include colloidal interactions, both the DLVO forces (van der Waals attraction and electrical repulsion) and

non-DLVO forces such as hydration effects, hydrophobic effects, viscous or hydrodynamic interactions, steric interactions and bridging (Gregory, 1989). These tend to impact the size and compactness of the floc matrix and the number and strength of bonds at the microparticle contacts. The size and shape of the microparticles, type of coagulant or coagulant aid used and water quality parameters can also impact the strength of the floc. Although the strength of flocs are of great practical importance, the effects of many of these factors on floc strength are still poorly understood (Gregory, 1989; Leentvaar and Rebhan, 1983). Generally it has been assumed that many of these factors are scale-invariant, and are accounted for by using the same water, including the particulate matter to be flocculated and coagulant in both the small and large scale systems.

The mixing of fluid which is required to promote agglomeration in flocculation will also cause forces to be placed on the floc which, if great enough, will cause break-up. Fluid induced stresses on the floc can be caused by shear stresses, drag stresses and differential pressure (i.e. normal stresses). Most flocculation processes occur in turbulent flow and, to determine turbulence induced stresses acting on particles, it is necessary to consider the structure and scale of turbulence in relation to particle size and motion in the fluid flow. Generally, turbulence production occurs at large scale with energy being transferred down through smaller scale eddies until it is dissipated at small scales. Of interest is the relation between the smallest length scales and particle size. The smallest sustainable eddy is given by the Kolmogorov's microscale (η) which, based on dimensional arguments is given by:

$$\eta = \left(\frac{v^3}{\varepsilon} \right)^{1/4}$$

(4.1)

where v is the kinematic viscosity, and ε, the energy dissipation rate per unit mass. When eddies are larger than the particle, the eddies tend to entrain particles, thus causing little surface stress, with laminar shear being the dominate stress. If eddies are smaller than

the size of the particles, these eddies can provide particle shear, surface drag and pressure forces. As a result the relation between η and particle size is of importance. When the floc size is greater than η, inertial effects in the fluid will be more likely to cause break-up. This is commonly referred to as the inertial convection subrange. Levich (1962) states that the break-up phenomena in this range is related to the fact that the turbulent velocity in a turbulent stream varies from one point to another. Therefore different dynamic pressures will be exerted at different points on the floc and will lead to break-up if these forces are great enough. The difference in dynamic pressures exerted on opposite sides of the drop, Q, with a diameter, d, is given by:

$$Q \propto \frac{\rho(v_1^2 - v_2^2)}{2} \tag{4.2}$$

where v_1 and v_2 are velocities separated by distance d, equal to the diameter of the particle. For large scale eddies, velocities vary little over small distances; it is small eddies in the range of the floc diameter that are responsible for greatest variation in v. In the inertial convection subrange Batchelor (1958) showed the turbulent velocity difference, v_λ, at a distance, λ, is given by:

$$v_\lambda \propto (\varepsilon\lambda)^{1/3} \tag{4.3}$$

Setting λ equal to the diameter of the floc (it is eddies of this size which are most significant) and substituting (4.3) into (4.2) the following is obtained:

$$Q \propto \rho\varepsilon^{2/3}d^{2/3} \tag{4.4}$$

The total dynamic force acting on the floc in the inertial convection subrange, F_{DI} is given as:

$$F_{DI} \propto \rho\varepsilon^{2/3}d^{8/3} \tag{4.5}$$

This force equation, although in a different form, has the same reliance on ε as that developed by Tambo and Hozumi (1979) and Parker et al. (1972) for flocculation of particles and is widely used in drop break-up studies (see for example Davies (1987); Hesketh et al. (1987); and Clark (1988)). Although the force exerted on the floc in the inertial convection subrange is similar for both Tambo and Hozumi (1979) and Parker et al. (1972), different approaches were used to relate this force to a maximum stable floc size. The maximum stable floc size is determined by relating the forces acting on the floc described by (4.5) for the inertial convection subrange to the ability of the floc particle to resist this force. For drops, this is simplified, as relations exist linking drop size and properties to its ability to resist forces acting on it. The general resisting force of a drop, F_R, is given as:

$$F_R \propto \sigma d \tag{4.6}$$

where σ is the interfacial tension. Equating (4.5) to (4.6) the maximum stable drop, d_{max} size is given as:

$$d_{max} \propto \sigma^{0.6} \varepsilon^{-0.4} \rho^{-0.6} \tag{4.7}$$

Equation (4.7), first proposed by Kolmogorov (1949) and Hinze (1955), has been successfully applied in many studies of the break-up of drops in the inertial convection subrange. For flocs a similar and universal relation for floc strength, F_R, is not available due to the many factors affecting it. Tambo and Hozumi (1979) related the binding force of a floc to:

$$F_R \propto \sigma d^{2(1-K_p/3)} \tag{4.8}$$

where K_p is the floc density function and ranges from 1.0 to 1.5. If K_p is equal to 1.5, (4.8) becomes equivalent to (4.6) and the formula for d_{max} is equivalent to (4.7). Based on

various values of K_p their formula for d_{max} for the interial convection subrange was given as:

$$d_{max} = K^* \varepsilon^{-(0.5 \text{ to } 0.4)}$$ (4.9)

Parker et al. (1972) assumed that the strength of the floc was dependent on τ_y, which is not directly related to floc diameter. As a result although the force on the floc was equivalent to (4.5) the equation for d_{max} differs and is given by:

$$d_{max} = C_1 \left(\frac{\varepsilon}{v} \right)^{-1} = C_1 \overline{G}^{-2}$$ (4.10)

where C_1 is a constant which incorporates a number of terms including τ_y. The far right-hand of the equation was obtained by:

$$\overline{G} = \sqrt{\frac{P}{V\mu}} = \left(\frac{\overline{\varepsilon}}{v} \right)^{0.5}$$ (4.11)

where P is the power input in the vessel and V the volume of the vessel.

As the mixing intensity in many flocculators is low and, hence, the Kolmogorov microscale, η, can be quite large, often the flocs are in the viscous subrange $d \ll \eta$. In this range, viscous stresses due to the motion of the larger eddies are responsible for forces placed on the floc and not inertial forces as in the inertial convection subrange. The viscous shear can be related to $\{\mu(du / dr)\}$ which is proportional to $\mu(\varepsilon / v)^{0.5}$. The force on the floc in the viscous subrange, F_{VS}, is given as:

$$F_{VS} \propto \mu(\varepsilon / v)^{0.5} d^2$$ (4.12)

For drops this equation can be equated to (4.6) and yields:

$$d_{max} \propto \sigma \mu^{-1} v^{0.5} \varepsilon^{-0.5}$$ (4.13)

Again this equation has been used su..:essfully for drops in the viscous subrange (Bourne and Baldyga, 1994). Parker et al. (1972) using a significantly different approach obtained a similar formula for flocs in the viscous subrange, given as:

$$d_{max} = C_2 (\varepsilon / v)^{-0.5} = C_2 G^{-1} \tag{4.14}$$

where again C_2 is a constant which incorporates a number of terms including τ_y but it is not equivalent to C_1.

Another approach for the viscous subrange was proposed by Kolmogorov (1949) in which the change in velocity v_λ is given by $\mu(\varepsilon / v)^{0.5}$, which is correct. However, this term was substituted in (4.2) for dynamic pressures exerted on opposite sides of the drop. Using this approach, d_{max} for a drop is given as:

$$d_{max} \propto (\sigma v / \rho \varepsilon)^{1/3} \tag{4.15}$$

This approach has been criticized by Levich (1962) and Shinnar (1961) as stresses are viscous if d << η and not inertial. Most recent work in drop breakup has used (4.13) rather than (4.15) (see for example Clark, 1988). However, it was this approach which was used by Tambo and Hozumi (1979) which resulted in the force acting on the floc being given as:

$$F_{VS} \propto (\varepsilon / v)d^4 \tag{4.16}$$

It is important to note the difference in the exponent on ε between (4.12) and (4.16).

Normally in turbulent flow the greatest change in velocity across the floc is due to turbulent fluctuating velocities and velocity gradients in the mean flow are much smaller. They are therefore commonly ignored. However, at solid boundaries such as vessel walls and the impeller surface, mean velocity gradients may approach or exceed those due to the turbulent velocity fluctuations. Levich (1962) and Thomas (1964) showed that for drops

near the wall of a pipe, shear due to mean velocity gradients can be greater than those due to turbulent fluctuating velocities. In simple shear flow the force on the floc, F_{ss}, can be expressed as:

$$F_{ss} \propto \tau d^2 \qquad (4.17)$$

where τ is the shear stress given as $\mu \dfrac{du}{dr}$.

Due to the lack of detailed hydrodynamic data on turbulence in flocculators, most experimental research has represented ε by the vessel average parameter $\overline{G}$, by using (4.11). The maximum floc diameter, d_{max}, is then related to mixing intensity as:

$$d_{max} \propto G^{-n} \qquad (4.18)$$

Table 4.1 gives experimental and theoretical values of n which have been reported in the literature. As shown in the table, values vary widely, making it difficult to choose the most appropriate value for scale-up. Much of the difficulty can be related to the fact that the vessel average $\overline{G}$ is used. Studies have shown that dissipation rates within an impeller-agitated vessel vary greatly and, in a flocculator, areas of high energy tend to dictate the maximum floc size. The relation between local values of dissipation rates and vessel-average values is highly dependent on the type of impeller and geometry of the vessel, resulting in different hydrodynamic conditions if different types of flocculators are used. In addition, most of the equations given above are non-linear in ε and spatial variation in energy dissipation in the flocculator cannot be accounted for by average values (Clark 1985). Trying to choose a scaling relation based on a theoretical basis is also complicated by the lack of a firm relationship describing floc strength characteristics.

An alternative approach is to obtain a more refined specification of hydrodynamics with an impeller-agitated vessel in which localized forces placed on a floc can be determined. Areas of higher forces will tend to govern floc size. Scaling relations can be

developed for local floc forces which will allow the matching of the floc forces in the small

and large scales. Noting that many of the factors that effect floc strength appear to be

independent of scale, if floc forces are the same so should be the performance of both

systems. Methodologies to accomplish this will be discussed.

4.3 Experimental

Results from two previously completed studies will be used to characterize the

hydrodynamics in an impeller agitated flocculator. General details on these studies can be

found in Stanley and Smith (1995) and Stanley et al. (1995). In addition, a significant

amount of additional information obtained from these studies will be reported herein which

was not presented in the previous publications. The first study involved the

characterization of hydrodynamics in a standard square jar test apparatus, which is used at

full-scale plants to determine coagulant doses and mixing requirements and has also been

used for many research studies. The jar test used was a standard 2 L (115mm x 115mm x

150mm) square jar test apparatus with a 76 mm diameter flat blade impeller, as described

by Hudson and Wagner (1981). Flow characteristics in this vessel were determined by

measurements with a 2-D laser doppler anemometer (LDA), which will be described later.

The primary purpose of the study was to determine variation in local hydrodynamic

characteristics within the vessel, relate them to vessel average parameters and see how these

characteristics changed with changes in impeller speed. The second study involved, once

again, the characterization of flow in a flocculator. However, this flocculator was

significantly different from the jar test, as it was the reactor zone of an upflow solids-

contacting clarifier which acts as the flocculator in this type of clarifier. The type of

clarifier investigated is currently used at the E.L. Smith Water Treatment Plant, a large (200

ML/d) facility in Edmonton, Alberta, Canada. Documentation of flow conditions in the

upflow solids-contacting clarifier was accomplished through the measurement of turbulent

flow in two small scaled models, measurement of mean flow characteristics in an

intermediate scale model and limited testing on the full-scale clarifier. The three model-scales, maintaining geometric similarity, used in the study were 1:55, 1:41 and 1:10, which correspond to impeller diameters of 76.6 mm, 103.7 mm and 427 mm, respectively. The full scale impeller diameter is 4270 mm. Figure 4.1 shows the impeller and draught tube. The two small scale models were constructed to represent only the flocculation zone of the clarifier and were constructed of transparent acrylic or polycarbonate as the velocity measurements were accomplished with the use of a LDA. The 1:10 model represents a faithful reproduction of the entire clarifier, complete with a tangential inflow pipe, flocculation zone, settling zone, tube settlers and perforated launders. Two of the primary purposes of this study were first to, determine the effect of scale on flow characteristics as the work covered impeller diameters from 76.6 mm to 4270 mm, and second to investigate whether methods of analyzing impeller-agitated flow which have been reported for relatively simple mixing systems (impeller placed in a large baffled tank) were appropriate for a more complex flow situation such as the impeller placed in a draught tube. It should also be noted that the type of impeller investigated is significantly different to those previously reported.

In the jar test vessel and the 1:55 and 1:41 scale clarifier models radial, axial and tangential velocities were measured with a Dantec 2-D LDA, in the forward scatter mode using a 300 mW Argon-ion laser. To allow measurement of reversing flows the frequency of one beam for each velocity component was shifted by 40 MHz using a Bragg cell. Bandpass input filters were set at a bandwidth of 0.4 MHz. Signal processing was accomplished with a Particle Dynamics Analyzer, covariance signal processor. It has the ability to handle higher data rates and lower signal-to-noise ratios than traditional counter and tracker signal processors. The laser system contains a built-in laser diode which generates calibration signals that are fed via a fibre optic cable to the receiving optics to ensure that the equipment is automatically calibrated. All velocity measurements were validated based on signal-to-noise levels and fringe counts. To eliminate velocity bias,

moments were calculated by residence time weighting. For the set-up used in this study the measuring volume at the beam crossing was 0.12 mm x 0.12 mm x 2.4 mm. Care was taken to ensure that the frequency of data collection was below the phase ambiguity noise limit. More details on the LDA system and concerns with the phase ambiguity noise limit can be found in Stanley and Smith (1995).

To measure velocities in the 1:10 model, a Nixon propeller meter attached to a Novonic Streamflow processor use used. Given the spatial limitations presented in the model only radial and tangential velocities could be measured. This meter was calibrated by means of a velocity measurement across a rectangular flume under conditions of steady flow. To measure the impeller's power consumption, torque was measured with a model TRPA5 Rotary Parallel Shaft torque transducer manufactured by Industrial Measurements Ltd. This device was connected to a special conditioning unit which gives readout in Nm directly.

Results from the measurements will be presented as they apply to forces acting on the floc. As mentioned, a more detailed presentation of general hydrodynamic conditions in these flocculators can be found in Stanley and Smith (1995) and Stanley et al. (1995).

4.4 Hydrodynamics of Impeller Agitated Flocculators

Figure 4.2 presents a typical impeller-agitated mixing vessel. The figure shows dimensions used to describe the geometry of the vessel. Also shown in Figure 4.2 are four zones in which the hydrodynamics of each of these zones will be described separately. A brief discussion of vessel average parameters will also be presented.

4.4.1 Vessel Average Parameters

Due to the complexities of impeller-generated turbulent flow the traditional approach in analysis and assessment has been based on vessel-average or bulk parameters. Through

dimensional analysis (Rushton, 1951) it has been shown that bulk mixing in impeller-agitated flow can be described by the following dimensionless quantities:

$$R = \frac{D^2 N}{v} \qquad (4.19)$$

$$N_p = \frac{P}{\rho D^5 N^3} \qquad (4.20)$$

where D is the diameter of the impeller, N is the rotation speed, v is the kinematic viscosity, g acceleration due to gravity, ρ the density of the fluid, P the power input into the tank, R is the Reynolds number (ratio of inertial to viscous forces), and N_p the power number (analogous to a drag coefficient). The Froude number Fr (ratio of inertial to gravitational forces) is also frequently included in these dimensionless quantities; however it has generally been founded that if impeller-agitated mixers are well baffled, the effect of Fr is effectively suppressed.

An additional parameter used to describe bulk flow is the flow number or the pumping number, N_q:

$$N_q = \frac{Q}{ND^3} \qquad (4.21)$$

where Q is the impeller generated flow rate. As discussed, in the field of coagulation and flocculation the root mean square velocity gradient $\overline{G}$, has long been used. The equation for $\overline{G}$ was given earlier in (4.11).

At sufficiently high Reynolds' numbers (fully turbulent flow) it has been found that the power number, N_p, becomes constant and should be constant for the same type of impeller at different scales. This was found to be the case for both the jar test impeller and the clarifier impeller. For the jar test impeller N_p became constant at a value of R greater than 2,000 and was equal to 2.1. However, only one scale was tested. For the clarifier impeller the value was constant for $R \geq 10,000$ and was the same for the different scales

investigated and equal to 3.0. Using N_p, $\overline{G}$ can be written in terms of vessel geometry and impeller properties, assuming fully turbulent flow:

$$\overline{G} \approx \sqrt{\frac{N_p D^5 N^3}{v(T^2 H)}} \tag{4.22}$$

If flocculator units are scaled keeping geometric similarity, the ratio between D:T:H will remain constant. If the same type of impeller is used in each system N_p should also remain constant. This allows all vessel dimensions to be given in terms of D and the following relation can be developed:

$$\overline{G} \propto N^{1.5} D \tag{4.23}$$

Noting that $\overline{G} \propto \left(\overline{\varepsilon}\right)^{0.5}$ the vessel average force on the floc in both the inertial convection subrange $(d \gg \eta)$ and the viscous subrange $(\eta \gg d)$ can be determined.

$$F_{DI} \propto \rho(N^3 D^2 / v)^{2/3} d^{8/3} \qquad (d \gg \eta) \tag{4.25}$$

$$F_{VS} \propto \mu(N^3 D^2 / v)^{0.5} d^2 \qquad (\eta \gg d) \tag{4.26}$$

For two geometrically scaled flocculators of impeller diameters D_1 and D_2, to keep vessel average forces on the floc equal in both systems, the following relation must be met.

$$\frac{N_1^{1.5} D_1}{N_2^{1.5} D_2} = 1 \tag{4.27}$$

This equation is valid for both the viscous and inertial subranges and is equivalent to keeping $\overline{G}$ constant. If the two vessel were not geometrically similar, a relationship could be developed equating (4.22) for both systems and using appropriate values for T, H, D and N_p.

As mentioned, use of vessel average parameters may not be appropriate and will be discussed in greater detail later.

4.4.2 Impeller Discharge Zone

The impeller discharge zone is the area within the vessel of highest velocity and turbulent kinetic energy. This zone has been successfully described by the analogy of the flow to swirling radial jet (Kolar, Filip and Curev, 1984; Kolar, Filip and Curev, 1985; Filip, Kolar and Curev, 1985a; Filip, Kolar and Curev, 1985b; Filip, Kolar and Curev, 1986; and Kresta and Wood, 1991). However, most of the studies above were modeling studies and experimental work, especially at multi-scales and complex flow such as that found in the clarifier investigated, had not been completed. To investigate the applicability of using the swirling radial jet analogy for the two flocculators analyzed, results from the LDA measurements in the impeller zone were compared to literature data available on swirling radial jets. Focus was placed on the clarifier impeller as the flow was more complicated and multi-scale testing was performed.

To characterize the swirling radial jet it must be recognized that the jet produced by the impeller has both a radial and tangential velocity component and therefore the axis of the jet does not follow the traditional radial and tangential coordinate systems used in mixing tank analysis. A new geometric variable, ξ, originally described by Kolar, Filip and Curev (1982) is used to represent the distance along the axis of the swirling radial jet.

$$\xi = \sqrt{r^2 + e^2} \tag{4.28}$$

where r is the radial distance from the center of the tank and e represents the ratio of the radial momentum to the angular momentum within the swirling radial jet. In practice, e may be fully defined for a given set of conditions from a single measurement of the radial and tangential velocities at the impeller's periphery. Details and formulation on this can be found in Stanley et al. (1995). This relationship allows coordinate ξ to be determined for any radius, r. The vector sum of the radial and tangential velocities may be made in order to define a new velocity, q, which is the local velocity along the axis of the swirling radial

jet. With the use of transforms of q and ξ, characteristics of the impeller-induced jet, such as the width of the jet and maximum jet velocity can be determined using traditional formulae for radial jets.

The first set of experiments was conducted on the free clarifier impeller (no draught tube in place). The 1:55 and 1:41 scale impellers were placed in a large tank (D/T = 0.22) and LDA measurements were taken to characterize the impeller discharge. Mean and fluctuating velocities were determined in three dimensions. For the two different scales and impeller speeds from 25 to 200 rpm it was found that both the mean velocities and fluctuating velocities scaled on the tip speed of the impeller. Figure 4.3 shows the resultant velocity, q, for the free impeller, scaled on the tip speed. To assess the applicability of the swirling radial jet, results from the impeller discharge were compared to published results for true radial jets by Rajaratnam (1976) and Heskestad (1966) for the change in maximum velocity along the axis of the jet, growth of the width of the jet and the ratio of the fluctuating velocity u' to mean velocity U. In each case, results from the impeller discharge zone compared favorably to results reported from true radial jets (Stanley et al. 1995), giving confidence in the use of the swirling radial jet analogy for the discharge zone.

To determine forces on flocs, it is required that local energy dissipation rates be determined in the discharge zone. A number of methods are available to determine dissipation rates; however for stirred tanks the most appropriate methods are based on the fact that all the kinetic energy, k, being transferred from the large scale eddies where turbulence production is occurring must be dissipated by the small scale eddies (Kresta and Wood, 1993; and Stanley and Smith, 1995). An estimate of kinetic energy, k, is given by:

$$k = \frac{\overline{u'_z}^2 + \overline{u'_r}^2 + \overline{u'_t}^2}{2}$$

(4.29)

Knowing the rate at which kinetic energy is transferred down through the eddies, an estimate of ε can be obtained from:

$$\varepsilon = A \frac{k^{\frac{3}{2}}}{L} \qquad (4.30)$$

where A is a constant and L is a characteristic length scale. From equation 4.29, if the turbulence is assumed to be isotropic $k^{1/2} \approx u'$. This relation, along with a description of the characteristic length scale can be used to develop an appropriate scaling relationship. Generally, the characteristic length scale, L, is determined by equating it to the Eulerian integral length scale. The analogy of the swirling radial jet is a powerful tool in determining L. Studies of jets have shown that the Eulerian integral length scale can be related to 1/2 of the total jet width (Antonia, et al., 1980). The initial width of the jet produced by a radial impeller has been shown by many to be equal to the width of the impeller blade and hence the Eulerian integral length scale can be related to 1/2 the blade width, near the impeller. Noting that the fluctuating velocities (u') scaled on the tip speed of the impeller $(N\pi D)$ and that L can be related to the width of the blade, the following scaling relation can be developed for ε, in the impeller discharge zone.

$$\varepsilon = K_\varepsilon \frac{(N\pi D)^3}{b} \qquad (4.31)$$

A similar scaling relation $((N\pi D)^3 / D)$ has been proposed by Kresta and Wood (1991); however, it is only applicable for comparison with other types of impellers when the D/b ratio (diameter to width of impeller) is constant, as D is being used to represent the length scale which is really dependent on b. For Rushton turbines, the most frequently studied turbine, the D/b ratio is 5. For the clarifier impeller the ratio is 3.95 and for the jar test impeller the ratio was 3. For this reason it is better to use $((N\pi D)^3 / b)$ as it does not require a constant D/b ratio for comparison purposes. Figure 4.4 shows dissipation rates for the clarifier impeller scaled using $((N\pi D)^3 / b)$. As described in Stanley et al. (1995), the use of this relationship should be applicable to many types of radial flow impellers. For the clarifier impeller $k^{\frac{1}{2}} / (N\pi D)$ was found to range from 0.26 to 0.31. For the jar test

impeller $k^{\frac{1}{2}} / (N\pi D)$ was found to be in the range of 0.26 . As $k^{1/2}$ is representing u' and

U_O is equal to the v_{tip}, the value reported for $k^{\frac{1}{2}} / (N\pi D)$ would be equivalent to u'/U_O.

The concept of a constant u'/U_O has long been recognized in turbulent jets. Antonia et al.

(1980) reported a value of u'/U_O of 0.32 for a circular jet and which was similar to the

value from Wygnanski and Fielder (1969) of 0.31 for the same kind of jet. For a radial jet,

u'/U_O was report by Heskestad (1966) to be 0.33. Note that values are similar to those

found for impellers, even though the device generating the jet are significantly different.

For the 1:10 scale clarifier model only mean velocities could be determined and in the full-

scale clarifier only a bulk flow determination could be made. However, it was found that

mean velocities scaled tip speed of the impeller, right from impeller diameters from 76.6

mm to 4267 mm. Given the above discussion of constant u'/U_O in jets and that this was

found to be the case in the two small-scale clarifier models in which u' could be measured,

equation 4.31 should be applicable for a wide range of situations. Values for K_ε were

found to be 0.032 for the clarifier impeller and to range from 0.033 to 0.047 for the jar test

apparatus. Analysis of data from Wu et al. (1989) for a Rushton turbine found that using

there reported results for ε, the calculated values for K_ε were found to varied from 0.018

to 0.07. Again close to values found in this study, even though their methods of

calculating ε were significantly different than those used in this study.

An important point to note about equation (4.31) is that the local energy dissipation

rate ε, is independent of the vessel geometry, and only dependent on the dimensions of the

impeller, D and b, and the impeller rotation speed N. This fact was highlighted in the study

of the clarifier impeller. Tests were done both with the free impeller (D/T = 0.22) and the

confined impeller in which the impeller was placed in the draught tube with D/T = 0.71,

which represents a reduction in vessel volume of about 10 times. Even with this great

reduction in vessel volume the value of K_ε remained constant, indicating that ε in the

discharge zone is truly independent of vessel dimensions and only dependent on impeller characteristics.

If one uses equation (4.31) the following relationships can be developed for the forces on the floc.

$$F_{DI} \propto \rho(N^3D^3 / bv)^{2/3}d^{8/3} \qquad (d >> \eta) \tag{4.32}$$

$$F_{VS} \propto \mu(N^3D^3 / bv)^{0.5}d^2 \qquad (\eta >> d) \tag{4.33}$$

It is interesting to note that if the flocculator is scaled based on 100% geometric similarity, the ratio b/D should remain constant and b can be written in terms of D. In this case with 100% geometrically similar flocculators, scaling the mixing based on keeping a constant $\overline{G}$ will also result in maintaining a constant local dissipation rate ε, in the impeller discharge zone. It should be emphasized that this only occurs if 100% geometric similarity is kept as all dimensions can be related to impeller diameter. It should also be noted, that although the forces have the same proportional relationship to N and D, the magnitude of the forces are quite different. For example in the jar test apparatus the local dissipation rate in the discharge zone is 4 to 6 times higher than the vessel-average dissipation rate. The magnitude of the difference in local to vessel average dissipation rates may also impact the range of turbulence the flocs fall into. As vessel-average dissipation rates are lower, the corresponding Kolmogorov's microscale, η, calculated on this vessel-average value will be larger. Generally, in most flocculation processes, calculation of η, based on vessel-average values indicates that the flocs are in the viscous subrange, for sizes of flocs normally found in water treatment. At higher $\overline{G}$ values, but still ones commonly used in flocculation, results from the jar test data indicate that η may approach and go below 100 μm in the impeller discharge zone, which is a typical size of flocs found in water and wastewater treatment.

4.4.3 Impeller Zone

The impeller zone is the area of the tank where energy is transferred to the flow. In this region there will be high turbulent kinetic energy, especially compared to the bulk of the vessel. However, the turbulent energy will be at a maximum at the outer edge of the impeller, as at that point all the energy that can be transfered will be. This will be equivalent to the turbulent energy at the start of the discharge jet described above. As a result although turbulent energy may be greater than the vessel average values it should never exceed that contained in the discharge jet. As the maximum force on the floc due to turbulent energy will be in the discharge jet, turbulent energy in this zone will not be discussed further. Another phenomena occurring in this zone is that high mean velocity shear stresses can occur on the surface of the impeller. The impeller can be thought of as a _)-slip boundary over which fluid is flowing. Wichterle et al. (1984) found that shear on the impeller surface could be adequately described by the theoretical expression describing boundary layer flow. By substituting appropriate impeller dimensions to describe velocity ($N\pi D$) and boundary layer length, $\propto D$, the following equation can be developed.

$$\tau_o = 6.3\mu N \left(\frac{D^2 N}{v} \right)^{1/2}$$

(4.34)

Wichterle et al. (1984) tested this relation by placing electrochemical sensors imbedded flush to the surface of a Rushton turbine. Results compared remarkably well. They found that shear stresses were great enough on the surface of the impeller that they may be significant break-up of drops, bubbles, and agglomerates, although no attempt was made to quantify this significance. Substituting (4.34) into (4.17) gives.

$$F_{ss} \propto \mu (N^3 D^2 / v)^{1/2}$$

(4.35)

Note that (4.35) is proportionally equivalent to (4.26) which was based on $\overline{G}$. Scaling on $\overline{G}$ will also keep the force due to impeller shear constant in both scales if they are scaled

based on 100% geometric similarity. Again however, the magnitude of the force due to shear and $\overline{G}$ may be different.

4.4.4 Vessel Wall Zone

Analysis of flow near the vessels walls has been almost completely ignored in the study of impeller-agitated flow. The reason for this is that most applications in mixing are concerned with the blending and homogenization of material. However, in flocculation, the flocs are relatively fragile and, as shown above, mean velocity shear may be significant in causing break-up. For blending and homogenization the effect of mean shear on the walls and impeller are small compared to turbulent mixing and hence the lack of consideration in the literature.

Figure 4.5 shows general flow patterns in the jar test apparatus. In the figure the swirling radial jet discharging from the impeller is evident and it can be seen that this jet impinges on the wall of the vessel. The study of jets impinging on a planar surface has shown that in the stagnation region high shear stress can occur at the surface.

Impinging jets have been a topic of study in classical fluid mechanics and applied mathematics for some time. However, the situation in an impeller-agitated tank is more complex than situations described in the fluid mechanics literature, due to the fact that the impinging jet is a swirling radial jet and there is an overlying water surface on the flow along the wall. Still, analysis of the phenomena based on the classical work should provide an estimate of shear stress in this region. This estimate shoudl provide an assessment on whether these shear stresses are significant and, most importantly should provide a basis for the scaling of these shear stresses. Figure 4.6 shows a typical jet impinging on a surface. Along the wall surface, velocities parallel to the surface grow rapidly from zero at the stagnation point to close to U_0 at the edge of the stagnation region ($r = r_o$). Often, as the fluid moves further away from the stagnation region, a hydraulic

jump will form. The flow in the stagnation point is one of the problems having an exact solution of the Navier-Stokes equations and was solved by Schlichting (1960). Based on laminar boundary layer theory, shear stress in the stagnation region $(0 \le r \le r_o)$, shear stress is described by the Schlichting-Shach formula:

$$\frac{\tau_o Q^2}{\rho v^4} = 5.95 \times 10^{-2} (Q / vr)^{7/2} (r / r_o)^{9/2} \tag{4.36}$$

where Q is the discharge in the jet. Experimental work has confirmed that this relationship describes shear stress in the stagnation region (Nakoryakov et al. 1978). Based on the above analysis the maximum shear stress occurs at $r = r_o$. However, as described by Watson (1964) if the flow is unstable as it approaches the surface the boundary layer may be turbulent, which could be the case in the impeller generated jet. Based on turbulent boundary layer theory and assuming Blasius' resistance equation holds, the shear stress can be given as:

$$\tau_o = 0.029 \rho U^2 \left(\frac{v}{Ur} \right)^{1/5} \tag{4.37}$$

Calculation of shear rates based on either (4.36) or (4.37) for typical jet values found in impeller agitated vessel showed little difference between them. If impeller dimensions are substituted to represent U and r, (4.37) can be rewrite as:

$$\tau_o = 0.029 \rho (N\pi D)^2 \left(\frac{v}{(N\pi D)(b/2)} \right)^{1/5} \tag{4.38}$$

and, using $\frac{b}{D} = \Lambda_1$, (4.38) can be simplified to:

$$\tau_o = 0.261 \rho \Lambda_1^{-1/5} N^{9/5} D^{8/5} v^{1/5} \tag{4.39}$$

The above equation describes the shear stress at $r = r_o = b/2$, which has been shown to be the point of maximum shear stress. However, if one considers (4.37) it can be seen that τ_o decreases only slightly with increasing distance along the wall. As a result,

relatively high shear stresses would be experienced for a considerable distance up and down the vessel wall from the stagnation point. Substituting this equation into (4.17) obtains the force on the floc due to the shear stress given as:

$$F_{ss} \propto \rho \Lambda_1^{-1/5} N^{9/5} D^{8/5} v^{1/5} d^2 \qquad (4.40)$$

and d_{max} for a drop would be given as:

$$d_{max} \propto \rho^{-1} v^{-1/5} \Lambda^{1/5} N^{-9/5} D^{-8/5} \sigma \qquad (4.41)$$

Note that both (4.40) and (4.41) depend on different exponents of N and D than the other relationships developed.

4.4.5 Bulk Flow Zone

Energy not dissipated in the impeller zone and the discharge zone must be dissipated in the bulk of the tank. As it has been noted that energy dissipated in the discharge zone can be many times greater than the average energy dissipation rate, dissipation rates in the bulk of the tank must be less than those in the discharge zone and even less than the average dissipation rate. This has been shown by many researchers (Kresta and Wood, 1991 and 1993; Weetman and Oldshue, 1988; Wu and Patterson, 1989; Wu et.al., 1989; and Stanley and Smith, 1995). As a result, in determining maximum floc size this zone tends to place the smallest forces on the floc. Although the rate of energy dissipation in this zone may be important for flocculation growth kinetics it should not be important for the maximum equilibrium floc size.

4.5 Discussion

Studies by Clark et al. (1994). Oldshue and Mady (1978) and Konno et al. (1983) have shown that scaling based on $\bar{G}$ may not be appropriate in many situations. Table 4.2

shows a summary of results from Konno et al. with the drop diameter given as the d_{50} based on volume fraction after 300 minutes of mixing. Tank and impeller dimensions, rotation speed and vessel average dissipation rates, $\bar{\varepsilon}$, were taken directly from their paper. Their work involved investigation of drop size using three tank sizes (128mm, 186mm and 300 mm) with two D/T ratios (1/2 and 2/3). For each D/T ratio impeller speeds were scaled based on a constant value of $\bar{\varepsilon}$. For D/T = 1/2, $\bar{\varepsilon}$ was kept at 0.078 m^2/s^3 which is equivalent to $\bar{G}$ = 279 s^{-1}. For D/T = 2/3, $\bar{\varepsilon}$ was 0.094 m^2/s^3 which is equal to $\bar{G}$ = 306 s^{-1}. Figure 4.7 shows the relation between drop size, d, and $\bar{\varepsilon}$. From thier figure it can be seen that $\bar{\varepsilon}$ does not explain the reduction in drop size as tank diameter, T, is increased. In addition, according to theory, the drop diameter should decrease with increasing $\bar{\varepsilon}$. As drops in their study were in the inertial convection subrange, drop diameter should vary as $d \propto \bar{\varepsilon}^{-0.4}$. In fact if one compares the drop diameters in tanks with D/T = 1/2 and D/T = 2/3 there should be a decrease in d, where results show a ge: eral trend towards increasing d.

Also given in Table 4.2 is the local dissipation rate, ε, in the discharge zone of the impeller. This was calculated based on impeller dimensions and speed using equation (4.31) with $K_\varepsilon = 0.03$, a value found to be appropriate for many impellers. Two important points can be seen by looking at the results of this calculation. As discussed, if the tanks were scaled based on 100% geometric similarity (same D/T) keeping a constant $\bar{\varepsilon}$ or $\bar{G}$ should result in a constant ε. However, the ratio of $\varepsilon/\bar{\varepsilon}$ will change if tank geometry is changed (different D/T). For D/T = 1/2, $\varepsilon/\bar{\varepsilon}$ = 5.3, while for D/T = 2/3, $\varepsilon/\bar{\varepsilon}$ = 2.3. This highlights one of the difficulties encountered in using vessel-average parameters such as $\bar{\varepsilon}$ or $\bar{G}$, as Table 4.2 shows that, although the vessel-average $\bar{\varepsilon}$ increased slightly from D/T = 1/2 to D/T = 2/3, the local dissipation rate, ε, actually decreased. It should be noted that many researchers in trying to recognize that local ε may be significantly greater than the vessel-average $\bar{\varepsilon}$, have assumed some ratio of $\varepsilon/\bar{\varepsilon}$, often taken from studies in which the geometry of the mixing vessel are different from the ones they are using. The above

analysis indicates that this is not appropriate unless geometry is almost exactly the same. Large differences occur even in the above case when only slight changes are made in tank geometry (D/T from 1/2 to 2/3). Figure 4.8 relates drop size to the local dissipation rate ε in the impeller zone. As the figure shows, use of ε still does not describe why drop size decreases with increasing T. However, by using ε instead of $\bar{\varepsilon}$, the drop size now shows the proper trend between the two sets of tanks with different D/T in terms of decreased drop size with increasing dissipation rate.

The final column in Table 4.2 shows the value of shear stress at the impinging jet calculated using equation (4.39). According to equation (4.41) the drop size should be linearly proportional to the inverse of the calculated shear stress. Figure 4.9 presents drop size plotted against the inverse of the shear stress $(\tau_o)^{-1}$. As shown in the figure drop sizes, for each D/T ratio plot linearly with $(\tau_o)^{-1}$. Although there is a slight shift in the data for D/T=1/2 and D/T=2/3 both have almost exactly the same slope indicating the same phenomena is occurring in both situations. The shift in linear relationship between the two D/T ratio can be related to using the same relationship to describe the velocity of the jet which is impinging on the vessel wall. Both velocities were assumed to be represented by $(N\pi D)$. However, in the case of D/T=1/2 the distance the jet must travel before hitting the wall is greater than in the case of D/T=2/3. Given the earlier discussion that the jet velocity decreases with distance from the source, the velocity for the jet in the D/T=1/2 vessels is probably over estimated in comparison to the D/T=2/3 case. This would cause an over estimation of the shear stress for D/T=1/2 compared to D/T=2/3. As Figure 4.9 plots $(\tau_o)^{-1}$ this would tend to shift the line towards smaller values of $(\tau_o)^{-1}$ as is shown in the figure. As a result, the shift in the two cases actually strengths the case that this wall shear is controlling drop diameter. Forces due to the impinging jet are the only factor which explains the phenomena of decreasing drop size with increasing scale. To the knowledge of the authors this has never been considered in impeller-agitated mixing before.

Similar results with the effect of increasing scale were found by Clark et al. (1994). In their study three flocculation vessel sizes were investigated (T= 434mm, 857mm and 1375 mm) with four different types of impellers. Mixing was scaled based on keeping $\overline{G}$ = 25 s⁻¹ in each vessel size. In their study they did not measure floc size but assessed flocculation performance based on turbidity and total particle count after 20 minutes of sedimentation. Results indicated that as tank diameter increased so too did settled water turbidity and particle counts, which would indicate that floc size is decreasing. Turbidities were almost double between the small and large scale vessels. An explanation for this was not determined and instead recommendations for further study were given, which were summarized earlier. Similar to what was done above for the Konno et al. study, various zones in their vessels were analyzed based on impeller type, tank geometry and impeller speed. Figure 4.10 shows the forces placed on the floc for various zones in the three vessels which used a Rushton impeller, made dimensionless by the vessel average floc force. The figure indicates that in all cases local forces (shear on impeller surface, dissipation in the impeller discharge zone and shear due to the impinging jet) are all greater than the vessel average floc force. As discussed, since $\overline{G}$ was used to scale mixing between the vessels which were 100% geometrically similar, forces due to shear on the impeller and floc forces in discharge zone should also remain constant with scale, although they are greater than the vessel-average values. Figure 4.10 there is a slight change in these parameters due to the fact that the D/T did not remain exactly constant between scales (D/T varied from 0.29 to 0.33). Also indicated in the figure is that the force due to the impinging jet increases with scale and is dominant at the two largest scales. Because of the low mixing rate $\overline{G}$ = 25 s⁻¹, which results in low jet velocities, especially at small scale, the shear due to the impeller and the imping. jet are about equal for the smallest tank. The impinging jet would again seem to explain the reported results as these forces tend to increase with scale and are dominant under most situations.

Finally, Oldshue and Mady (1978) completed a study in which coagulated water from the same rapid mixer was flocculated in two small-scale batch flocculators, measuring 460 mm and 760 mm in diameter. A Rushton-type impeller was used with a D/T ratio of 0.2 in each. Various mixing intensities ($\overline{G}$) were investigated for each flocculator and settled water turbidities were assessed. It was found for the small tank that the optimum $\overline{G}$ was 116 s^{-1} while for the larger tank the optimum $\overline{G}$ was 59 s^{-1}. The investigators concluded that there appears to be a trend toward decreasing optimum $\overline{G}$ values with increasing tank size. Based on (4.40) the force on the floc due to the impinging jet is $\propto N^{9/5}D^{8/5}$. Although values of $\overline{G}$ are almost a factor of two different between the two systems. values of ($N^{9/5}D^{8/5}$) calculated at the optimum mixing intensities for both systems are very similar (0.085 for T = 760 mm and 0.09 for T = 460 mm). Again it appears that the force on the floc due to the impinging jet explains the reported results form this multi-scale flocculation study.

The above discussion highlights that vessel average parameters such as $\overline{\varepsilon}$ and $\overline{G}$ are not appropriate for the design, assessment and operation of flocculation facilities. These parameters are not even good surrogates for local hydrodynamic characteristics as indicated in the Konno et al. (1988) study where a small change in geometry (D/T) resulted in an increase in $\overline{\varepsilon}$, but a decrease in local forces on the drops. Much of the difficulty in scale-up of flocculation can be related to a number of factors. First, until recently little detailed information on hydrodynamics within impeller agitated vessels has been available. As a result, researchers have had to rely on easily measured vessel average parameters to describe flow conditions. Secondly, measurement of an undisturbed floc size is difficult which is compounded by the lack of good relationships relating floc characteristics such as size to strength. Another factor is that most studies of flocculation are at a single scale and as a result only one impeller diameter is investigated. With constant D, only impeller speed, N, is varied in these studies. When D is constant, it is difficult to determine if floc size, varied as N$^{-1.5}$ which theory (based on $\overline{G}$) states or varied as N$^{-1.8}$, which would be

the case for the impinging jet, especially given the errors associated with measuring floc size. The difference in floc size with the exponent on D cannot be assessed unless multi-scale tests are completed.

By obtaining more detailed hydrodynamic data on mixing in flocculation it was possible to assess various forces on flocs. These local forces tend to govern floc characteristics as, in most flocculation units, the circulation time is much shorter than the total residence time. As a result, although areas of high floc forces are localized, flocs come in contact with these zones many times during their residence time in the flocculator. The analogy of the discharge stream from the impeller to a swirling radial jet highlighted the need to consider the impinging of this jet on the vessel walls. Although this has never been considered before in flocculation, it has long been known in fluid mechanics that an impinging jet can produce high shear stress. Analysis of this shear stress appears to explain many of the difficulties found in previous scale-up studies. However, further work is required to characterize better shear forces due to the impinging jet, as the situation found in many impeller-agitated vessels is more complex than has been previously reported in the fluid mechanics literature.

4.6 Conclusions

Based on characterization of flow in two types of flocculators with a laser doppler anemometer, forces on flocs were assessed for various zones in an impeller-agitated flocculator. It was found that local forces within the vessel can be much greater than those calculated based on vessel-average values. Of importance, it was found that the highest forces on flocs occur due to high energy dissipation rates in the discharge stream from the impeller, mean shear stress due to fluid flowing over the impeller blades and mean shear stress as a result of the discharge jet impinging on vessel walls. The later may be the most

significant and may explain many of the difficulties found in scaling up mixing for

flocculation. Although high shear stresses as a result of impinging jets have been

recognized in classical fluid mechanics for some time, their effect been ignored in mixing

for flocculation. Results also indicate that vessel-average parameters such as $\bar{\varepsilon}$ and $\bar{G}$ are

not appropriate for the design, assessment and operation of flocculation facilities as local

forces on the floc are not represented by them.

4.7 References

Antonia, R., Satyaprakash, B. & Hussain, A. (1980). Measurements of Dissipation Rate and Some other Characteristics of Turbulent Plane and Circular Jets, *Phys. Fluids*, **23**, *4*, April, 695-700.

Batchelor, G.K. 1958. *The Theory of Homogeneous Turbulence*, Cambridge Univ. Press, Cambridge, England.

Bourne, J.R. and Baldyga, J. 1994. Drop breakup in the viscous subrange: a source of possible confusion. *Chemical Engineering Science*, **49**, 7, 1077-1078.

Camp, T.R. and Stein, P.C. (1943). Velocity gradient and internal work in fluid motion. *Jour. Boston Soc. Civil Engineering* **30**, 10, 219-237.

Clark, M.M. (1985). Critique of Camp and Stein's RMS velocity gradient. *Journal of Environmental Engineering*, *111*, 6, 741-754.

Clark, M.M. 1988. Drop breakup in a turbulent flow - I. Conceptual and Modeling Considerations. *Chemical Engineering Science*, **43**, 3, 671-679.

Clark, M.M., Srivastava, R.M., Lang, J.S., Trussel, R.R., McCollum, L.J. Baily, D., Christie, J.D., and Stolarik, G. (1994). Selection and Design of Mixing Processes for Coagulation. American Water Works Association Research Foundation and American Water Works Association, Denver, CO. 150p.

Davies, J.T. 1987. A physical interpretation of drop sizes in homogenizers and agitated tanks, including the dispersion of viscous oils. *Chemical Engineering Science*, **42**, 1671-1676.

Filip, P., Kolar, V. & Curev, A.G. (1985-a). Space Flow Geometry of the Radial Free, Wall and Liquid Jets with Swirl. *Applied Scientific Research*, **42**, 185-196.

Filip, P., Kolar, V. & Curev, A.G. (1985-b). Complex Swirling Radial Jets, *Z. Angew. Math. u. Mech*, **65**, *9*, 441-446.

Filip, P., Kolar, V. & Curev, A.G. (1986). A Note on the Radial Wall Jet with Swirl, *Acta Mechanica*, **60**, 41-47.

Gregory, J. (1989). Fundamentals of Flocculation. *Critical Reviews in Environmental Control. Vol.* **19**, 3. pp. 185-230.

Heskestad, G. (1966). Hot-wire measurements in a radial turbulent jet. Trans. ASME, J Appl. Mech. 417-424.

Hesketh, R.P., Russel, T.W.F. and Etchells, A.W. 1987. Bubble size in horizontal pipelines. *A.I.Ch.E.J.*, **33**, 663.

Hinze, J.O. 1955. Fundamentals of the hydrodynamic mechanism of splitting in dispersion processes. *A.I.Ch.E.J.*, **1**, 289-295.

Hudson, H.E. Jr. and Wagner. E.G. (1981). Conduct and use of jar tests. *Journal of the AWWA,* **73**, 4, 218-224

Kolar, V., Filip, P. & Curev, A.G. (1982). The Swirling Radial Jet, *Applied Scientific Research,* **39**, 329-335.

Kolar, V., Filip, P. & Curev, A.G. (1984). Hydrodynamics of a Radially Discharging Impeller Stream in Agitated Vessels, *Chemical Engineering Communications,* **27**, 313-326.

Kolar, V., Filip, P. & Curev, A.G. (1985). The Swirling Radial Jet Model and its Application to a Radial Impeller Stream, from *5th European Conference on Mixing,* Wurzburg, West Germany, 10-12 June, 1985, 483-490.

Kolmogorov, A.N. 1949. Disintegration of drops in turbulent flows. *Dokl. Akad. Nauk. SSSR* **66**, 825-828.

Konno, M., Aoki, M. and Saito, S. 1983. Scale effect on breakup process in liquid-liquid agitated tanks. *Journal of Chemical Engineering of Japan,* 16, 4, 312-319.

Kresta, S.M. and Wood, P.E. (1991). Prediction of the three dimensional turbulent flow in stirred tanks. *A.I.Ch.E.J.,* **37**, 448-460.

Kresta, S.M. and Wood, P.E. (1993). The flow field produced by a pitched blade turbine: Characterization of the turbulence and estimation of the dissipation rate. *Chemical Engineering Science,* **48**, 10, 1761-1774.

Leentvaar, J. and Rebhun, M. 1983. Strength of ferric hydroxide flocs. *Water Research,* **17,** 8, 895-902.

Levich, V.G. 1962. *Physiochemical Hydrodynamics.* Prentice-Hall, Inc. Englewood Cliffs, N.J. 700p.

Matsuo, T. and Unno, H. 1981. Forces acting on floc and strength of floc. *Journal of Environmental Engineering, ASCE,* **107,** 3, 527-545.

Nakoryakov, V.E., Pokusaev, B.G. and Troyan, E.N. 1978. Impingement of an axisymmetric liquid jet on a barrier. *International Journal of Heat and Mass Transfer,* **21,** 1175-1184.

Parker, D.S., Kaufman, W.J. and Jenkins, D. 1972. Floc break-up in turbulent flocculation processes. *Journal of the Sanitary Engineering Division. ASCE,* **88,** 1, 79-99.

Rajaratnam, N. (1975). *Turbulent Jets,* Elsevier Science Publishers Ltd., Amsterdam.

Rushton, J.H. 1951. The Use of Pilot Plant Mixing Data, *Chemical Engineering Progress,* **47,** 9, 485-488.

Schlichting, H., 1960. *Boundary Layer Theory.* McGraw Hill, New York, 747p.

Shinnar, R. 1961. On the behavior of liquid dispersions in mixing vessel. *Journal of Fluid Mechanics,* **10,** 259-275.

Stanley, S.J. and Smith, D.W. (1995). Measurement of turbulent flow in a standard jar test apparatus. *Journal of Environmental Engineering, ASCE,* (Accepted for publication, Feb. 1995).

Stanley, S.J., Yaremko, B. P., and Smith, D.W. 1995. Characterization of Impeller-Agitated Flow in a Upflow Solids-Contacting Clarifier. *Journal of Environmental Engineering, ASCE,* (Submitted for publication).

Tambo, N. and Hozumi, H. (1979). Physical Characteristics of Flocs - II. Strength of Floc. *Water Research,* **13,** 421-427.

Thomas, D.G. 1964. Turbulent disruption of flocs in small particle size suspensions. *A.I.Ch.E.J.*, 10, 517-523.

Watson, E.J. 1964. The radial spread of a liquid jet over a horizontal plane. *Journal of Fluid Mechanics*, 20, 3, 481-499.

Weetman, R.J. and Oldshue, J.Y. (1988). Power, flow, and shear characteristics of mixing impellers. *Proc. 6th Eur. Conf. on Mixing*, Pavia, Italy, BHRA Fluid Eng. Cntr., Springer, 43-50.

Wichterle, K., Kadlec, M., Zak, L. and Mitschka, P. 1984. Shear rates on turbine impeller blades. *Chemical Engineering Communications*, 26, 25-32.

Wu, H. and Patterson, G.K. 1989. Laser doppler measurements of turbulent flow parameters in a stirred mixer. *Chemical Engineering Science*, 44, 2207-2221.

Wu, H., Patterson, G.K. and van Doorn, M. 1989. Distribution of turbulence energy dissipation rates in a Rushton turbine stirred mixer. *Expts Fluids*, 8, 153-160.

Wygnanski, I. and Fielder, H. (1969). Some measurements in the self-preserving jet. *J. Flui Mech.*, 38:577-612.

Table 4.1. Value of exponent n for the function $d_{max} \propto G^{-n}$ (after Amirtharajah et al. 1991)

Reference	n	Regime of Turbulence	Kind of flocs	Type of Data used
Thomas (1964)	5 1	Inertial subrange Viscous subrange	Modeling	Theoretical formula (checked with experimental data)
Tambo et al. (1970, 1979)	0.6 to 0.8 0.56 to 0.66	Inertial subrange Viscous subrange	Model floc and aluminum hydroxide kaolinite floc	Theoretical formula and experimental study
Parker et al. (1971, 1972)	2 1	Inertial subrange Viscous subrange	Model floc Ferric and aluminum floc	Theoretical formula and experimental study
	0.5 0.5 0.17 to 0.37	Inertial subrange Viscous subrange	Model floc Model floc Activated sludge floc	Theoretical formula Experimental study
Tomi et al. (1978)	2 0 1	Inertial subrange Viscous subrange Intermediate	Modeling	Theoretical formula
Leentvaar et al. (1983)	1 0.6	Inertial subrange Viscous subrange	Ferric chloride floc	Experimental study with polymer
Francois (1987)	0.7 to 1.5 0.3 to 0.5	Inertial subrange Viscous subrange	Aluminum floc	Experimental study

Table 4.2. Summary of results from Konno et al. (1983)

D/T ratio	Tank Diameter (m)	Impeller Diameter (m)	Impeller Speed, N (s⁻¹)	Drop Diameter (μm)	Vessel Ave., $\bar{\varepsilon}$ (m²/s³)	Discharge jet, ε (m²/s³)	Impinging jet, τ_o (kg/ms²)
	0.128	0.064	2.73	235	0.078	0.415	1.50
1/2	0.186	0.093	2.13	205	0.078	0.415	1.75
	0.30	0.150	1.55	175	0.078	0.415	2.12
	0.128	0.085	1.82	280	0.094	0.217	1.14
2/3	0.186	0.124	1.42	230	0.094	0.217	1.33
	0.30	0.20	1.02	200	0.094	0.209	1.57
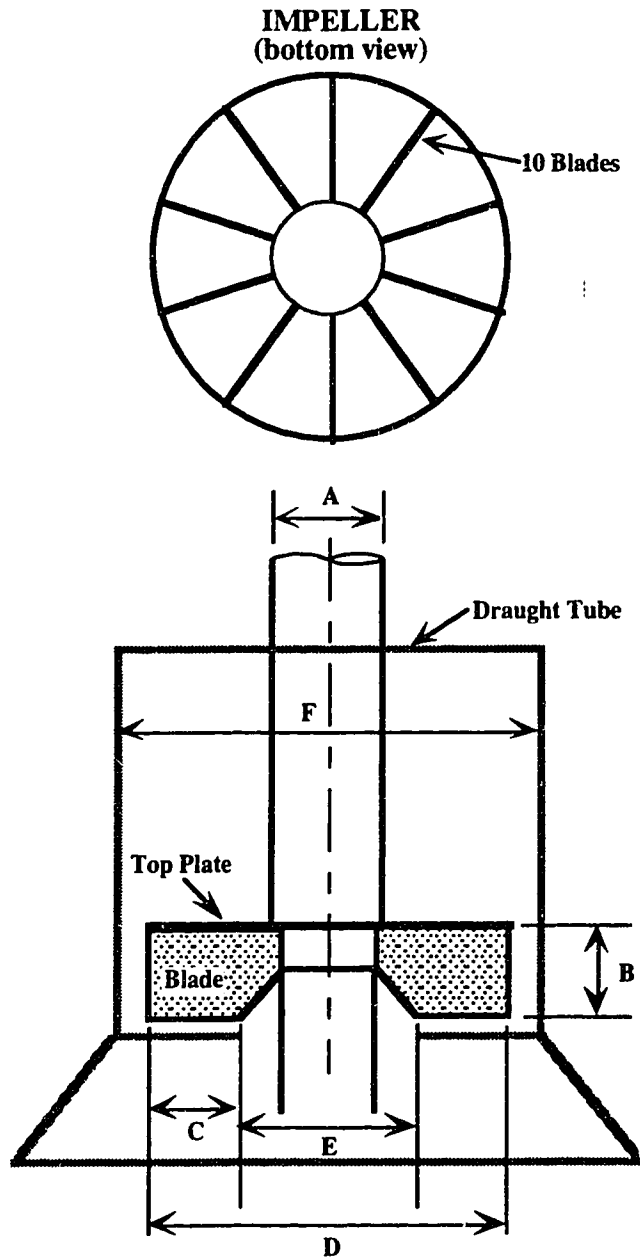
IMPELLER
(bottom view)

All dimensions in mm

Dimension	1:55	1:41	1:10	Full-scale
A	24.6	33.3	140	1369
B	19.4	26.3	108	1083
C	18.5	25.0	103	1029
D	76.6	103.7	427	4267
E	39.7	53.7	221	2210
F	107.9	146.0	601	6007

Figure 4.1. Description of clarifier impeller and draught tube.
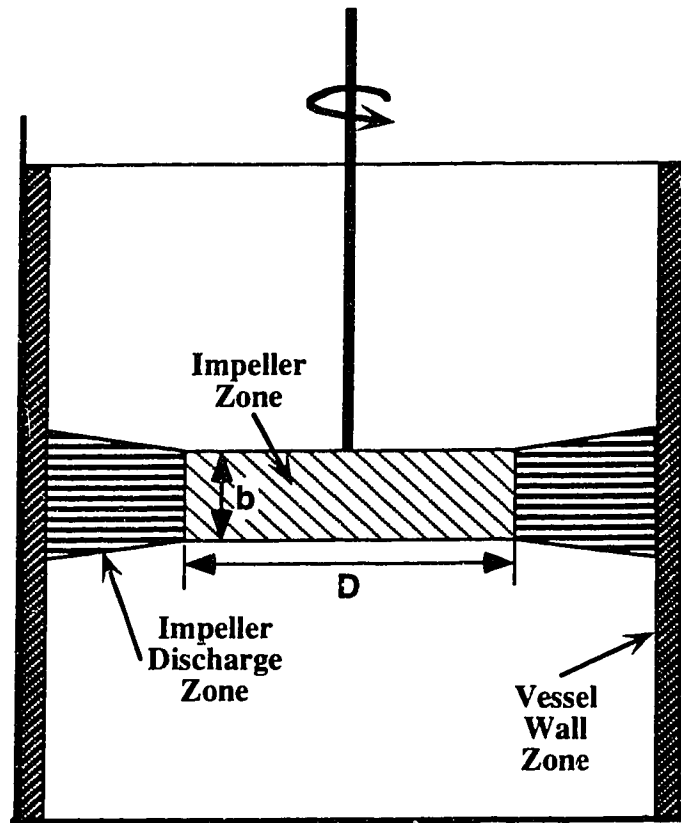
Figure 4.2. Typical impeller agitated flocculator with various vessel zones.
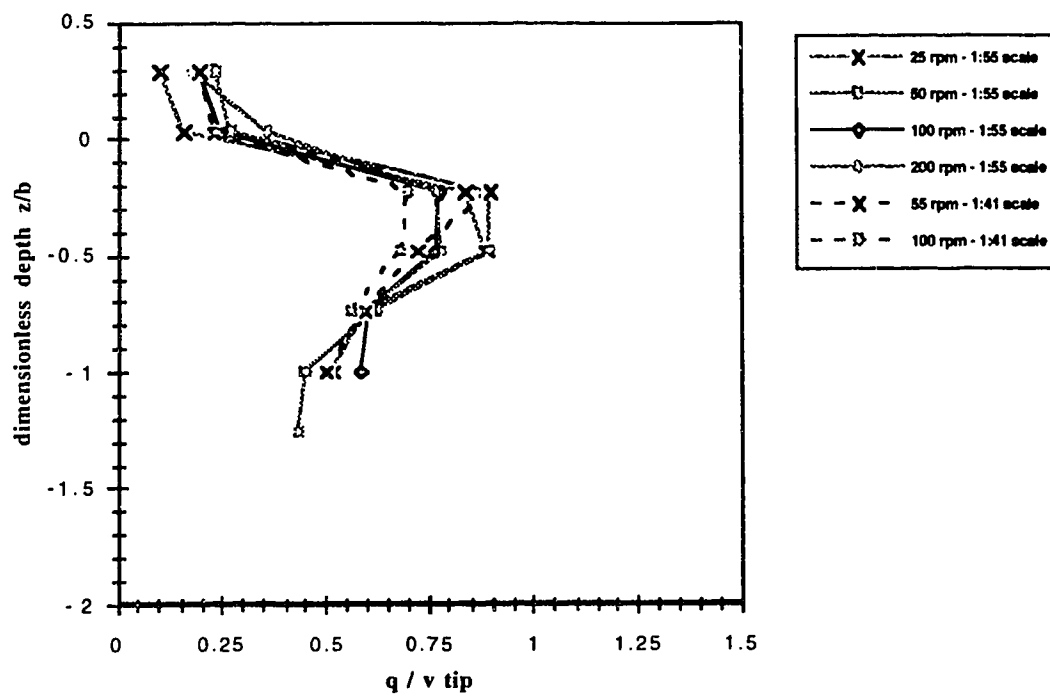
Figure 4.3. Resultant velocity, q, for free clarifier impeller, made dimensionless by v_{tip}, $(N\pi D)$
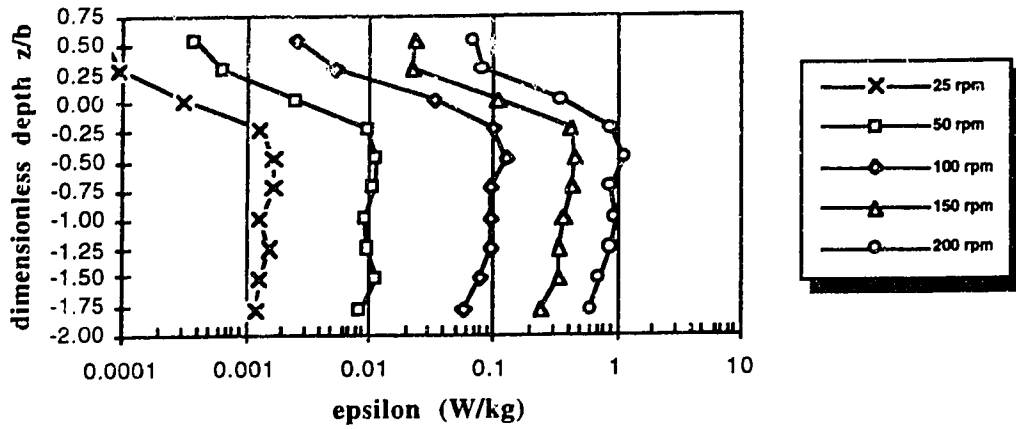
a)
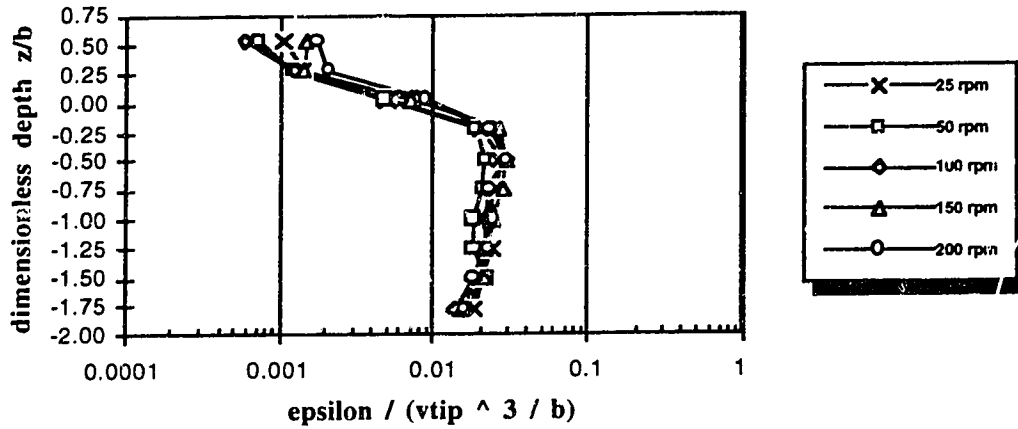
b)

Figure 4.4. Local dissipation rates near the impeller. Free impeller; 1:55 scale; d=76.6mm; b=19.4 mm; 2r/d=1.175. a) dimensional; b) dimensionless-normalized by $\varepsilon / ((N\pi d)^3 / b)$
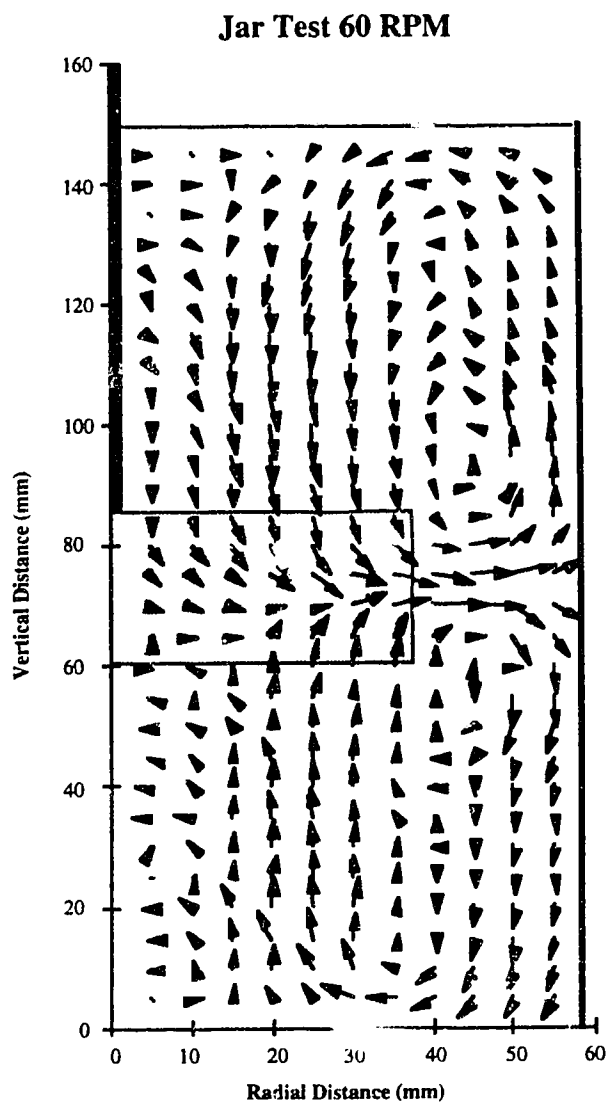
Jar Test 60 RPM

Figure 4.5. General flow patterns with in jar test at 60 RPM.
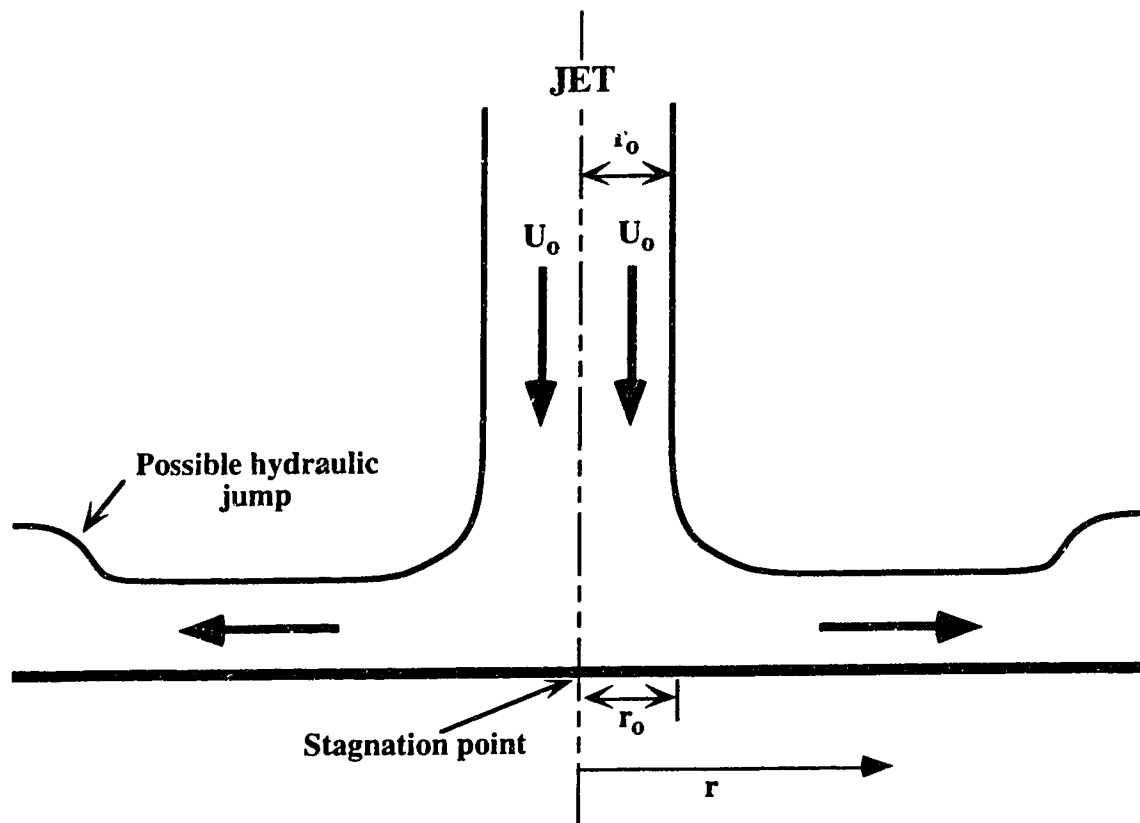
Figure 4.6. Impinging jet on a planar surface.
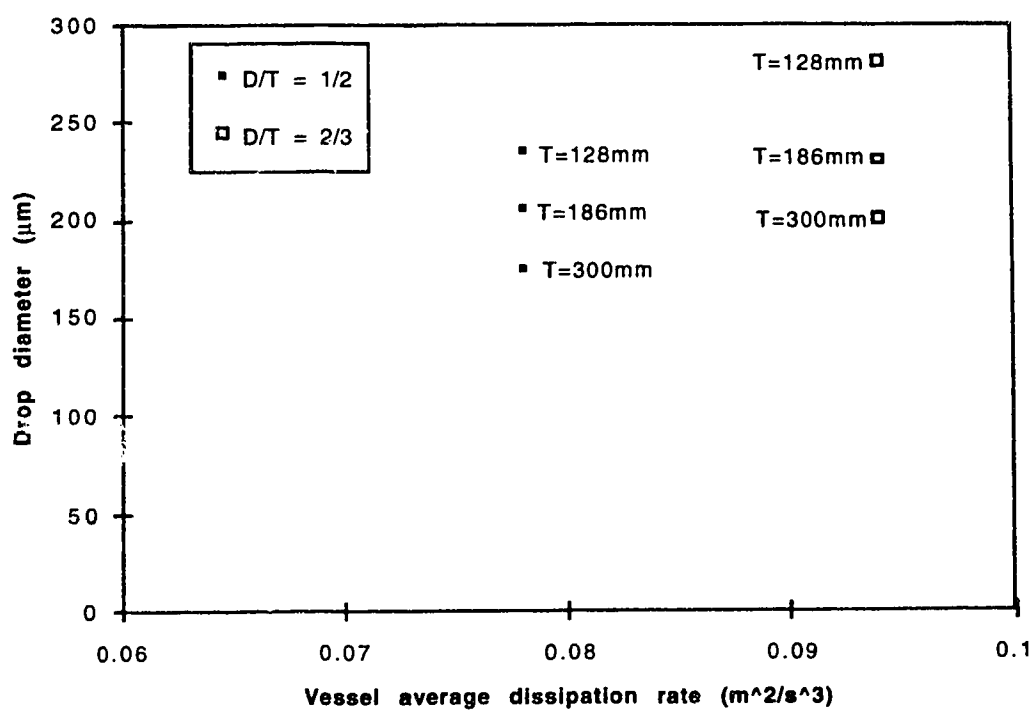
Figure 4.7. Drop diameter versus the vessel average dissipation rate, $\bar{\varepsilon}$.
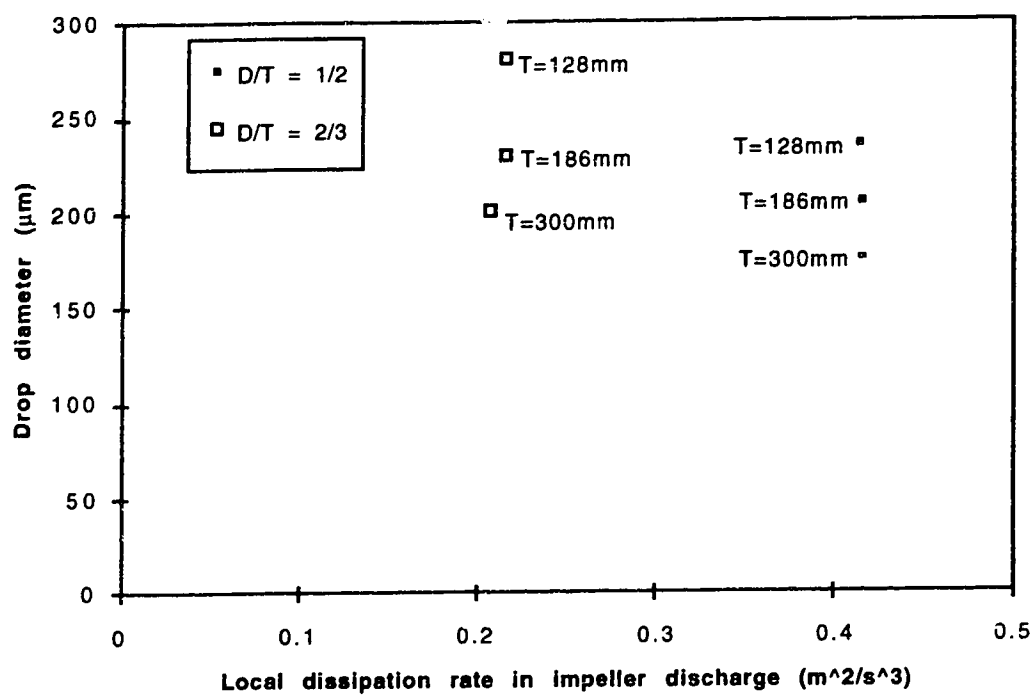
Figure 4.8.   Drop diameter versus the local dissipation dissipation rate in impeller discharge zone, ε.
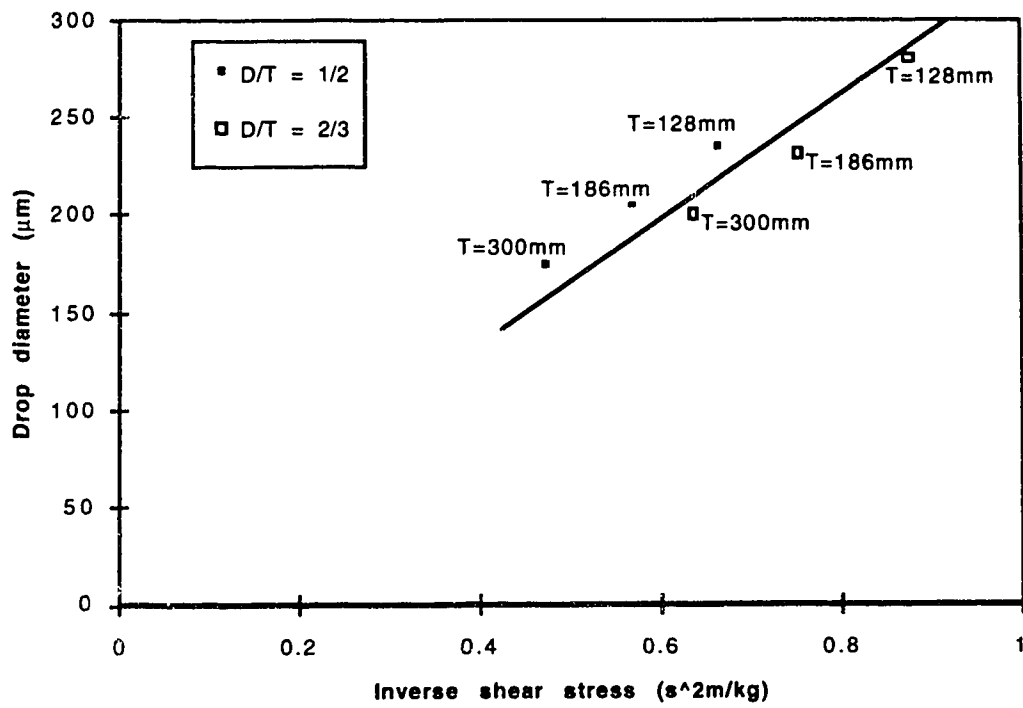
Figure 4.9.   Drop diameter versus the inverse of wall shear stress due to the impinging jet, $(\tau_o)^{-1}$
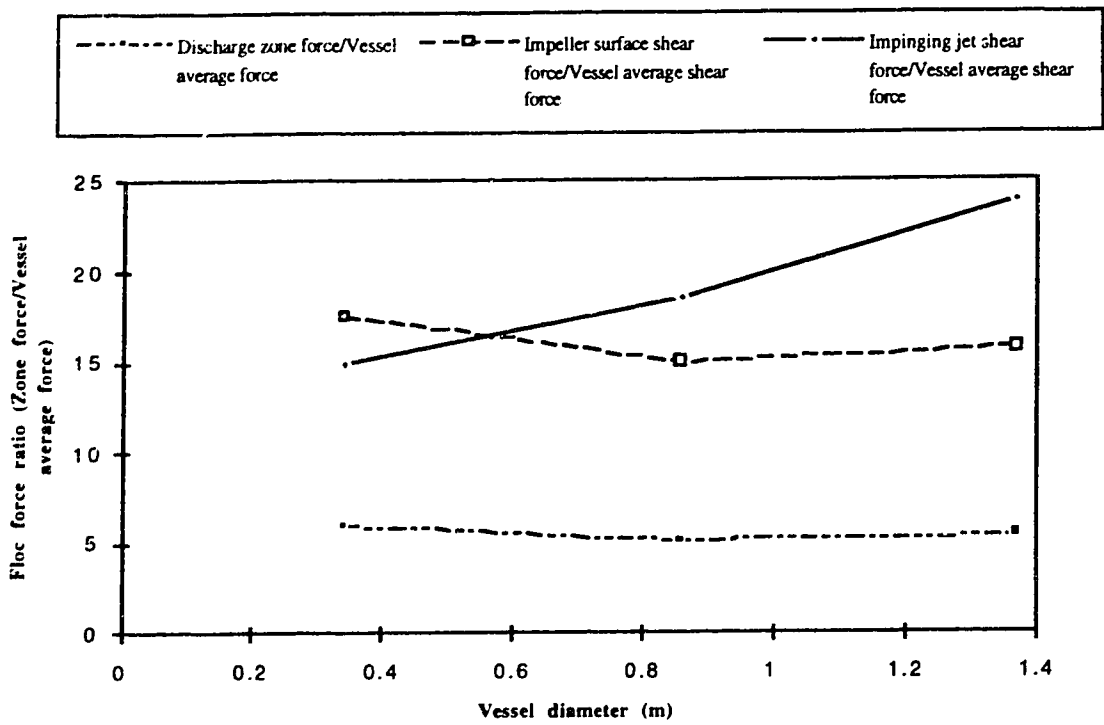
Figure 4.10. Variation in force on a floc, made dimensionless by vessel average floc force.

Chapter 5
General Summary and Conclusions

5.1 General Overview

Chapters 2, 3, and 4 show a general progression in the understanding of impeller agitated mixing and the impact it may have on the flocculation process. The investigation of turbulent flow in the jar test apparatus highlighted the variation in velocities and energy dissipation within an impeller agitated mixing vessel. In this initial component of the study, due to the complex flow characteristics found in impeller-agitated mixers, significant effort was spent developing fundamentally sound methods of measurement and analysis of turbulent flow in mixing vessels. This included investigation of problems associated with the phase ambiguity noise limit in laser doppler anemometer (LDA) velocity measurements, accounting for pseudo-turbulence caused by blade passage, investigating methods for determining local energy dissipation rates given the inability of the LDA to measure the full turbulent spectrum, and determination of appropriate turbulent length scales to describe the flow. In addition, experimental conditions such as seeding requirements, optimum forward scattering angle, and laser settings such as the input filter bandwidth setting, velocity validation requirements, methods to eliminate velocity bias and the measuring volume used, were also all investigated during the this initial component of the study. Information gained from this exercise was used in the remaining portions of the research. Details on many of these factors can be found in Appendix A.

Results from the jar test experiments indicated that near the impeller region, local energy dissipation rates could be significantly higher than vessel-average parameters. The investigation of the jar test initiated the process of developing scaling relationships for local hydrodynamic parameters in impeller agitated vessels. Similar to most other studies of

impeller-agitated mixing it was found that mean and turbulent fluctuating velocities near the impeller scaled on the tip speed of the impeller $(N\pi D)$. Using this fact and by determining the dissipation rate based on the transfer of kinetic energy it was shown that, similar to Kresta and Wood (1991), the local dissipation rate in the impeller discharge could be scaled by $((N\pi D)^3 / D)$. At this stage of the study it was noted however, that D in the denominator was really being used to represent the Eulerian integral length scale, which is approximately equal to the one-half width of the impeller. Justification of this was related to the discharge from the impeller behaving like a turbulent jet. As discussed in Chapter 2, $((N\pi D)^3 / D)$ can only be used to scale similar impellers where the b/D ratio is constant. Of significance is that the local dissipation rate, ε, in the impeller discharge zone is independent of tank volume. Many other researchers who have investigated local energy dissipation rates have reported results in terms of $\varepsilon / \bar{\varepsilon}$, where the vessel average dissipation rate, $\bar{\varepsilon}$, is dependent on vessel volume (see for example Wu and Patterson, 1989). In relating results based on $\varepsilon / \bar{\varepsilon}$ to other types of vessels, extreme care must be taken as this ratio is highly dependent on vessel geometry.

Chapter 3 involved the expansion of the characterization of turbulent flow in flocculators to the reactor zone of an upflow solids-contacting clarifier. The primary purpose of this work can be divided into two broad objectives. First, to investigate whether methods of analyzing flow characteristics used for relatively simple mixing vessel such as the jar test apparatus, are applicable for more complex flow systems such as that found in the reactor zone of the clarifier. Secondly, this component of the study involved the investigation of four geometrically scaled mixing vessels with impeller diameters ranging from 76.6 mm to 4267 mm. This allowed investigation of how local hydrodynamic parameters changed with scale.

Of significance in this section of the study was the expansion of the concept of representing flow from the impeller by a swirling radial jet. Although this had been

proposed earlier, in the chemical engineering field (Kolar, Filip and Curev, 1984; Kolar, Filip and Curev, 1985; Filip, Kolar and Curev, 1985a; Filip, Kolar and Curev, 1985b; Filip, Kolar and Curev, 1986; and Kresta and Wood, 1991) few multi-scale studies, especially under complex flow conditions (the reactor zone) had been completed. It was not only found that the impeller discharge could be represented by the swirling radial jet, but also that characteristics of this jet were similar to traditional radial jets. As the mean and turbulent fluctuating velocities were again shown to scale on the tip speed of the impeller, use of the radial swirling jet analogy allowed the refinement of the scaling of local dissipation rates by using $((N\pi D)^3 / b)$ and it was found the $\varepsilon / ((N\pi D)^3 / b)$ was relatively constant for a wide range of impellers. Study of the clarifier reactor zone showed that the local dissipation rate, ε, was truly independent of vessel volume as $\varepsilon / ((N\pi D)^3 / b)$ was constant for both D/T = 0.22 and D/T = 0.71, which represents a reduction in vessel volume of about 10 times. It was also found that localized values of G were much higher than those calculated based on the vessel-average power input.

Chapter 4 involved the investigation of localized forces on the floc in an impeller-agitated mixer. This started with a review of previous work that had been completed on forces on a floc and floc size. It was found that in most of the previous work, similar relations were developed describing fluid forces on the floc. However, it was found that different relationships had been developed relating floc size to mixing intensity. The differences in these relationships could be related to the different approaches used to assess floc strength. It was also found that in the few multi-scale flocculation studies that have been completed, all tend to show that greater forces are placed on the floc, indicated by smaller floc size, with increasing scale of the flocculator, even though the vessel-average $\bar{G}$ remains constant. Using relationships developed from the characterization of turbulence in the flocculators, local forces on the floc were determined for various localized zones within the flocculator. Zones considered were the impeller zone, the impeller discharge zone, the walls of the vessel and the bulk of the tank. It was found that local forces within the vessel

can be much greater than those calculated based on vessel-averag̲ values. Of importance, it was found that high forces on flocs occur due to high dissipation rates in the discharge stream from the impeller, shear stress due to fluid flowing over the impeller blades and mean shear stress as a result of the discharge jet impinging on vessel walls. Although it was found that the floc forces can be much greater in the impeller zone and the impeller discharge zone compared to vessel-average forces, it was also found that in geometrically scaled flocculators, scaling of the mixing based on $\bar{G}$ will also result in the scaling of these forces. Hence, by keeping $\bar{G}$ constant, these forces although greater than vessel-average ones, should be the same in both scales and do not explain trends found in the multi-scale flocculation studies. The analogy of the swirling radial jet lead to consideration of the impingement of this jet on the vessel walls. Although the impinging jet has not been considered before in flocculant mixing, high shear stresses in the region of impinging jets have long been recognized in classical fluid mechanics. Floc forces due to the impinging jet were determined to be dominant under most mixing conditions found in flocculation. In addition, it is important how these forces change with scale, as it tends to explain many of the difficulties that have been experienced in trying to scale-up flocculation systems.

One of the most significant findings of this study is that $\bar{G}$ is not appropriate for the design, assessment and operation of flocculation facilities. It appears that $\bar{G}$ is not even a good surrogate for local hydrodynamic characteristics as local characteristics change dramatically with changes in geometry, which are not represented by $\bar{G}$. Further discussion of this is presented in the next section.

5.2 Use of $\overline{G}$ for Scaling Mixing for Flocculation

A number of the components of this study have shown that the classical use of $\overline{G}$ as a scaling parameter for mixing in flocculation may be inappropriate. Listed below are a number of results which question the use of $\overline{G}$ for scale-up.

1) Results for both the jar test apparatus and the clarifier impeller show that the distribution of flow and energy in the mixing vessel is not homogeneous. Much higher velocities and energy dissipation rates occur near the impeller. As many of the equations governing flocculation kinetics and floc size are non-linear in dissipation rate, the use of simple ve vel-average parameters such as $\overline{G}$ do not account for these variations. Although this has been recognized before (Clark, 1985), no detailed hydrodynamic data have been available for flocculant mixing to quantify the fact.

2) Many of the local hydrodynamic parameters are independent of vessel volume. Both the energy dissipation rate in the impeller discharge zone and the mean shear produced by flow over t! impeller blades are only dependent on impeller geometry and speed. As a result there is not a simple relationship between the vessel average $\overline{G}$ or $\overline{\varepsilon}$ and local dissipation rate ε. The ratio of $\varepsilon/\overline{\varepsilon}$ is highly dependent on the geometry of the tank. This ratio will remain constant between two sizes of vessels if they are scaled using 100% geometrical similarity. As shown however, if relatively small changes are made in the geometry of the vessel, this may result in situations where the vessel-average $\overline{G}$ will increase, but the local ε actually decreases, with the opposite case also being possible. This

significantly limits the use of $\bar{G}$ to select optimum mixing conditions from other studies unless the geometry of the vessels are similar. It also questions the use of $\bar{G}$ for jar tests as, normally, the jar test vessel is significantly different from the full-scale flocculator it is supposed to represent. This finding also brings into question results from some other researchers in the flocculation and coagulation field, who have recognized that energy dissipation rate is not homogeneous and tried to account for it by simply multiplying the vessel average value by some constant. For example, Amirtharajah and Trussel (1986) used data from Cutter (1966) who studied a Rushton turbine and found the $\varepsilon/\bar{\varepsilon}$ ratio for the Rushton turbine system to be 56.5. Amirtharajah and Trussel used the same ratio for their system which was a baffled tank backmix reactor for rapid mixing, which varied significantly in geometry from the system studied by Cutter (1966). Based on this, they made a number of inferences about rapid mixing. As discussed, the ratio could be significantly different for their system in comparison to that used by Cutter.

3) Analysis of forces on the floc found that, in many cases, the dominant force can result from high shear stresses caused by the impinging jet. Of importance is that these forces do not scale similarly to $\bar{G}$, even if vessel sizes are scaled based on 100% geometric similarity. These forces will increase with increasing mixing vessel size even if $\bar{G}$ is kept constant. This tends to explain many of the results from multi-scale flocculation studies.

The above discussion highlights some of the difficulties in using $\overline{G}$ for scaling

flocculant mixing. Although these problems exist, it is also important to consider that there

are many facilities which operate successfully that have been designed based on $\overline{G}$. This

can be partly related to experience of designers and a number of "rules of thumb" which are

also used in design. Many of these "rules of thumb" tend to account for some of the

problems described above. Most standard texts on water treatment provide design

guidelines based on $\overline{G}$ and also add that the tip speed of the impeller should never exceed

some value. ASCE-AWWA (1990) states for high-energy flocculators ($\overline{G}$ = 50 to 75 s⁻¹)

maximum tip speed of the impeller should not exceed 3 m/s. For low-energy flocculators

($\overline{G}$ = 20 to 45 s⁻¹) the maximum tip speed should be limited to 0.3 to 0.75 m/s. In a

sense, this limits the force on the floc by the impinging jet as this force is dependent on

velocity of the jet which is directly related to tip speed on the impeller. The importance of

impeller tip speed found in this study tends to be supported by experiences found in

practical flocculator designs.

5.3 Scaling of Mixing for Flocculation

Although the work presented in this study is more theoretical in nature, results do

tend to indicate scaling parameters which are important in the scaling of the flocculant

mixing process. The dominant force on the floc appears to be the result of the impinging

jet. To keep forces on the floc due to the impinging jet equivalent at both scales, equations

developed in Chapter 4 indicate that ($N^{9.5}D^{8/5}$) should be kept constant between the scales.

Figure 5.1 shows the results from the Oldshue and Mady (1978) study, where water from

the effluent of the rapid-mix stage of a surface water treatment plant was tested. Water

from the rapid-mix stage was flocculated in two small-scale batch flocculators, one

measuring 460 mm in diameter and the other 760 mm. Both had a impeller diameter, D, to

tank diameter, T, ratios of 0.2 and used a Rushton-type impeller. As shown by the figure the optimum $\bar{G}$ for the smaller vessel was 116 s^{-1} while for the larger vessel it was 59 s^{-1}. If their data is replotted with settled water turbidity versus $(N^{9/5}D^{8/5})$, one can see in Figure 5.2, that both curves tend to collapse onto each other. This indicates that $(N^{9/5}D^{8/5})$ or the force exerted on the floc by the impinging jet is a more appropriate scaling factor. It should also be remembered that similar results were found when data from Konno et al. (1983) on drop diameter were analyzed in a similar manner.

Due to general lack of multi-scale flocculation data further work is required to confirm the use of this scaling factor, although it does explain results from Oldshue and Mady (1978), Konno et al. (1983), Clark and Fiessinger (1991), and Clark et al. (1994).

5.4 Limitations of Study

As with any study there are a number of limitations which must be considered when using the results of this study. These are listed below:

1) This study only investigated radial discharge impellers. Although these are often used in flocculation, many other types of impellers are also used. The other types most commonly used are axial flow impellers and rake-type impellers. In the study of Clark et al. (1994) these two other types of impeller were also investigated with similar findings: poorer performance with increasing scale even though $\bar{G}$ remained constant. Figure 5.3 shows a typical axial flow impeller. As shown, the discharge from the axial flow impeller impinges on the bottom of the tank. Often the axial flow impeller is placed in the bottom third of the tank to ensure high enough velocities occur at the bottom of the tank to stop sedimentation. As a

result, velocities of this downward jet hitting the bottom of the tank could be a significant source of high floc forces, similar to the jet impinging on the walls for the radial impellers. Kresta and Wood (1993) found that, for axial flow impellers, the downward velocities also scale on tip speed of the impeller. Based on that result, the scaling of forces due to the downward jet impinging on the bottom should scale similarly to that of the radial impellers and would explain the similar finding in scaling of these types of impellers for flocculation. The third type of impeller used, the rake impeller, is really only used in flocculation and as a result no detailed turbulent flow information is available for it. Explanation of why this type of impeller also shows similar trends will require further study, starting with characterization of the flow it produces.

2. Two other important characteristics of flocculators which were not considered as part of this study are circulation time, t_c, residence time, t_d and the relation between the two. The circulation time represents the time an element of fluid takes to circulate around the tank. During one circulation this element of fluid and flocs contained in it will come in contact with all zones of the flocculator and the fluid forces that each of these zone exerts on the floc. For small scale batch flocculators $t_c \ll t_d$. Preliminary assessment of the jar test apparatus showed that t_c was in the order of seconds where t_d is the flocculation time which is normally 10 to 30 minutes. As a result during the flocculation time the flocs will come into contact with areas of high floc forces numerous times and these zones will tend to dictate floc characteristics. Normally, constant between small and large scale systems. However, leads to

increase with increasing scale. As t_c approaches t_d the influence of zones of high floc forces on floc characteristics would tend to decrease as the contact time with these zones would be less. The exact influence of this is unknown however and will require further study. Another important factor in scaling up is residence time, t_d. Normally full-scale systems are flow through systems and not batch systems where it is easy to match the residence time. As mixing is applied to the flocculators, these flocculators tend to behave more as a continuous flow stirred tank reactor (CFSTR) than a plug flow reactor (PFR). It is therefore important that the residence time distribution of the two systems to be scaled are matched. However, in flocculation, little work has been completed to assess this.

5.3 Conclusions

Major conclusions from this study can be divided into two broad areas. One deals with the measurement and analysis of flow in impeller-agitated mixers and the other involves the impact of mixing on flocculation. Conclusions on general analysis of mixing in vessels are presented below followed by the conclusions on the role of mixing in flocculation.

1. There are significant variations in velocity and energy with in an impeller agitated mixer.

2. Both mean and turbulent fluctuating velocities produced by radial flow impellers scale on the tip speed of the impeller.

3. Flow from the discharge from radial flow impellers can be represented by a swirling radial jet and characteristics of this jet are similar to those found for true radial jets.

4. Based on conclusions 2 and 3 it was shown that energy dissipation in the discharge region of the impeller scales on $((N\pi D)^3 / b)$. Values of $\varepsilon / ((N\pi D)^3 / b)$ were found to be relatively constant for the two types of impellers investigated and similar to values reported for other radial flow impellers. Of importance is that energy dissipation in this region is totally independent of the volume of the tank and only dependent on impeller geometry and speed.

5. Based on conclusion 4, the ratio of $\varepsilon / \bar{\varepsilon}$ is not constant and varies based on the geometry of the tank.

Conclusion involving the role of mixing in flocculation include:

1. Local forces on the floc exceed those calculated based on vessel-average parameters. It was found that the highest forces on flocs occur due to high energy dissipation rates in the discharge stream from the impeller, shear stress due to fluid flowing over the impeller blades and shear stress as a result of the discharge jet impinging on vessel walls.

2. Forces caused by the impinging jet appear to be dominant and the scaling of these forces tend to explain many of the results found by multi-scale flocculation studies.

3. Although more study is required, it appears that scaling based on matching forces placed on the floc by the impinging jet is an improvement over traditional methods.

4. The use of $\bar{G}$ is not appropriate for the design, assessment and operation of flocculation facilities. It appears that $\bar{G}$ is not even a good surrogate for local hydrodynamic characteristics as the ratio between local characteristics and vessel average characteristics change dramatically with changes in geometry.

5.6 Recommendations

This study involved the investigation of local hydrodynamics of mixing vessels as a refinement over the traditional use of vessel-average parameters. Detailed measurement and analysis of flow in impeller-agitated vessels highlighted a number characteristics of these systems. However, additional research is required to confirm some of these findings with other types of flocculators used and to relate these findings more closely to flocculator performance. Further advancement in the field of coagulation and flocculation will require greater knowledge of a number of aspects of this field. Based on the results of this study a number of recommendation for further study are given below:

1. There is a general need for more multi-scale flocculation studies. Most studies in the area of flocculation involve testing at only one scale, which provide little information on scale-up. Multi-scale studies should look both at details of mixing and flocculation performance with changing scale. Of importance is that performance measures are not limited just to traditional assessment methods such as turbidity reduction but also removal of organics

and specific chemical and microbial contaminants and how
performance of the flocculator for these various parameters change
with scale and mixing intensity.

2. Other types of flocculators used in practice need to be investigated.
   Of importance are axial flow impellers and rake-type impellers. For
   these systems initial work should focus on the characterization of the
   flow these systems produce.

3. Due to the fragile nature of flocs formed in water treatment there is a
   need to develop better methods of assessing floc size and
   characteristics. Clark et al. (1994) recommended there is a need to
   improve nondestructive methods of evaluating floc size as well as
   developing better methods to characterize floc density.

4. A major problem in relating mixing characteristics to floc size is the
   lack of a sound relationship which relates floc characteristics to floc
   strength. More work is required to determine how colloidal
   interactions impact the strength of the floc.

5. Further work is required to describe better both the force produced
   by the impinging jet and the impact they have on flocs. Analysis of
   this phenomenon in this study was based on a much less complex
   situation, taken from classical fluid mechanics, than what actually
   occurs in impeller-agitated mixing vessels. Work should focus on
   the impingement of a swirling radial jet on a surface.

5.7 References

Amirtharajah, A. and Trussel, S.L. 1986. Destabilization of particles by turbulent rapid mixing. *Journal of Environmental Engineering*, 112, 6, 1085-1108.

Clark, M.M. (1985). Critique of Camp and Stein's RMS velocity gradient. *Journal of Environmental Engineering*, 111, 6, 741-754.

Clark, M.M. and Fiessinger, F. 1991. Mixing and Scale-up. In *Mixing in Coagulation and Flocculation*. A. Amirtharajah, M.M. Clark, and R. Trussel. AWWA Research Foundation, Denver, CO. 282-308.

Clark, M.M., Srivastava, R.M., Lang, J.S., Trussel, R.R., McCollum, L.J. Baily, D., Christie, J.D., and Stolarik, G. (1994) Selection and Design of Mixing Processes for Coagulation. American Water Works Association Research Foundation and American Water Works Association, Denver, CO. 150p.

Cutter, L.A. 1966. Flow and turbulence in stirred tanks. *AIChE Jour.*, 12, 35-46.

Filip, P., Kolar, V. and Curev, A.G. (1985-a). Space Flow Geometry of the Radial Free, Wall and Liquid Jets with Swirl. *Applied Scientific Research*, 42, 185-196.

Filip, P., Kolar, V. and Curev, A.G. (1985-b). Complex Swirling Radial Jets, *Z. Angew. Math. u. Mech*, 65, 9, 441-446.

Filip, P., Kolar, V. and Curev, A.G. (1986). A Note on the Radial Wall Jet with Swirl, *Acta Mechanica*, 60, 41-47.

Kolar, V., Filip, P. and Curev, A.G. (1982). The Swirling Radial Jet, *Applied Scientific Research*, 39, 329-335.

Kolar, V., Filip, P. and Curev, A.G. (1984). Hydrodynamics of a Radially Discharging Impeller Stream in Agitated Vessels, *Chemical Engineering Communications*, 27, 313-320.

Kolar, V., Filip, P. and Curev, A.G. (198). The Swirling Radial Jet Model and its Application to a Radial Impeller stream, from *5th European Conference on Mixing*, Wurzburg, West Germany, 10-12 June, 1985, 483-490.

Konno, M., Aoki, M. and Saito, S. 1983. Scale effect on breakup process in liquid-liquid

agitated tanks. *Journal of Chemical Engineering of Japan*, 16, 4, 312-319.

Kresta, S.M. and Wood, P.E. (1991). Prediction of the three dimensional turbulent flow in

stirred tanks. *A.I.Ch.E.J.*, 37, 448-460.

Kresta, S.M. and Wood, P.E. (1993). The flow field produced by a pitched blade turbine:

Characterization of the turbulence and estimation of the dissipation rate. *Chemical*

Engineering Science, 48, 10, 1761-1774.

Oldshue, Y.J. and Mady, O.B. 1978. Flocculation performance of mixing impellers.

Chemical Engineering Progress, 74, 8, 103-108.

Wu, H. and Patterson, G.K. 1989. Laser doppler measurements of turbulent flow

parameters in a stirred mixer. *Chemical Engineering Science*, 44, 2207-2221.
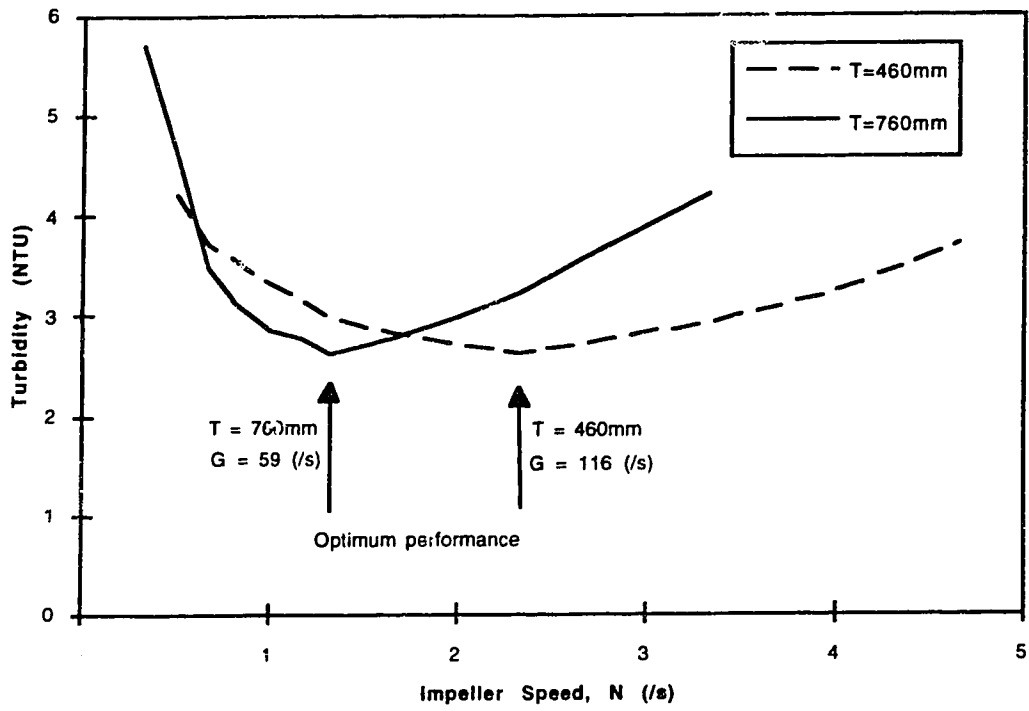
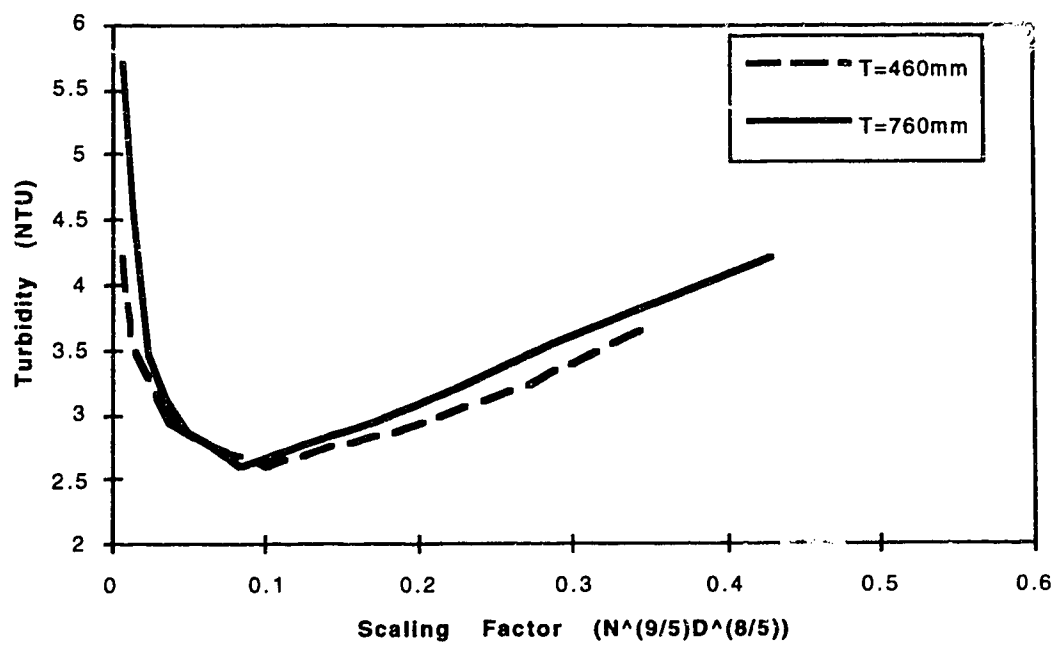Figure 5.1.   Multi-scale flocculation study results from Oldshue and Mady (1978)

Figure 5.2. Multi-scale flocculation study results from Oldshue and Mady (1978), Settled water turbidity vs. $(N^{9/5}D^{8/5})$
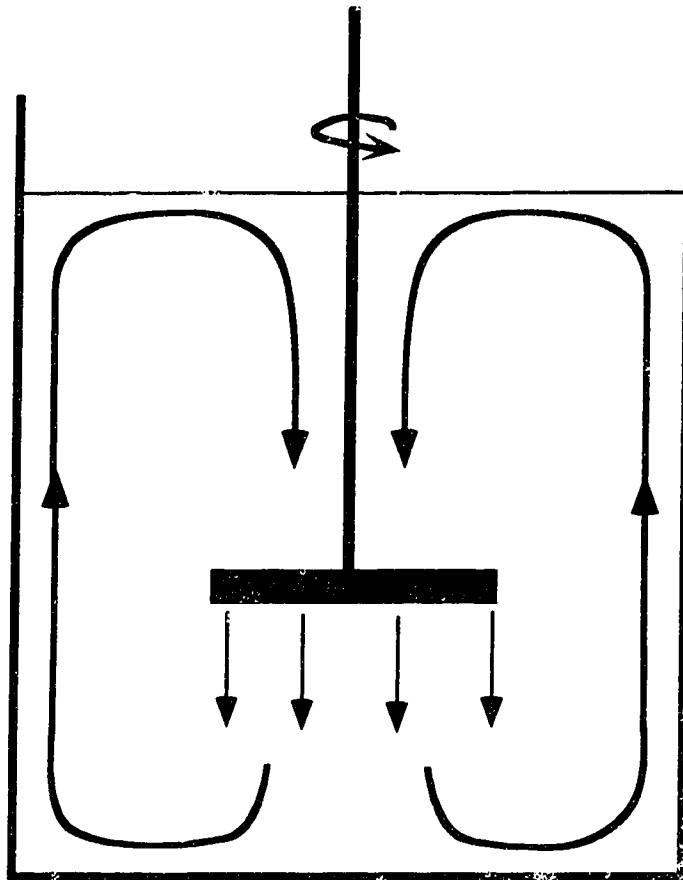
Figure 5.3. Typi of axial flow impeller.

APPENDIX A

Measurement of Turbulent Flow with a Laser Doppler Anemometer

A.1 Introduction

As the use of a laser doppler anemometer (LDA) is new to the field of
environmental engineering a brief description of the theory of LDA velocity measurement is
presented along with the set-up used in this experimental study and brief overview of
methods used to analyze the data. Further details on the LDA system used in this study can
be four `    ` ∩ANTEC (1989).

A.2   . ιι.   .DA Theory

The operating theory of the LDA is normally explained through the use of the
simple fringe model. A continuous wave laser is split into two parallel beams which pass
through spherical lens which causes these beams to intersect at the focal point of the lens.
A set of plane parallel interference fringes with a spacing dependent on the wavelength of
the laser and the angle between the two beams is produced at the intersection point of the
two beams. Figure A.1 shows the probe volume with the developed fringes. Small
particles, which can be naturally in the water or added by seeding, move with the velocity
of the fluid and will pass through the beams intersection point and the fringes. As these
particles pass the fringe system they will scatter light which is intensity modulated at the
rate at which the particles pass the fringe system; that is the particle velocity component
perpendicular to the plane of the fringes divided by the fringe spacing. The scattered light
is collected by receiving optics which convert it into an electrical signal by a high speed
photodetector. The frequency of the electrical signal, which is proportional to the particle
velocity, is then measured with an electronic device.

If the fringes are stationary as would be the case in the above discussion it would
not be possible to determine the sign of the velocity of the particle (fluid). To obtain
   .   ation on the sign of the velocity a small frequency shift is introduced in the
transmitting optics to one of the crossing laser beams. As a result the fringe pattern is no

longer stationary but moves perpendicularly to the fringe planes such that the light intensity

at any point   ulated at the shift frequency. Particles moving through the probe

volume will scatter light modulated such that the difference between the modulation

frequency and the shift frequency is proportional to the true velocity. For example, if a

particle is moving in an opposite direction to the fringe movement, the modulated frequency

would increase compared to the shift frequency; for particles moving in the same direction

of the fringe movement the modulated frequency would decrease. In the system used in

this study the frequency shift was accomplished with the use of a Bragg Cell which

produces a 40 MHz shift.

To obtain velocity values the signal obtained from the receiving optics must be

processed. The most common processors used include frequency trackers, counters, burst

spectrum analyzers and covariance processors. All of these signal processors do the same

task; demodulate the LJ , signal to determine the Doppler frequency. In general, trackers

are inexpensive but have limited bandwidths and are usually limited to liquid flows.

Counters have higher bandwidths but require a high signal-to-noise ratio and are subject to

large errors. Both the burst spectrum analyzer and covariance processors provide wide

bandwidths, high data rates and are able to handle low signal-to-noise ratios. As the

system used in this study used a covariance processor, the theory of this type of processor

will be briefly explained.

These processors use covariance processing techniques in which the phase detector,

the frequency detector and the sophisticated burst detector all utilize powerful analog

correlation techniques (Lading and Anderson, 1988). In the frequency detector, the signal

from one photodetector is split into two, one of which is delayed by a known time. This

corresponds to shifting the phase of that signal by the known delay multiplied by the

unknown frequency. The two signals are input to a phase detector, which measures their

phase difference. Finally, the measured phase difference divided by the known delay time

yields the unknown frequency of the signal. In the phase detector, signals from the two signals are fed to an analog cross correlator. A second correlator compares the two signals, but with one of them 90° out of phase. The integration parts of the cross correlators are gated by a burst detector. The outputs of the two correlators are proportional to the cosine and the sine of the original phase difference. By taking their ratio, the amplitudes and gate period cancel and performing an arctan operation using a PROM yields the required phase difference.

Velocities from the processor are then feed to a computer for further analysis, including calculation of mean velocities, fluctuating velocity and other turbulent quantities.

A.3. Experimental Set-up

The system used in this study was the 2-D DANTEC Particle Dynamics Analyzer with 55X Modular LDA transmitting optics, 55X10 receiving r₁tics, 55X08 photomultipliers and 58N10 processor. Figure A.2 shows the set-up of the laser and the experiments.

The laser was configured as outlined in Table A.1. The two laser wavelengths for the different velocity components were 488 nm (blue) and 514.5 nm (green). For both the transmitting and receiving optics either 310 mm or 600 mm lens were used, depending on the configuaration of the vessel to be analyzed. With a beam spacing of 39 mm for the 310 mm and 610 mm lenses this produced probe volumes of 0.12 mm X 0.12 mm X 2.4 mm or 0.24 mm X 0.24 mm X 2.4 mm, respectively. The bandpass filters were set at a bandwidth of 0.4 MHz. This bandwidth was chosen to minimize noise but ensured that all velocities encountered were contained within the selected bandwidth. The system as configured requires four photomultipliers (PMT). Each PMT has an individual high voltage supply, with each being adjusted to account for normal variations in sensitivity

between PMTs. Adjustments were made by comparing signals on a two channel oscilloscope.

As shown, in Figure A.2 the laser was operated in the forward scatter mode with a deflection angle of 60° from true forward scatter. This was found to produce the cleanest signal as well as allow the widest range of velocity measurements in the impeller zone minimizing blockage of the signal by the impeller blade. In the set-up the laser system remained stationary and the mixing vessel was moved to change the position of the velocity measurement. This was accomplished by placing the mixing vessel on a 3-dimensional moveable table in which the position of the vessel could placed at the desired coordinate within ±0.25 mm. Positions were determined by placing a grid on the mixing vessel studied.

A.4 Analysis of Velocity Data

From the raw velocity data obtained, a number of turbulent flow parameters were determined. These included mean velocities, turbulent fluctuating velocities, and the autocorrelation function. As discussed in Chapter 2, in making velocity measurements with a LDA it is important to consider the phase ambiguity noise limit. Detailed discussion of this was presented in Chapter 2 and will not be presented here.

The velocity is determined by fringe spacing and the frequency of the Doppler signal. Each time a particle passes through the measuring volume and produces a validated signal an instantaneous velocity can be determined. Velocity samples were validated based on signal-to-noise levels and fringe counts.

Generally, in the analysis of turbulence, instantaneous turbulent velocities, u_i, are divided in a mean component, $\overline{U_i}$ and a fluctuating component, u_i' which is defined as:

$$u_i' = u_i - \overline{U_i} \qquad\qquad (A.1)$$

At each measurement point between 5,000 and 10,000 instantaneous velocities were measured. The mean of the velocity in LDA measurements can not normally be calculated by taking a simple average as this can lead to velocity biases. Generally velocity distributions given by LDA measurements are somewhat correlated with particle velocity. This results as fast moving particles are more likely to be detected than slow moving particles. In addition, particles passing through the outer edges of the measurement volume are less likely to be detected. To account for this bias, mean velocities were calculated based on residence time weighting as shown below:

$$\overline{U} = \sum u_i \delta t / \sum \delta t \qquad (A.2)$$

In turbulence the fluctuating velocity is normally given by the root-mean-square velocity. For residence time weighted velocities this is given as:

$$u' = \sqrt{(\sum (u_i - \overline{U})^2 \delta t / \sum \delta t)} \qquad (\text{A}.3)$$

The autocorrelation function was determined as follows:

$$R_E(\tau) = \frac{\overline{u'(t)u'(t-\tau)}_{tot}}{\overline{u'^2}} \qquad (A.4)$$

where τ is the time between velocity measurements analyzed.

A.5 References

Arik, E.B. 1989. New developments in instrumentation for fluid dynamic measurements. In Modern Techniques and Measurements in Fluid Flows, S. Xiong and S. Xijiu, Ed., Beijing, China, International Academic Publishers, 1-6.

DANTEC 1989. Particle Dynamics Analyzer: Users Manual. DANTEC

Lading, L. and Anderson, K. 1988. A convariance processor for laser anemometry and particle sizing. Procceedings of the Fourth International Symposium on Application of Laser Anemometry to Fluid Mechanics, Lisbon, Spain.

Table A.1 Laser Specifications

| Component	Experimental Setting
Argon-Ion Laser	Power = 300 mW λ = 514.5nm
Bragg Cell	40 MHz frequency shift
U velocity	λ = 514.5 nm
V velocity	λ = 488 nm
Transmitting lens	$f = 310mm$ or $f = 600mm$ (depending on set-up)
Beam Spacing	39 mm
Fringe Spacing $f = 310mm$ $f = 600mm$	U = 4.10 μm V = 3.89 μm U = 7.91 μm V = 7.51 μm
Gaussian Beam Diameter	0.82
Beam Collimator	1.1
Beam Expander	1.85
Number of Fringes	30
Measurement Volume $f = 310mm$ $f = 600mm$	0.12 mm X 0.12 mm X 2.4 mm 0.24 mm X 0.24 mm X 7.0 mm
Receiving optics lens	$f = 310mm$ or $f = 600mm$ (depending on set-up) $\delta = 60°$
Forward scatter deflection	
Validation Level	-4 dB
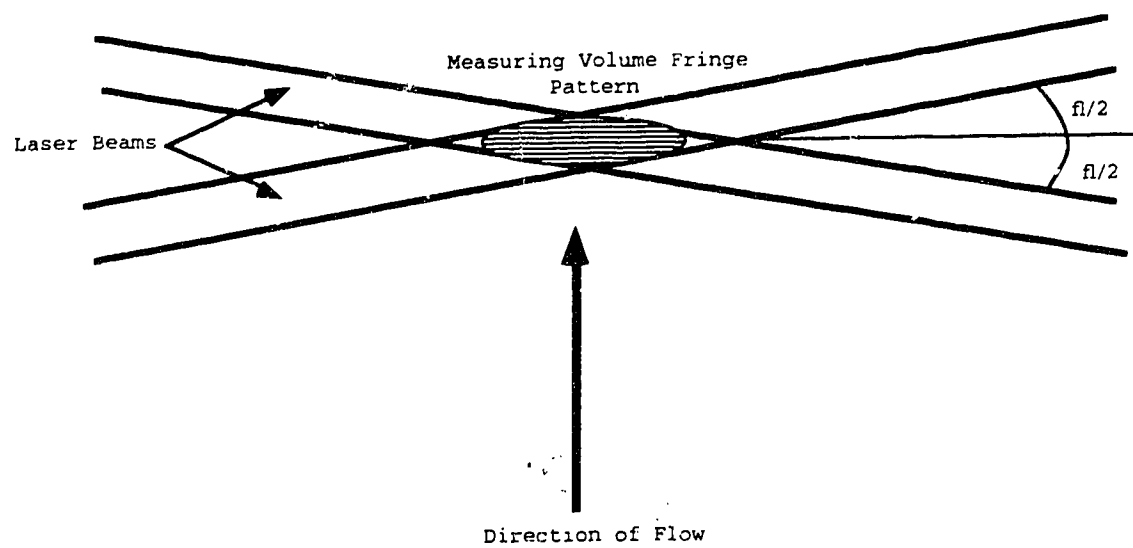
Figure A.1. Simple Fringe Model
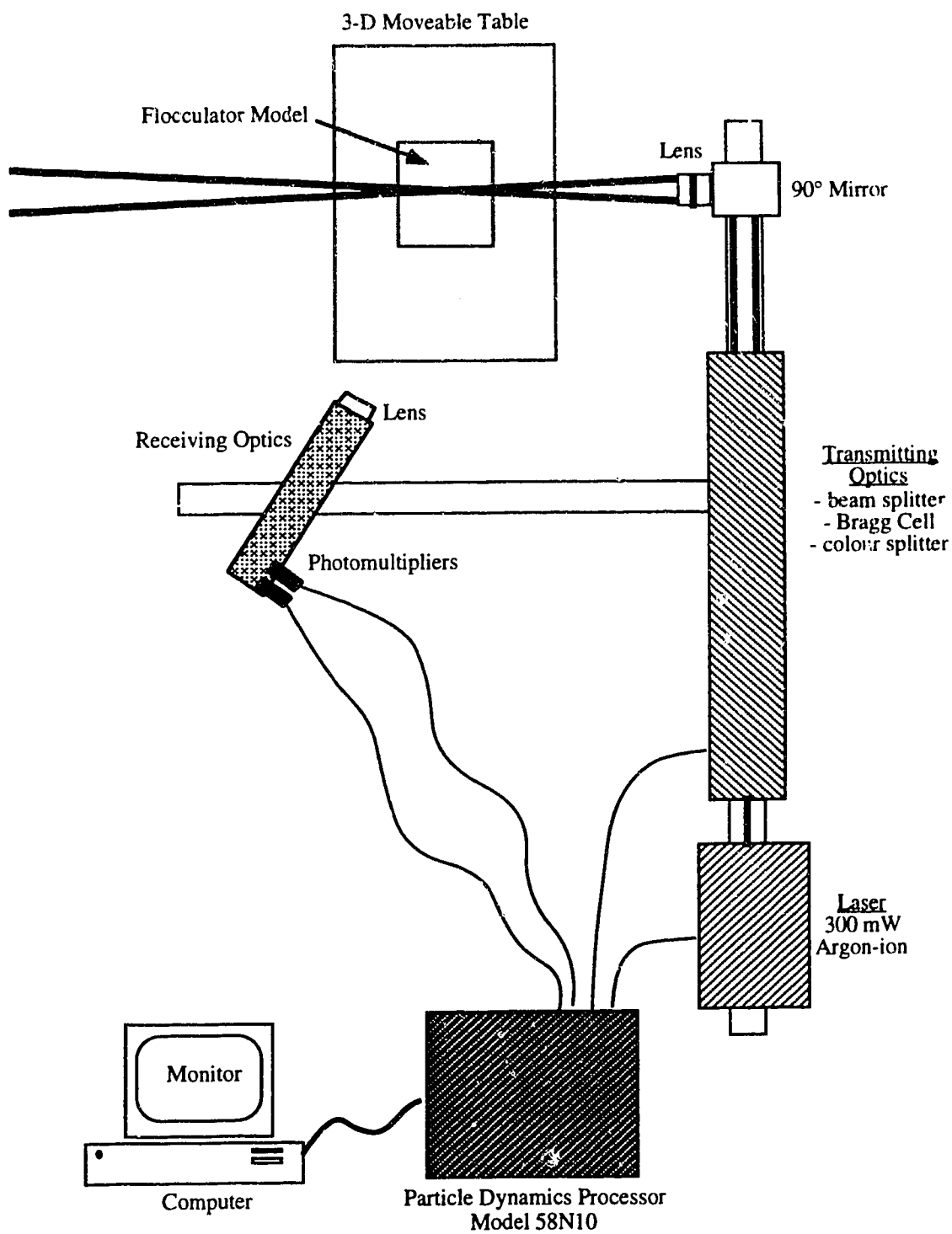
Figure A.2. LDA Experimental Set-up.

APPENDIX B

Curriculum Vitae

CURRICULUM VITAE

Stephen John Stanley, P. Eng.

PERSONAL:

Address:	12220 - 42 Avenue
	Edmonton, Alberta
	T6J 0W9
Telephone:	(403) 435-9445 (residence)
	(403) 492-4738 (business)

CURRENT POSITION: (July 1993 to present)

Title:
Assistant Professor
Environmental Engineering and Science Program
Department of Civil Engineering
University of Alberta
Edmonton, Alberta

Function:
Teaching and developing courses in the environmental engineering field at both the undergraduate and graduate level. Supervise graduate student research related to environmental engineering.

EDUCATION:

Sept. 1988 - present	Ph.D. Candidate in Environmental Engineering Department of Civil Engineering University of Alberta Thesis topic: Hydrodynamics of flocculation Advisor: Dr. D.W. Smith
1988	M.Sc. in Hydrotechnical Engineering Department of Civil Engineering University of Alberta Thesis topic: Ice jam analysis in a complex reach Advisor: Dr. R. Gerard
1985	B.Sc. in Civil Engineering University of Alberta

REGISTRATION:

Professional Engineer, Province of Alberta, No. 44421

AWARDS:

Keefer Medal, Canadian Society for Civil Engineering, Outstanding Paper in the *Canadian Journal for Civil Engineering*, 1992.

RESEARCH INTERESTS:

Water quality assessment, unit processes in water and wastewater treatment, environmental hydraulics and fluid mechanics, river mixing and hydrology, and ice jam analysis.

PREVIOUS EMPLOYMENT:

1990-93   Research Associate, Environmental Engineering and Science Program, University of Alberta

1990   Sessional Lecturer, Department of Civil Engineering, University of Alberta.

1988-90   Graduate Research and Teaching Assistant, Environmental Engineering and Science Program, Department of Civil Engineering, University of Alberta.

1986-88   Graduate Research and Teaching Assistant, Water Resource Engineering, Department of Civil Engineering, University of Alberta.

1985-86   Research Engineer, Department of Civil Engineering, University of Alberta.

1981-84   Engineering summer student, Lethbridge Northern Irrigation District.

RESEARCH AND CONSULTING PROJECTS:

Northern River Basin Study (a $13 million study by federal and provincial governments)
- Group coordinator for the drinking water group.

Transportation, Drainage Branch, City of Edmonton (1992 - present)
Project: • Review of wastewater treatment plant flow improvement study

Edmonton Board of Health, Environmental Health Division, Edmonton, Alberta (1992 - present)
Project: • Review of landfill application under the Public Health Act

Proctor and Gamble Inc., Grande Prairie, Alberta (1992 - present)
Project: • Pulp mill effluent treatment studies

Alberta Environment, Environmental Protection Services, Edmonton, Alberta (1992 - present)
Projects: • Assessment of lagoon treatment
• Mixing in coagulation and flocculation
• Effect of hydraulic shear on pipe biofilms

Water Branch, Public Works, City of Edmonton (1992 - 1993)
Project: • Special consultant (open consulting agreement)

Alberta Research Council, Combustion/Gasification Group, Edmonton, Alberta (1991-1992).
Project: • Characterization of Granular Activated Carbon.

Stanley Associates Engineering Ltd. and City of Edmonton, Environmental Services. (1991-1993)

Project: • Expert review team - E.L. Smith - Lime Waste Treatment.

David A. Poole Consultants Ltd, Vancouver, B.C. (1990 - 1992)

Project: • Filter pilot plant study at Rossdale Water Treatment Plant, Edmonton , Alberta.

City of Edmonton, Environmental Services, Edmonton Alberta (1988 - present)

Projects: • Urban Storm Water Literature Review (1993)
              • CT study E.L. Smith (1992-93)
              • Rossdale filter study, Phase III (1992-1993)
              • Assessment of polymers as filter aids, E.L. Smith (1992)
              • Review of a risk assessment for the Rossdale water intake
              • Filter pilot plant study, Phase II (1991-92).
              • Lime sludge dewatering effluent studies for E.L. Smith Water Treatment Plant (1991).
              • Mass balance study of the softening clarifier and thickener at E.L. Smith Water Treatment Plant (1990).
              • Field investigation of the decay of chlorinated discharges from water treatment plants (1990-91).
              • Alum clarifier performance study (1989-90).
              • Impact assessment of chlorinated discharges from water treatment plants (1989-90).
              • Water softening: Costs and benefits. (1989)

Department of Municipal and Community Affairs, Government of the Northwest Territories, Yellowknife, NWT. (1989-present)

Projects: • Site investigation of the Rankin Inlet wastewater marine outfall (1990-91).
              • Water quality analyses for selected N.W.T. Communities (1990 -91).
              • Ice reduction on potable water reservoirs.(1989-90).

Tradewinds Scientific Ltd, Ottawa, Ontario

Project: • Friction testing of airport runways in Alberta (1988-89)

Environment Canada and Indian and Northern Affairs Canada, Yellowknife, NWT.

Projects: • Ice jams and flood forecasting, Hay River, N.W.T. (1987-88).
              • Updating ice jam flood levels (1992-93)

Steve E. Hrudey & Associates Ltd. and D.W. Smith and Associates Ltd. Edmonton, Alberta.

Project: • A critical assessment of drinking water in Edmonton. (1986)

Indian and Northern Affairs Canada, Whitehorse, Yukon.

Project: • Ice jam flooding on the Yukon River, Dawson, Yukon (1986)

PUBLICATIONS

Publications in Refereed Journals:

Stanley, S.J. and Smith, D.W. 1995. Scaling of forces on a floc particle. Journal of Environmental Engineering, American Society of Civil Engineering. (Submitted).

Suthaker, S., Smith, D.W. and Stanley, S.J. 1995. Statistcal data evaluation and reliability-based design for water filtration. Journal of Environmental Engineering, American Society of Civil Engineering. (Submitted).

Prince, D.S., Smith, D.W. and Stanley, S.J. 1995. Intermittent Discharge Lagoons for use in Cold Regions. Journal of Environmental Engineering, American Society of Civil Engineering., (Accepted, Dec. 1994).

Stanley, S.J. and Smith, D.W. 1995. Characterization of impeller-agitated flow in an upflow solids-contacting clarifier. Journal of Environmental Engineering, American Society of Civil Engineering. (Accepted May, 1995).

Suthaker, S., Smith, D.W. and Stanley, S.J. 1995. Filtrate Turbidity Improvement of Existing Mono-media Filters based on a Pilot Plant Study. Environmental Technology, (Accepted for publication, Jan. 1995)

Makepeace, D.K., Smith, D.W. and Stanley, S.J. 1994. Urban Storm Water Quality: Summary of Contaminant Data. Critical Reviews in Environmental Science and Technology (Accepted, August).

Zhu, H., Smith, D.W., Zhou, H. and Stanley, S.J. 1995. Selection of Polymers as Filter Aids for Softened Water. Water Research (Accepted, July)

Smith, D.W. and Stanley S.J. 1994. Progress towards the development of clean-up protocols for contaminated sites in Canada. ASCE Journal of Professional Issues in Engineering, Education and Practice, 121, 1, 67-70.

Suthaker, S., Smith, D.W. and Stanley, S.J. 1995. Filtrate Turbidity Improvement of Existing Mono-media Filters based on a Pilot Plant Study. Canadian Journal of Civil Engineering. (Accepted May, 1995).

Prince, D.S., Smith, D.W. and Stanley, S.J. 1994. Performance of lagoons which experience seasonal ice cover. Water Environment Research, (Accepted, June, 1995).

Stanley, S.J. and Smith, D.W. 1995. Measurement of turbulent flow in a standard jar test apparatus. Journal of Environmental Engineering, American Society of Civil Engineering. (Accepted February, 1995).

Stanley, S.J. and Smith, D.W. 1993. Lagoons and Ponds. Water Environment Research. 65,4, 344-349

Suthaker, S., Smith, D.W. and Stanley, S.J. 1993. Characteristics and quantity of lime sludge from solid contact clarifiers and their implications on gravity thickening. Environmental Technology, 14, 1001-14.

Zhou, H., Smith, D.W. and Stanley, S.J. 1993. Modeling of Concentration Profiles of Dissolved Ozone in Bubble Columns. Journal of Environmental Engineering, American Society of Civil Engineering 120, 821-840..

Milne, G.D., Stanley, S.J. and Smith, D.W. 1993. Residual Chlorine Decay in a Broad Shallow River. Water Research 27,6, 993-1001.

Stanley, S.J. and Gerard, R. 1992. Probability analysis of historical ice jam flood data for a complex reach: a case study. Canadian Journal of Civil Engineering, 19, 875-885.

Zhou, H., Smith, D.W. and Stanley, S.J. 1992. Characterization and Treatment of Lime Sludge Dewatering Effluents. Canadian Journal of Civil Engineering, 19, 794-805.

Stanley, S.J. and Smith, D.W. 1992. Lagoons and Ponds. Water Environment Research, 64, 4, 367-371.

Stanley, S.J., Smith, D.W. and Milne, G.D. 1992. Microorganism survival in an ice-covered marine environment. Journal of Cold Regions Engineering, American Society of Civil Engineering, 6, 2, 58-72.

Stanley, S.J. and Gerard, R. 1992. Ice jam forecasting procedure: Hay River, N.W.T. Canadian Journal of Civil Engineering, 19, 212-223.

Stanley, S.J. and D.W. Smith. 1991. Reduction of ice thickness on northern water reservoirs. Journal of Cold Regions Engineering, American Society of Civil Engineering, 5, 3, 106-124..

Stanley, S.J. and Smith, D.W. 1991. Modelling chlorinated discharges from water treatment plants: a case study. Canadian Journal of Civil Engineering, 18, 6, 985-994.

Papers published in conference proceedings:

Prince, D.S., Smith, D.W. and S.J. Stanley. 1994. Performance and factors effecting performance of lagoons in cold regions. 7th International Cold Regions Engineering Specialty Conference, Edmonton, Alberta, 539-556.

Stanley, S.J. and Smith, D.W. 1994. Hydrodynamics of mixing in drinking water treatment. Proceedings CSCE Annual Conference, Winnipeg, Man., Vol. III, 50-59.

Suthaker, S., Smith, D.W. and Stanley, S.J. 1994. Comparing filter media alternatives for improving drinking water quality. Proceedings CSCE Annual Conference, Winnipeg, Man., Vol. III, 40-49.

Zhu, H., Smith, D.W., Zhou, H., Stanley, S.J. and Kellondonk, D. 1994. Selection of a polymer filter aid for softened water. Proceedings CSCE Annual Conference, Winnipeg, Man., Vol. III, 159-168.

Smith, D.W. and Stanley, S.J. 1993. Urban and Industrial Pollution and Clean Up in Canada: The Balance between Clean Up and Effects on Devlopment. Proceedings, Urban Development and the Environmental Challenge, Institution of Civil Engineers, London, England, pp. 33-36.

Stanley, S.J., Smith, D.W., and Prince, D.S. 1993. Determination of CT Values to Measure the Adequacy of Water Treatment Disinfection. CSCE Annual Conference 403-412.

Stanley, S.J. and Smith, D.W. 1991. A Technical and Economic Evaluation of Ice Reduction Methods for Northern Potable Water Reservoirs. International Symposium on Cold Region Development, 16-21 June 1991, Edmonton, Alberta pp. 60.

Stanley, S.J. and Smith, D.W. 1991. Clarifier Performance Data: A Valuable Tool in Clarifier Design. Proceeding of the 1991 Annual Conference, Canadian Society of Civil Engineering, Vancouver, B.C. Vol. 4. pp. 375-384.

Milne, G.D., Stanley, S.J. and Smith, D.W. 1991. Mixing and Decay of Chlorinated Water Treatment Plant Discharges to the North Saskatchewan River. Proceeding of the 1991 Annual Conference, Canadian Society of Civil Engineering, Vancouver, B.C. Vol. 4. pp. 249-258.

Stanley, S.J. and Gerard, R. 1990. Ice jam forecasting procedure: Hay River, N.W.T. Proceedings: Canadian Society for Civil Engineering, Annual Conference, Hamilton, Ontario. Volume V. pp. 301-321.

Stanley, S.J. and Smith, D.W. 1989. Water Softening: Benefits and Costs. Proceedings: Canadian Society for Civil Engineering, Annual Conference, St. Johns, Newfoundland. Vol. IV. pp. 653-671

Gerard, R. and Stanley, S.J. 1988. Ice jams at a lake: the situation at Hay River, Northwest Territories, Canada. Proceedings of the International Association of Hydraulic Research Ice Symposium, Sapporo, Japan. Vol. 3, pp 157-167.

Stanley, S.J. and Gerard. R. 1988. Probability analysis of historical ice jam flood data for a complex reach: a case study. Proceeding of the 5th Annual Workshop on River Ice/Ice Jams, Winnipeg, Manitoba, pp. 115-138.

Reports and other published material

Zhu, H., Smith, D.W., Zhou, H. and Stanley, S.J. 1995. Selection of Polymers as Filter Aid for E.L. Smith Water Treatment Plant Softened Water. Environmental Engineering Technical Report 95-1.

Prince, D.S., Smith, D.W. and Stanley, S.J. 1994. An Abridgement of "Evaluation of Lagoon Treatment in Alberta. Prepared for Alberta Environmental Protection, 54p.

Liem, E., Stanley, S.J., Smith, D.W. and Prince, D. 1994. Detention time evaluation for some Rossdale Water Treatment Plant Process Tanks. A report prepared for Water Branch, Public Works, City of Edmonton. 55p.

Stanley S.J. 1994. Review of lime waste recycling in a water treatment plant. A report prepared for Water Branch, Public Works, City of Edmonton. 25p.

Emde, K.M.E., Smith, D.W. and Stanley S.J. 1994. Health Records Study. Prepared for Northern River Basin Study. 35p.

Prince, D.S., Smith, D.W. and Stanley, S.J. 1994. Review and Synthesis of Existing Information on Consumptive Use of Drinking Water and Available Drinking Water Quality Data. Prepared for Northern River Basin Study. 80p.

Makepeace, D.K., Smith, D.W. and Stanley S.J. 1993. Urban Stormwater Literature Review. A report prepared for Water Branch, Public Works, City of Edmonton. 83p.

Stanley, S.J. 1993. Rossdale Raw Water Intake Mixing Study. A report prepared for Water Branch, Public Works, City of Edmonton. 83p.

Stanley S.J., Smith, D.W. and Prince D.S. 1993. Hydraulic Tracer Test on Clarifier C-2, E.L. Smith Water Treatment Plant. A report prepared for Water Plants Engineering, Public Works, City of Edmonton, 14p.

Stanley S.J. and Smith, D.W. 1993. Investigation of hydrodynamics in coagulation and flocculation. Canadian Civil Engineer, Vol. 10, No. 9, 5-7.

Prince, D.S., Smith, D.W. and Stanley, S.J. 1993 Evaluation of Lagoon Treatment in Canada. A report prepared for Alberta Environmental Protection, Edmonton, Alberta, 187p.

Jasek, M., Stanley, S.J., and Gerard, R. 1993. An update of historical flooding at Hay River, N.W.T., A report prepared for Indian and Northern Affairs Canada, Yellowknife, N.W.T.

Suthaker, S., Stanley, S.J. and Smith, D.W. 1992. Filter Ripening Sequence Study. A report prepared for Water Plants Engineering, City of Edmonton.

Stanley, S.J. and Smith, D.W. 1992. The role of mixing in coagulation and flocculation. A report prepared for Standards and Approvals Division, Alberta Environment.

Stanley, S.J., Smith, D.W., and Emde, K.M.E. 1992. The effect of hydraulic shear on water distribution pipe biofilms. A report prepared for Standards and Approvals Division, Alberta Environment.

David A. Poole Consultants Ltd. 1992. Rossdale Filter Study. Prepared for Environmental Services, City of Edmonton, Edmonton, Alberta.

Suthaker, S., Stanley, S.J. and Smith, D.W. 1992. Rossdale Filter Study, Phase II Report. Available as Environmental Engineering Technical Report 92-2, Department of Civil Engineering, University of Alberta, Edmonton, Alberta.

Smith, D.W., Kenefick, S. and Stanley S.J. 1992. Evaluation of Activated Carbon. A proprietary report for the Coal and Hydrocarbon Processing Department, Alberta Research Council, Edmonton, Alberta.

Milne, G.D., Stanley, S.J., and Smith, D.W. 1991. Assessment of Chlorinated Discharges from the City of Edmonton's Two Water Treatment Plants. Available as Environmental Engineering Technical Report 91-4, Department of Civil Engineering, University of Alberta, Edmonton, Alberta.

Stanley, S.J., Smith, D.W. and Milne, G.D. 1991. Site Investigation of the Rankin Inlet, NWT Wastewater Marine Outfall. Available as Environmental Engineering Technical Report 91-2, Department of Civil Engineering, University of Alberta, Edmonton, Alberta.

Suthaker, S., Stanley, S.J. and Smith, D.W. 1991. Mass balance study of softening clarifier and thickener at E.L. Smith Water Treatment Plant. Available as Environmental Engineering Technical Report 91-3, Department of Civil Engineering, University of Alberta, Edmonton, Alberta.

Zhou, H., Smith, D.W. and Stanley, S.J. 1991. Lime sludge dewatering effluent studies for E.L. Smith Water Treatment Plant (Draft Report). Available as Environmental Engineering Technical Report 91-1, Department of Civil Engineering, University of Alberta, Edmonton, Alberta.

Stanley, S.J. and Smith, D.W. 1990. Water reservoir ice reduction study. A report for the Government of the Northwest Territories. Available as Environmental Engineering Technical Report 90-3. Department of Civil Engineering, University of Alberta, Edmonton, Alberta.

Stanley, S.J. and Smith, D.W. 1990. Clarifier performance study. A report for the City of Edmonton. Available as Environmental Engineering Technical Report 90-2, Department of Civil Engineering, University of Alberta, Edmonton, Alberta.

Stanley, S.J. and Smith, D.W. 1990. Chlorine plume study: City of Edmonton's Water Treatment Plants. A report for the City of Edmonton. Available as Environmental Engineering Technical Report 90-1, Department of Civil Engineering, University of Alberta, Edmonton, Alberta.

Stanley, S.J. and Smith, D.W. 1989. Water Softening: Benefits and Costs. A report for the City of Edmonton. Available as Environmental Engineering Technical Report 89-1, Department of Civil Engineering, University of Alberta, Edmonton, Alberta.

Gerard, R. and Stanley, S.J. 1988. Ice jams flood forecasting, Hay River, N.W.T. A report for Environment Canada and Indian and Northern Affairs Canada, Yellowknife, N.W.T. Available as Water Resources Engineering Report 88-6, Department of Civil Engineering, University of Alberta, Edmonton, Alberta.

Stanley, S.J. 1988. Ice Jam Analysis in a Complex Reach. M.Sc. Thesis, Department of Civil Engineering, University of Alberta, Edmonton, Alberta.

Gerard, R. and Stanley, S.J. 1986. A preliminary appraisal of meteorological and streamflow effects on break-up, Yukon River at Dawson. A report for Indian and Northern Affairs Canada, Whitehorse, Yukon. Available as Water Resources

Engineering Report 86-1, Department of Civil Engineering, University of Alberta, Edmonton, Alberta.

Daniel W. Smith and Associates. 1986. Microbiological Water Quality of the North Saskatchewan River. A proprietary report for S.E. Hrudey and Associates, Edmonton, Alberta.